



Faculty of Applied and Computer Sciences
Department of Chemistry

Amino acid-capped metal selenide nanoparticles: Their synthesis, characterization, optical and magnetic properties

By

Kopano Edward Mokubung

Student Number: 211090360

**A dissertation submitted in fulfilment of requirements for the degree;
Magister Technologiae: Chemistry**

Supervisor: Prof M.J. Moloto [BSc. Hons, MSc, PhD. (Chemistry)]

Co-supervisor: Prof N. Moloto [BSc. Hons, MSc, PhD. (Chemistry)]

Date: April 2018

Declaration

I, _____ hereby declare that this work has not previously been accepted in substance for any degree and is not being concurrently submitted in candidature for any degree.

Signed.....

Date.....

Abstract

Quantum dots (QDs) have already proven features that can be considered to improve their properties for biological applications. Metal selenide nanoparticles possess semiconducting behaviors that can vary with structural and optical properties evolving from their synthesis. An aqueous medium through a simple, non-toxic and environmentally friendly colloidal route for the preparation of water-soluble CdSe, Cu₂Se, FeSe semiconductor nanoparticles has been developed. Different capping molecules with multi-functional moieties (-COOH, -NH₂ and -OH) namely, L-cysteine, L-glutamic acid and L-phenylalanine, have been employed in the preparation of cadmium selenide, copper selenide and iron selenide semiconductor nanoparticles as capping molecules. The synthesized metal selenide nanoparticles were characterized by Fourier Transform Infrared (FTIR), UV-Vis spectroscopy, Photoluminescence spectroscopy (PL), X-ray Diffraction (XRD), Vibrating Sample Magnetometer (VSM) and Transmission Electron Microscopy (TEM). The FTIR spectroscopy confirmed the binding moiety through the surface of the nanoparticles which is pH dependent. The XRD patterns confirmed a cubic phase of CdSe and Cu₂Se while FeSe revealed a hexagonal phase for the synthesized nanoparticles. The optical absorption as a function of wavelength for the prepared nanoparticles at different temperature is investigated. The morphology of the nanoparticles dominated through this method was spherical in shape. Amino acids capped metal selenide nanoparticles were successfully synthesized by aqueous medium through a simple colloidal route. The absorption spectra of all samples prepared were blue shifted as compared to their bulk counterparts which signify quantum confinement effect. The optical absorption measurements show some dependency of the temperature values used in the synthesis of nanoparticles. The effect of temperature and pH on the growth and morphology of nanoparticles was investigated. X-ray diffraction patterns confirms the structure, single cubic and hexagonal phase for the synthesized nanoparticles. TEM studies of metal selenide nanoparticle show that particle size increases with the increase in reaction temperature. The vibrating sample magnetometer (VSM) shows almost linear without any hysteresis loop for copper selenide, which indicated the absence of magnetism and exhibits paramagnetic nature than diamagnetic properties while iron selenide revealed twofold ferromagnetic behavior in low fields and paramagnetic behavior in up fields.

Dedication

For you my loving parents and friends

Acknowledgements

I will begin my acknowledgement by sincerely thanking God for giving me courage and strength to complete my studies and my supervisors, Prof M.J. Moloto and Prof N. Moloto for their guidance during the period of completing this project by providing numerous help was the main essence that keeps me working till the end. I would also like to express my gratitude to him for granting me freedom and positive attitude in completing this research.

Secondly, I will like to thank my fellow research team mates – Wanda Bout and Khumblani Mnqiwu for their assistance, valuable comments and ideas on this work. Next, special thanks also goes to Dr Poslet Shumbula and Mr Sanele Nyembe in helping with the characterization techniques and those who have helped me for being so supportive and keep me motivated along the way.

I would like to take this opportunity to thank the following Dimakatso Mncira, Nomsa Mathabi, Thulani Mokubung, Mokgethi Mokubung and my late Mother Busisiwe Julia Mokubung, siblings for giving me support constantly to overcome all the obstacles faced in completing this project and the degree programme.

Lastly, I would like thanks NRF, Vaal University of Technology and University of Witwatersrand for laboratory space and equipment used for the research.

Conferences Presentations

1st VUT interdisciplinary research and postgraduate conference (Oral)

Title: Direct synthesis of water soluble cadmium selenide nanoparticles capped with hydrophilic stabilizer. Science Park, Vanderbijlpark (Sebokeng), South Africa 09-10 November 2016.

Nanoscience Young Researchers' Symposium 2016 Program (Oral)

Title: Size tuning of cysteine capped CdSe nanoparticles using an alternative source of selenium. Mintek, Randburg, South Africa 18 November 2016.

SACI INORGANIC 2017 Incorporating the Carman Symposium (Poster)

Title: Direct synthesis and characterization of cysteine-capped water-soluble copper selenide quantum dots. Arabella Hotel & spa, Kleinmond, Hermanus, Western Cape, South Africa 25-29 June 2017.

Publications

K.E. Mokubung, M.J. Moloto, N. Moloto, Low temperature synthesis of L-cysteine capped Cu₂Se quantum dots, Materials letters, *to be submitted*.

Table of Contents

Declaration	i
Abstract	ii
Dedication	iii
Acknowledgements	iv
Conferences Presentations	v
Publications	v
List of Figures	ix
CHAPTER 1	1
INTRODUCTION AND LITERATURE REVIEW	1
1.1 Semiconducting nanocrystals.....	1
1.2 Surface chemistry.....	4
1.3 Chemistry of selected amino acids as capping agents	5
1.3.1 L-cysteine.....	6
1.3.2 L-glutamic acid	6
1.3.3 L-phenylalanine	7
1.4 Metal selenide nanoparticles.....	8
1.4.1 CdSe nanoparticles.....	8
1.4.2 Cu _x Se _y nanoparticles	10
1.4.3 Fe _x Se _y nanoparticles.....	12
1.5 Parameters that influence size and shape of nanocrystals.....	13
1.6 Methods for the preparation of semiconductor nanocrystals	15
1.6.1 Colloidal routes.....	15
1.6.2 Hot injection routes.....	17
1.6.3 Single-molecule precursors.....	18
1.7 Application of nanotechnology	19
1.7.1 Light-emitting devices	19
1.7.2 Biomarkers	20
1.7.3 Dual-modality probes.....	21
1.8 Problem Statement	23
1.9 Aims and Objectives	23

CHAPTER 2	24
EXPERIMENTAL	24
2.1 Chemical used	24
2.2 Apparatus	24
2.3 Synthesis	25
2.3.1 Preparation of Selenium source S^{2-}	25
2.3.2 Preparation of L-cysteine-capped CdSe nanoparticles.....	25
2.3.3 Preparation of L-cysteine-capped Cu_xSe_y nanoparticles	26
2.3.4 Preparation of L-cysteine-capped Fe_xSe_y nanoparticles.....	26
2.3.5 Preparation of nanoparticles capped with L-glutamic acid and L-phenylalanine	26
2.4 Characterization techniques	27
2.3.2 Infrared spectrometer	27
2.3.3 Optical characterization	27
2.3.4 X-ray diffraction analysis.....	27
2.3.5 Electron microscopy	27
 CHAPTER 3	 28
RESULTS AND DISCUSSION	28
SYNTHESIS, CHARACTERIZATION OF L-CYSTEINE, L-GLUTAMIC ACID AND L-PHENYLANILINE CAPPED METAL SELENIDE NANOPARTICLES	28
3.1 L-Cysteine-capped metal selenide nanoparticles	29
3.1.1 FTIR spectral analysis of metal selenide nanoparticles capped with L-cysteine	29
3.1.2 Cadmium selenide nanoparticles capped with L-cysteine	30
(a) Optical properties	30
(b) Structural characterization	32
3.1.3 Copper selenide nanoparticles capped with L-cysteine	35
(a) Optical properties	35
(b) Structural characterization	37
(c) Magnetic properties.....	39
3.1.4 Iron selenide nanoparticles capped with L-cysteine	40
(a) Optical properties	40
(b) Structural characterization	41
(c) Magnetic properties.....	44

3.2	L-Glutamic acid capped metal selenide nanoparticles.....	45
3.2.1	FTIR spectral analysis of metal selenide nanoparticles capped with L-glutamic acid.....	45
3.2.2	Cadmium selenide nanoparticles capped with L-glutamic acid.....	46
(a)	Optical properties.....	46
(b)	Structural characterization	47
3.2.3	Copper selenide nanoparticles capped with L-glutamic acid.....	50
(a)	Optical properties.....	50
(b)	Structural characterization	51
(c)	Magnetic properties.....	54
3.2.4	Iron selenide capped with L-glutamic acid	55
(a)	Optical properties.....	55
(b)	Structural characterization	56
(c)	Magnetic properties.....	59
3.3	L-Phenylalanine capped metal selenide nanoparticles.....	60
3.3.1	FT-IR analysis of L-phenylalanine capped metal selenide nanoparticles.....	60
3.3.2	Cadmium selenide nanoparticles capped with L-phenylalanine	61
(a)	Optical properties.....	61
(b)	Structural characterization	63
3.3.3	Copper selenide nanoparticles capped with L-phenylalanine	66
(a)	Optical properties.....	66
(b)	Structural characterization	68
(c)	Magnetic properties.....	71
3.3.4	Iron selenide capped with L-phenylalanine	72
(a)	Optical properties.....	72
(b)	Structural characterization	73
(c)	Magnetic properties.....	76
CONCLUSIONS AND FUTURE WORK		77
3.4	Conclusions.....	77
3.5	Future work and recommendations.....	78
3.6	References.....	79

List of Figures

Fig. 1. 1 Molecular structure of l-cysteine.....	6
Fig. 1. 2 Molecular structure of l-glutamic acid	7
Fig. 1. 3 Molecular structure of l-phenylalanine.....	7
Fig. 3. 1 FT-IR spectra of (a) free L-cysteine, (b) L-cysteine-capped CdSe, (c) L-cysteine-capped Cu _x Se and (d) L-cysteine-capped Fe _x Se _y	29
Fig. 3. 2 Absorption spectra (i) and Tauc's plot (ii) of L-cysteine-capped CdSe nanoparticles prepared at (a) 55° C, (b) 75° C and (c) 95° C.....	31
Fig. 3. 3 Emission spectra of L-cysteine-capped CdSe nanoparticles prepared at (a) 55° C, (b) 75° C and (c) 95° C	31
Fig. 3. 4 XRD patterns of L-cysteine-capped CdSe nanoparticles prepared at (a) 55° C, (b) 75° C and (c) 95° C.....	33
Fig. 3. 5 TEM images and size distribution curve of L-cysteine-capped CdSe nanoparticles prepared at (a and b) 55° C, (c and d) 75° C and (e and f) 95° C	34
Fig. 3. 6 Absorption spectra (i) and Tauc's plot (ii) of L-cysteine-capped Cu _x Se nanoparticles prepared at (a) 55° C, (b) 75° C and (c) 95° C.....	36
Fig. 3. 7 Emission spectra of L-cysteine-capped Cu _x Se nanoparticles prepared at (a) 55° C, (b) 75° C and (c) 95° C	36
Fig. 3. 8 XRD patterns of L-cysteine-capped Cu _x Se nanoparticles prepared at (a) 55° C, (b) 75° C and (c) 95° C.....	37
Fig. 3. 9 TEM images and size distribution curve of L-cysteine-capped Cu _x Se nanoparticles prepared at (a and b) 55° C, (c and d) 75° C and (e and f) 95° C	38
Fig. 3. 10 VSM spectra of L-cysteine-capped Cu _x Se nanoparticles prepared at 75° C	39
Fig. 3. 11 Absorption spectra of L-cysteine-capped Fe _x Se _y nanoparticles (a) 55° C, (b) 75° C and (c) 95° C	40
Fig. 3. 12 Emission spectra of L-cysteine-capped Fe _x Se _y nanoparticles (a) 55° C, (b) 75° C and (c) 95° C	41
Fig. 3. 13 XRD patterns of L-cysteine-capped Fe _x Se _y nanoparticles (a) 55° C, (b) 75° C and (c) 95° C....	42
Fig. 3. 14 TEM images and size distribution curve of L-cysteine-capped Fe _x Se _y nanoparticles (a and b) 55° C, (c and d) 75° C and (e and f) 95° C	43
Fig. 3. 15 VSM spectra of L-cysteine-capped Fe _x Se _y nanoparticles at 75° C.....	44

Fig. 3. 16 FT-IR spectra of (a) free L-glutamic acid, (b) L-glutamic acid-capped CdSe, (c) L-glutamic acid-capped Cu _x Se and (d) L-glutamic acid-capped Fe _x Se _y	45
Fig. 3. 17 Absorption spectra of L-glutamic acid-capped CdSe nanoparticles prepared at (a) 55 °C, (b) 75 °C and (c) 95 °C	46
Fig. 3. 18 Emission spectra of L-glutamic acid-capped CdSe nanoparticles prepared at (a) 55 °C, (b) 75 °C and (c) 95 °C	47
Fig. 3. 19 XRD patterns of (cubic) and (* impurities) phase of L-glutamic acid-capped CdSe nanoparticles prepared at (a) 55 °C, (b) 75 °C and (c) 95 °C.....	48
Fig. 3. 20 TEM images and size distribution curve of L-glutamic acid-capped CdSe nanoparticles prepared at (a and b) 55 °C, (c and d) 75 °C and (e and f) 95 °C	49
Fig. 3. 21 Absorption spectra (i) and Tauc's plot (ii) of L-glutamic acid-capped Cu _x Se nanoparticles prepared at (a) 55 °C, (b) 75 °C and (c) 95 °C.....	50
Fig. 3. 22 Emission spectra of L-glutamic acid-capped Cu _x Se nanoparticles prepared at (a) 55 °C, (b) 75 °C and (c) 95 °C	51
Fig. 3. 23 XRD patterns of L-glutamic acid-capped Cu _x Se nanoparticles prepared at (a) 55 °C, (b) 75 °C and (c) 95 °C	52
Fig. 3. 24 TEM images and size distribution curve of L-glutamic acid-capped Cu _x Se nanoparticles prepared at (a and b) 55 °C, (c and d) 75 °C and (e and f) 95 °C	53
Fig. 3. 25 VSM spectra of L-glutamic acid-capped Cu _x Se nanoparticles prepared at 75 °C.....	54
Fig. 3. 26 Absorption spectra of L-glutamic acid-capped Fe _x Se _y nanoparticles prepared at (a) 55 °C, (b) 75 °C and (c) 95 °C.....	56
Fig. 3. 27 Emission spectra of L-glutamic acid-capped Fe _x Se _y nanoparticles prepared at (a) 55 °C, (b) 75 °C and (c) 95 °C	56
Fig. 3. 28 XRD patterns of L-glutamic acid-capped Fe _x Se _y nanoparticles prepared at (a) 55 °C, (b) 75 °C and (c) 95 °C	57
Fig. 3. 29 TEM images and size distribution curve of L-glutamic acid-capped Fe _x Se _y nanoparticles prepared at (a and b) 55 °C, (c and d) 75 °C and (e and f) 95 °C	58
Fig. 3. 30 VSM spectra of L-glutamic acid-capped Fe _x Se _y nanoparticles at 75 °C	59
Fig. 3. 31 FT-IR spectra of (a) free L-phenylalanine, (b) L-phenylalanine-capped CdSe, (c) L-phenylalanine-capped Cu _x Se and (d) L-phenylalanine-capped Fe _x Se _y	60
Fig. 3. 32 Absorption spectra of L-phenylalanine-capped CdSe nanoparticles prepared at (a) 55 °C, (b) 75 °C and (c) 95 °C	62

Fig. 3. 33 Emission spectra of L-phenylalanine-capped CdSe nanoparticles prepared at (a) 55 °C, (b) 75 °C and (c) 95 °C	62
Fig. 3. 34 XRD patterns of L-phenylalanine-capped CdSe nanoparticles prepared at (a) 55 °C, (b) 75 °C and (c) 95 °C	64
Fig. 3. 35 TEM images and size distribution curve of L-phenylalanine-capped CdSe nanoparticles prepared at (a and b) 55 °C, (c and d) 75 °C and (e) 95 °C.....	65
Fig. 3. 36 Absorption spectra of L-phenylalanine-capped Cu _x Se nanoparticles prepared at (a) 55 °C, (b) 75 °C and (c) 95 °C.....	67
Fig. 3. 37 Emission spectra of L-phenylalanine-capped Cu _x Se nanoparticles prepared at (a) 55 °C, (b) 75 °C and (c) 95 °C	67
Fig. 3. 38 XRD patterns of L-phenylalanine-capped Cu _x Se nanoparticles prepared at (a) 55 °C, (b) 75 °C and (c) 95 °C	69
Fig. 3. 39 TEM images and size distribution curve of L-phenylalanine-capped Cu _x Se nanoparticles prepared at (a) 55 °C, (b) 75 °C and (c) 95 °C.....	70
Fig. 3. 40 VSM spectra of L-phenylalanine-capped Cu _x Se nanoparticles at 75 °C	71
Fig. 3. 41 Absorption spectra of L-phenylalanine-capped Fe _x Se _y nanoparticles prepared at (a) 55 °C, (b) 75 °C and (c) 95 °C.....	72
Fig. 3. 42 Emission spectra of L-phenylalanine-capped Fe _x Se _y nanoparticles prepared at (a) 55 °C, (b) 75 °C and (c) 95 °C	73
Fig. 3. 43 XRD patterns of L-phenylalanine-capped Fe _x Se _y nanoparticles prepared at (a) 55 °C, (b) 75 °C and (c) 95 °C	74
Fig. 3. 44 TEM images and size distribution curve of L-phenylalanine-capped Fe _x Se _y nanoparticles prepared at (a) 55 °C, (b) 75 °C and (c) 95 °C.....	75
Fig. 3. 45 VSM spectra of L-phenylalanine-capped Fe _x Se _y nanoparticles prepared at 75 °C.....	76

List of abbreviations

QDs	Quantum dots
NCs	Nanocrystals
1D	1 Dimensions
2D	2 Dimensions
<i>T</i>	Temperature
a. u	Arbitrary unit
E_g	Band gap
° C	Degrees Celsius
θ	Theta
eV	Electron Volt
g	Gram
FWHM	Full width at half maximum
nm	Nanometer (10^{-9})
<i>F</i>	Flux
<i>C</i>	Coverage
MPA	Mercaptopropionic
UV-Vis	UV-Visible
PL	Photoluminescence
XRD	X-ray Diffraction
TEM	Transmission electron microscopy
VSM	Vibrating sample magnetometer

CHAPTER 1

INTRODUCTION AND LITERATURE REVIEW

1.1 Semiconducting nanocrystals

Semiconducting nanostructures with reduced dimensionality have attracted considerable scientific interest due to their unique properties arising from the interplay between quantum confinement and surface related effects. However, the dimensions of these nanostructures is smaller than twice the Bohr radius of the exciton in the bulk material, quantum confinement occurs, causing a different electronic and optical behavior of the nanostructures compared to bulk materials (Seguini *et al.*, 2013). These objects, most often referred to as quantum dots or nanoparticles typically have dimensions in the range of 1-100 nm and are highly dispersed, that is, have a large ratio of surface atoms to those located in the crystal lattice. The particle size is also important in relation to the excitonic radius of the bulk material (Malik *et al.*, 2000). However, as the particle size is reduced, the ratio of the surface atoms in relation to those in the crystal lattice increases, thereby increasing the significance of the surface in determining the properties of the material. The increase in the band gap of the nanocrystalline material with the corresponding reduction of particle size is explained by the phenomenon described as the quantum size effect (O'Brien & Malik, 2005).

This effect is a consequence of the confinement of the charge carriers within the dimensions of the nanocrystals. Therefore, valence band and conduction band split giving rise to discrete energy levels rather than a continuous band of the bulk material. The close proximity of the electron-and-hole pair in nanosized semiconductors has made it impossible to ignore the Coulombic interaction between the electron and hole and they consequently assume a higher state of kinetic energy than the bulk material (O'Brien & Malik, 2005). These heterostructures consist of nanometer-scale islands of one type of semiconductor either embedded in a different semiconductor or free-standing on a suitable substrate. The materials are chosen such that electrons and holes are confined to the island, resulting in a discrete spectrum for the confined charges, however, quantum dots suffer from unavoidable variation in their size, and hence, their energy levels (Landin *et al.*, 1998). Quantum confinement of both the electron and the hole in all three dimensions leads to an increase

in the effective band gap of the material with decreasing crystallite size. Consequently, both the optical absorption and emission of quantum dots shift to higher energies as the size of the quantum dots decreases. Although nanocrystallites have not yet completed their evolution into bulk solids, structural studies indicate that they retain the bulk crystal structure and lattice parameter. Recent advances in the synthesis of highly monodisperse nanocrystallites have paved the way for numerous spectroscopic studies assigning the QD electronic states and mapping out their evolution as a function of size. The size and shape of semiconductor nanoparticles control their widely varying electrical and optical properties (Nirmal *et al.*, 1995; Alivisatos, 1996; Lieber, 1998). However, bare nanocrystals (NCs) have low emission intensity due to the non-radiative transition caused by the trap states and might be unstable in luminescence spectrum when exposed to air and light due to photo-oxidation at their surface. This has placed some limits on the use of the nanocrystals. To control the nanocrystals surface and increase the photochemical stability of II-VI nanocrystals, great efforts have been made; inorganic passivation has mostly used the method. By coating nanocrystal with a wider band gap material, the surface of core nanocrystal can be electronically passivated, which can boost the amount of luminescence and reduce photochemical degradation (Li *et al.*, 2009; Dabbousi *et al.*, 1997).

The research has also revealed that core-shell structures are more chemically or thermally stable than corresponding plain core structure (Y. Liu *et al.*, 2006). However, the epitaxial growth methods have drawbacks which produce nanoparticles that are attached to a substrate in a matrix, and therefore limits the range of their applications. A major breakthrough for the synthesis of high-quality cadmium chalcogenides nanocrystals using dimethyl cadmium ($\text{Cd}(\text{CH}_3)_2$) as the cadmium precursor, the synthesis of CdSe nanocrystals using this precursor has been well developed (Murray, Nirmal, *et al.*, 1993). The growth of compound semiconductor NCs, the requisite supersaturation and subsequent nucleation can be triggered by rapid injection of metal-organic precursors developed by (C. B. Murray *et al.*, 2000). The reaction was carried out in hazardous conditions with extreme temperatures. Trindade and O'Brien then developed the single-source precursor route where the molecular compounds, containing both elements of the semiconductor, to produce nanosized material is used. One obvious advantage in using the single-source approach is that hazardous and volatile compounds such as $(\text{CH}_3)_2\text{Cd}$ are not involved in the high-temperatures and method opens a way of obtaining a wide range of nanodispersed semiconductors

with specific properties by tailoring the precursor (Trindade & O'Brien, 1997). Different shaped CdSe nanocrystals have just been achieved by growth of the nanoparticles in a mixture of hexyl phosphonic acid and tri-octylphosphine oxide (Manna *et al.*, 2000; Peng *et al.*, 2000). Flat triangular CdS nanocrystals can be generated by using reverse micelles to induce the growth of the crystals (Pinna *et al.*, 2001). Recent advances show more possibilities for rational synthesis of 1D and 2D nanocrystals by either a mild solution process (Pacholski *et al.*, 2002) or even simple double jet crystallization at room temperature in aqueous solution (Yu *et al.*, 2002). Growth control is difficult to obtain, even if one restricts the set of relevant parameters to temperature T , flux F and coverage c , if the growth temperature is chosen too low, the deposited atoms will just stick to the surface without having enough thermal energy to diffuse. However, when the temperature is too high, interatomic bonds are too easily overcome and one observes an ensemble of monomers and small polymers of adatoms performing random walks on the surface. Another important factor to influence the growth result is the time between the end of deposition and the capping of the quantum dot layer with another material, the so-called growth interruption time. During this growth interruption, the adatoms can relax to energetically favorable positions and approach thermodynamic equilibrium. Since there is a striking difference between kinetically controlled growth and a thermodynamically dominated size distribution (Meixner *et al.*, 2002).

The effect of a growth interruption can be dramatic. Furthermore, the initial stages of growth of quantum dots are most important for ordering effects, since here the monolayer islands can respond more easily to energetic changes in their vicinity. The morphology and spatial arrangement of these ‘‘platelets’’ will then determine the arrangement of the fully grown dots (Kunkel *et al.*, 1990; Priester & Lannoo, 1995). Therefore, the growth interruption during the transition from two dimensional to three-dimensional growth can improve the quality of the quantum dot layer considerably. There is a critical need to investigate a direct aqueous synthesis route that is benign to the environment, simple, cost-effective and friendly to human health, which will produce highly luminescent water-soluble nanoparticles that are well dispersed and ready for bio-applications.

1.2 Surface chemistry

The quantum (QDs) synthesis can be tailored to specific requirements, with core-shell and coating characteristics all affecting photochemical properties. QDs may be manufactured with diameters from nanometers to micrometers and size distribution can be controlled using precise growth techniques involving high annealing temperatures (Santra *et al.*, 2001; Raab & Stephanopoulos, 2004). The choice of shell and coating are gaining importance, as the shell stabilizes the nanocrystal and to some extent alter the photophysical properties whilst the coating confers properties to the QDs which allow its incorporation into the desired application. Bare core nanocrystals have proven that crystalline structure of the nanoparticles lends itself to imperfections (Raab & Stephanopoulos, 2004), which results in emission irregularities, particularly blinking, in which single QDs switch between fluorescent and non-fluorescent states despite continuous illumination (Kuno, 2003). The cores are highly reactive due to their large surface area, volume ratio resulting in a very unstable structure which is particularly prone to photochemical degradation. Capping core nanocrystals with ZnS has been shown to increase stability and performance producing QDs with improved luminescence, higher photochemical stability and higher quantum yields at room temperature (Manna *et al.*, 2002; Hines & Guyot-Sionnest, 1996). However, ZnS capping alone is not sufficient to stabilize the core, particularly in biological solutions, but a serendipitous by-product of modification to render QDs biologically compatible.

Solubilization of QDs is essential for many biological applications but presents a significant challenge. Non-water soluble QDs can be grown easily in hydrophobic inorganic solvents, but solubilization requires sophisticated surface chemistry alteration. Methods to make nanocrystals to be biocompatible without affecting their key properties mostly based on exchange of the original hydrophobic surfactant layer with a hydrophilic one (Bruchez *et al.*, 1998; Gerion *et al.*, 2001; Kim & Bawendi, 2003), or the addition of a second layer such as the amphiphilic molecule which may also contain another functional group. A natural polymer with one amino group and two hydroxyl groups has been used for intracellular delivery of specific molecules (Alonso *et al.*, 1997), and can be attached to the QD surface. Other methods for increasing solubility include encapsulation in phospholipid micelles (Dubertret *et al.*, 2002), the addition of dithiothreitol (Pathak *et al.*, 2001), oligomeric ligands (Kim & Bawendi, 2003), and the addition of the second

layer of poly-(maleic anhydride alt-1-tetradecane) to the QD's surface. Silica and mercaptopropionic acid (MPA) are also commonly used (Gerion *et al.*, 2001; Bruchez *et al.*, 1998), and allow bioconjugation to ligands of interest. MPA achieves this through carboxyl groups on its surface. The colloidal properties of solubilized nanoparticles, including the charge and hydrodynamic status, will be altered depending on the method used, meaning that the solubilization strategy will need to be tailored according to the biological system being used (Luccardini *et al.*, 2006). The increase in diameter brought about by such modifications, and conjugation with biomolecules may make intracellular delivery more difficult and could increase toxicity (Weng & Ren, 2006). Another challenge is that there is no technique which consistently allows preparation of QDs with control over the ratio of biomolecules per QD and their orientation on the surface. A current strategy based on modifying COOH groups on the QD surface for covalent attachment of amine groups is limited by problems of reproducibility and aggregation (Mattoussi *et al.*, 2000).

1.3 Chemistry of selected amino acids as capping agents

Amino acids are a main group of biological materials that are necessary for bod activity (Karami & Sheikhshoaie, 2017). Amino acids can be derived in two important categories included essential and nonessential amino acids. Essential amino acid cannot make by the human body. Amino acids are organic compounds containing amine (-NH₂) and carboxyl (-COOH) functional groups, along with a side (R group) specific to each amino acid. They can be classified according to the core structure functional groups, polarity, pH level and side chain group. Early on the history of biochemical research it was realized that controlling the pH is of critical importance for the proper function of biological processes. These studies implied that basic sites are usually protonated and acidic sites usually deprotonated in solution, and hence molecules containing both basic and acidic functional group, like peptides and proteins, typically end up in a zwitterionic form (Wytenbach *et al.*, 2000). However, amino acids exist as zwitterions and are neutral electrically at around pH 7. Therefore, the intercalation of amino acids and protein are expected to be difficult. By using the co-precipitation method and reconstruction method, it is sometimes possible to intercalate neutral molecules, which could not be intercalated by ion-exchange method (Nakayama *et al.*, 2004). Zhang *et al* demonstrated one-dimensional plasmon coupling by self-assembly of gold

nanospheres into branched chain networks using 2-mercaptoethanol as a coupling agent (Zhang *et al.*, 2007). Selvakannan *et al* reported tryptophan lysine capped gold nanoparticles by spontaneous reduction of the H₂AuCl₄ solution by the amino acid at higher temperatures or reduction by NaBH₄ followed by capping the particles with the amino acid. They found that use of an amino acid can result in some degree of cross-linking of the gold nanoparticles during the reduction processes (Selvakannan *et al.*, 2004).

1.3.1 L-Cysteine

Cysteine is an amino acid with the chemical formula HO₂CCH-(NH₂)-CH₂SH. It is a low molecular weight metal-binding ligand. The molecular structure of cysteine is shown in Figure 1.1. This amino acid has three deprotonation sites, i.e., carboxylic acid, amine and thiol sites, which are potential metal ion binding sites. Cysteine is a water-soluble amino acid, it is also more stable and non-toxic compound that possesses a good stabilizing capability and prevents the aggregation of nanoparticles (Koneswaran & Narayanaswamy, 2009). It is a powerful antioxidant and detoxifier. Cysteine was selected for the possible additional benefit of containing double bonded oxygen (carboxylic group) and amine groups for further conjugation, while thiol group caps the nanoparticle.

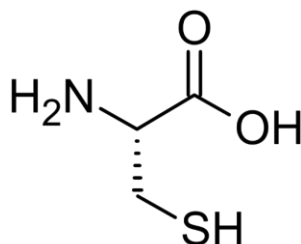


Fig. 1. 1 Molecular structure of l-cysteine

1.3.2 L-Glutamic acid

Glutamic acid is an α -amino acid with formula C₅H₉O₄N. Its molecular structure could be idealized as HOOC-CH(NH₂)-(CH₂)₂-COOH, with two carboxyl groups -COOH and one amino group -NH₂. In highly basic solution the doubly negative anion ⁻OOC-CH(NH₂)-(CH₂)₂-COO⁻. Its

biological properties such as non-toxicity, biocompatibility, and non-immunogenicity qualify it as an important biomaterial for applications in medicines (Shih, 2001).

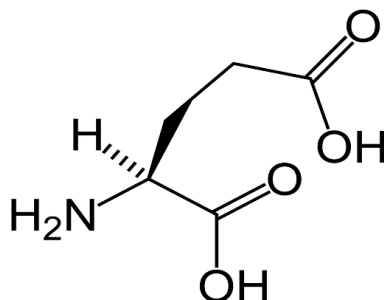


Fig. 1. 2 Molecular structure of l-glutamic acid

1.3.3 L-Phenylalanine

Phenylalanine is an α -amino acid with formula $C_9H_{11}NO_2$. It can be viewed as a benzyl group substituted with the methyl group of alanine, or a phenyl group in place of a terminal hydrogen of alanine. The essential amino acid is classified as neutral, and nonpolar because of the inert and hydrophobic nature of the benzyl side chain. It exhibits UV radiation absorption properties, can also reduce metal salts to form zero valent nanoparticles without adding any reducing agent (Nayak & Shin, 2006).

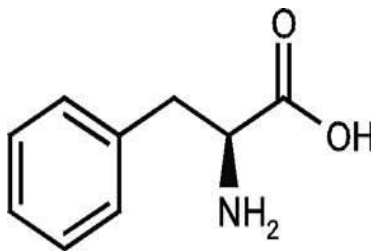


Fig. 1. 3 Molecular structure of l-phenylalanine

1.4 Metal selenide nanoparticles

1.4.1 CdSe nanoparticles

Synthetic reaction using high temperature solution from organometallic precursors to prepare high quality colloidal semiconductor nanocrystals (quantum dots, QDs), and the advances that followed to improve and understand their photoemission properties, there has been increasing interest in understanding their fundamental physical properties and developing applications that take advantage of some of the unique features of these materials (Clapp *et al.*, 2004). Recently, several methods have been developed to disperse QDs in aqueous solution for use in biological applications. Functionalization of the water-soluble QD surface allows the formation of QD bioconjugates that can bind specifically to target molecules and form stable conjugate complexes (Clapp *et al.*, 2004). The unique properties and utility of nanoparticles arise from a variety of attributes, including the similar size of nanoparticles and biomolecules such as proteins and polynucleic acids. Biomacromolecule surface recognition by nanoparticles as artificial receptors provides a potential tool for controlling cellular and extracellular processes for numerous biological applications such as transcription regulation, enzymatic inhibition, delivery and sensing (De *et al.*, 2008).

Numerous approaches such as homogeneous phase precipitation, reverse micelle, and organometallic approach and its variants have been applied to prepare CdSe and CdS nanocrystals. The highly luminescent semiconductor nanocrystals have also been prepared through organometallic approach. However, these reactions are carried out in the organic phase or aqueous phase, and both nucleation and growth of the nanocrystals only happened in a homogeneous system. It is very difficult for organic-phase approaches to synthesize oil-soluble nanocrystals by using various water-soluble precursors (De *et al.*, 2008). The composition, size, shape, and the surface of QD has been achieved in recent years by using chemical synthesis routes. Water-based synthesis of semiconductor nanocrystals with thiols as capping ligands has been developed as an alternative to original organometallic route, where reaction is carried out in airless conditions at relatively high temperatures in the presence of stabilizing agents such as trioctylphosphine (Pan *et al.*, 2007), trioctylphosphine oxide (Kim *et al.*, 2005), and hexadecylamine (Burgin *et al.*, 2008). However, the precursor used is highly toxic, explosive, and pyrophoric. Bifunctional molecules,

like organic molecules with both thiol and carboxylic acid, amine or alcohol functional groups have been widely adopted as capping molecules for CdSe and other II-VI group semiconductor nanoparticles (Deng *et al.*, 2006). Rogach *et al.*, in 1999 described the first aqueous preparation of CdSe QDs using different mercapto-alcohols and mercapto acids (R-SH) as stabilizers. Reaction was conducted at 100 °C with $\text{Cd}^{2+}:\text{Se}^{2-}:\text{R-SH}::2:1:4.8$ based on the conditions used earlier for the preparation of CdS and CdTe nanoclusters (Rogach *et al.*, 1999). The mercaptoacetic acid achieves this through the free carboxylic group (-COOH) and silica through the presence of thiol groups (-SH) on its surface.

It has been reported that the TOPO ligand on semiconductor nanoparticles surface may be replaced with heterobifunctional linker molecules, which provides both hydrophilic character and functional groups for further bioconjugation (Bruchez *et al.*, 1998). Gaponik *et al.*, 2002 synthesized nanocrystal after ligand exchange (Gaponik *et al.*, 2002). They showed that CdTe nanoparticles had better quantum yields with thioglycolic acid as capping agent than with 3-mercaptopropionic acid as the capping. Han *et al.*, 2006 reported the synthesis of small-sized CdSe QDs (1-3 nm) by reacting CdCl_2 and Na_2SeSO_3 solution with mercaptoacetic acid (MAA) as stabilizing agent under high-intensity ultrasonic irradiation (Han *et al.*, 2006). However, (Liu *et al.*, 2008) reported CdSe QDs with aromatic ligands: α -toluenethiol, thiophenol, and p-hydroxythiophenol to enhance the photoluminescence quenching and photoelectric properties of the QDs. Other thiol compounds such as L-cysteine (Wang *et al.*, 2011), thioacetamide (Williams *et al.*, 2007), glutathione (Cao *et al.*, 2009), 11-mercaptoundecanoic acid (Zhong *et al.*, 2006), have been widely studied for capping the CdSe QDs and promise many biological applications. MAA has been also employed in the hydrothermal synthesis of metal sulfide (CdS, CuS, ZnS etc) nanocrystals, where it acts both as sulfur source as well stability agent and makes an important role in the anisotropic growth of metal sulfide crystals to nanorods, nanowire and flower-like shapes. The effect of MAA concentration, on shapes and size of prepared nanoparticles have been investigated by various researchers (Salavati-Niasari *et al.*, 2010; Zhang *et al.*, 2003).

1.4.2 Cu_xSe_y nanoparticles

Nanostructured materials exhibiting size quantization effect are of enforced allegation owing to their peerless dimension-dependent properties and promising applications as building blocks in electronics, optoelectronics, and sensors in bio-imaging. Semiconductor quantum dots (QDs) one of the most important class of nanostructured materials are nanometer-size fragments of the corresponding bulk crystals with nearly equal size distribution and circular in shape with good luminescence properties, which have been active targets for chemist, material scientist, and nanotechnologist in recent years due to their size-dependent properties, flexible processing, and easier synthetic protocols. Chemically synthesized semiconductor nanostructures and their assembly with controlled size are of key importance in material chemistry, material science, and nanotechnology because of their importance in optoelectronics, photovoltaic devices, and solar cells due to their unique dimension-dependent and exceptional properties, which differ from those of their bulk counterpart. Recently wide ranges of techniques have been developed to synthesize metal chalcogenide with control of their microstructure and particle size. Copper chalcogenides have been studied to a lesser extent to its closest of kin chalcogenides nanoparticulate (especially CdS, CdSe, CdTe, ZnS, ZnSe, ZnTe, PbS, PbTe, and PbSe) (Wang *et al.*, 1999; Li *et al.*, 1999; Li *et al.*, 2001; Li *et al.*, 1998).

Copper chalcogenides have large number of applications in various devices such as in solar cells, superionic conductors, photodetectors, photothermal conversion, electroconductive electrodes, microwave shielding, coating, thermoelectric cooling, optical filter, and as an optical recording material (Bawendi *et al.*, 1992; Zhang *et al.*, 1997; Lakshmikumar & Rastogi, 1994; Kaito *et al.*, 1998). Many pioneering reports have described synthetic route for copper selenide nanostructures preparation, focusing on their structural characterization and their photoluminescence properties (Zhu *et al.*, 2000; Kemmler *et al.*, 2002; Xu *et al.*, 2002; Xie *et al.*, 2002). Copper selenide may be found in many phases and structural forms: different stoichiometries such as CuSe, Cu_2Se , Cu_2Se_x , CuSe_2 , $\alpha\text{-Cu}_2\text{Se}$, Cu_3Se_2 , Cu_5Se_4 , Cu_{7-x}Se , etc. as well with non-stoichiometric form such as Cu_{2-x}Se and can be constructed into several crystallographic forms (monoclinic, cubic, tetragonal, hexagonal, etc.) (Shafizade *et al.*, 1978). The properties of these compositions make copper selenide an ideal candidate for scientific research. Therefore, considerable progress on the

study of copper selenide has been made in recent years. It has been reported that thermal stability and band gaps of copper selenide vary depending on their stoichiometries (Haram & Santhanam, 1992; García *et al.*, 1999). The composition and the crystal structure of the final products are usually dependent on the preparation method (Gerber & Vining, 1976; Lakshmi *et al.*, 2001; Heyding, 1966; Lakshmi *et al.*, 2000). However, obtaining novel nanomaterials with controllable size or shape under mild conditions and with safe precursor at lower temperature with a relatively quicker process is an issue that has engaged many researchers. Copper selenide, is a p-type semiconductor having excellent electrical and optical properties, and is suitable for photovoltaic application. Recently, researchers developed a general aqueous solution phase strategy to grow nanostructured metal chalcogenides through electromagnetic stirring refluxing technique under mild conditions which is low cost and effective method (Kumar & Singh, 2009; Kumar *et al.*, 2010; Kumar & Singh, 2010; Kumar & Singh, 2010). In a synthesis of copper selenide QDs, copper chalcogenides have a variety of applications. Some reports have briefly stated the preparation of copper selenide nanostructures, which could mainly address the fluorescence and structural properties. Copper selenide may arise in different phases and structures in the previous reports. Preparation method plays a major role in obtaining the crystal structure and size. However, there is growing interest in using amine–chalcogen complexes as a better choice for preparing numerous QDs.

In general, metal halide and elemental chalcogens are not reactive enough to form II-VI QDs by a solvothermal route. However, by the incorporation of an amine into a reaction mixture, nanoparticles can be obtained easily at moderate temperatures (below 140 °C) as result of the high reactivity of the amine–chalcogen complex (Kaviyarasu *et al.*, 2016). The reaction conditions are always required to be conducted under an inert atmosphere, and it is still a problem how to obtain the requested phase of copper selenide through a facile and safe process. Although the size and shape of the semiconductor nanocrystals play an important role on their properties, the micromorphology of the copper selenide has not been well studied yet in the literature (Zhang *et al.*, 2010). The two phases of copper selenide, $\text{Cu}_2\text{-}\delta\text{Se}$ and CuSe were achieved via a green acetate-paraffin method, without the use of poisonous solvents such as trioctylphosphine (TOP) and tributylphosphine (TBP). The whole synthesis process was carried out open to air. The phase of the final products was controllable by adjusting the reaction parameters. The morphology results

were well presented, and CuSe nanoplates with good dispersivity in water were obtained (Zhang *et al.*, 2010). (Kumar & Singh, 2011) reported the simple aqueous solution method leaving behind contaminants. Surface energy and interparticle affinity for size-dependent diffusion have been shown elegantly leading to the evolution of copper selenide in the nanometer-size regime by inexpensive, straight forward, and element directed wet chemical method which is free from any capping agent, chelating agent, surfactant, or template. Liu *et al.* described phosphine-free routes, which have been implemented by directly dissolving Se powder or other Se precursors in high-boiling-point solvents such as octadecene, oleylamine (OLA), olive oil, and paraffin (Liu *et al.*, 2012). Kumar *et al.*, 2010 successfully obtained the different pure phases of copper selenides in ethylene glycol/hydrazine hydrate/water solutions via the solvothermal method under ambient conditions using copper chloride, copper sulphate, copper nitrate, copper acetate, elemental copper and elemental selenium powder as the raw materials (Kumar *et al.*, 2010). The diffusion of copper into selenium in dispersed phase using the solvothermal method leaving behind contaminants. Surface energy and interparticle affinity for size-dependent diffusion have been shown elegantly leading to the evolution of copper selenide hexagonal nanoplates (in different phases like CuSe, β -Cu₂Se, Cu₂Se and Cu_{2-x}Se,) in the nanometer size regime by an inexpensive, straightforward method that is free from any capping agent, chelating agent, surfactant.

1.4.3 Fe_xSe_y nanoparticles

Transitional metal chalcogenides are important class of binary inorganic materials which have been extensively investigated in the past decades for their photovoltaic (Mitzi *et al.*, 2008; Ennaoui *et al.*, 1993), thermoelectric (Poudel *et al.*, 2008), semiconducting (Jungwirth *et al.*, 2002), superconducting (Murray, Norris, *et al.*, 1993) , and nanosensing applications (Schcning & Kloock, 2007). Iron chalcogenides are particularly useful for their magnetic, semiconducting and spintronic applications (Takemura *et al.*, 1997). However maximum interest in iron chalcogenides originated after the unexpected discovery of superconductivity in PbO type tetragonal FeSe (Hsu *et al.*, 2008). The Fe–Se compounds, including FeSe, FeSe₂, Fe₃Se₄ Fe₇Se₈ etc, are important family members of Se-based materials. Recently more attention was given to iron selenide because of its unusual structure and electronic properties. Iron selenide system presents two homogeneous and stable phases, α -FeSe and FeSe₂ (Kim *et al.*, 1997; Campos *et al.*, 2004; Wu *et al.*, 2008), and

a variety of structures. The α -FeSe phase crystallizes in the tetragonal and in the hexagonal structure. The FeSe₂ crystallizes in the orthorhombic marcasite type and in the cubic structure. In case of iron chalcogenide compounds, much attention has been given to its potential as an absorber in solar cell (Arico *et al.*, 1991). Several methods have been employed in the preparation of iron selenide thin films such as molecular beam epitaxy (Takemura *et al.*, 1997), milling pure elemental powder of iron and selenium (Campos *et al.*, 2003) and selenization of amorphous iron oxide thin films prepared by spray pyrolysis (Ouertani *et al.*, 2005; Ouertani, Ouerfelli, Saadoun & Bessaï, 2005). Wu *et al.*, 2007 have successfully fabricated FeSe thin films by metal organic chemical vapor deposition on Si substrate with a large thermal mismatch. X-ray photoelectron spectroscopy and X-ray diffraction measurements indicate that the films show the single tetragonal phase of FeSe (Wu *et al.*, 2007). Pawar *et al.* have deposited iron selenide thin films onto stainless steel and fluorine-doped tin oxide (FTO) glass substrates by the electrodeposition process in a potentiostatic mode using ferric chloride and selenium dioxide salts (Pawar *et al.*, 2007). The deposition mechanism and growth of the films were investigated by cyclic voltammetry. (Thanikaikarasan *et al.*, 2009) have deposited FeSe thin films on indium-doped tin oxide coated conducting glass (ITO) substrates at various bath temperatures using an electrodeposition technique. (Ouertani *et al.*, 2005) developed a non-toxic technique to synthesize FeSe₂ thin films, which consists of the selenization of thin layers of amorphous iron oxide pre-deposited by spray pyrolysis. All these methods utilize enormous amount of energy for the material formation and moreover, they are time-consuming. In addition, when there is a large difference in the melting points of constituents [iron (1535 8C) and selenium (217 8C)], it becomes difficult to obtain FeSe compound with desired stoichiometry by electrodeposition techniques.

1.5 Parameters that influence size and shape of nanocrystals

One of the challenges in advanced materials is the control of the inorganic nanocrystal morphology. In fact, the shape of nanocrystals influences the physical properties. This is observed for metals, oxides, and semiconductors. Such changes in the physical properties produce a wide range of electrical, optical and magnetic properties and open a new domain of both fundamental and technological interest (Filankembo *et al.*, 2003). Crystallographic control over the nucleation and growth of nanoparticles has been most widely achieved using colloidal methods. In most cases,

a metal salt precursor is reduced in solution in the presence of stabilizing agents, which prevents aggregation or improves the chemical stability of the formed nanoparticles. The nucleation process is critical for obtaining shaped metal nanoparticles, the formation or addition of small seed particles that serve as nucleation sites for metal reduction can not only determine the crystallographic growth of the resulting nanoparticle but can also drastically change the kinetics of nanocrystal growth. Shape control of metal nanocrystals can be carried out via either homogeneous or heterogeneous nucleation (Tao *et al.*, 2008). The use of binary capping molecules such as trioctylphosphine oxide (TOPO) and hexyl phosphonic acid (HPA) is useful for its ability to generate shape anisotropy in CdSe, and also for its intrinsic hexagonal structure (Lee *et al.*, 2003). Iron nanorods formed by stabilizer-induced aggregation processes of iron nanospheres was reported by (Park *et al.*, 2000), and CdTe nanowires via crystal dipole-induced self-assembly of CdTe nanospheres was demonstrated by (Tang, 2002).

Talapin *et al.* reported on the synthesis of CdSe nanocrystals from cadmium oxide and trioctylphosphine selenide (TOP-Se) at a high temperature of 250–300 °C gives highly crystalline CdSe nanocrystals with tunable sizes, however introducing hexadecylamine (HDA) as a co-surfactant to the CdSe nanocrystals during their growth allows a considerable improvement of their PL properties (Talapin *et al.*, 2001). Yang *et al.* described the synthesis of CdSe semiconductor nanocrystals which particle size was varied from around 2 nm to 4.5 nm by rapid and exact temperature control in a micro-flow-reactor (Yang *et al.*, 2009). The CdSe QDs with three different sizes (~3 nm, ~4 nm and ~5 nm) were synthesized by the well-known hot injection technique, yielding narrow size and shape distribution of particles. The obtained hydrophobic CdSe QDs were further functionalized with L- and D-penicillamine molecules and the performed ligand exchange process additionally resulted in the transfer of the QDs to the aqueous phase was reported by (Tohgha *et al.*, 2013). Liu *et al.* synthesized Cu₂Se via the hydrothermal co-reduction method using CuSO₄·5H₂O, SeO₂, and hydrazine hydrate as the raw materials at temperatures of 150, 180 and 200 °C for 24h which yielded monodispersed particles with rectangular morphology (Liu *et al.*, 2009).

1.6 Methods for the preparation of semiconductor nanocrystals

There are numerous methods to produce nanomaterials with different structures. However, which are generally divided into two approaches commonly referred as ‘top-down’ and ‘bottom-up’ methods. Under controlled conditions, both approaches can be viewed as different forms of microstructures. The top-down approach involves the fabrication method that uses the simple removal or successive cutting of bulk material to reduce its size to nanoscale materials. This fabrication method uses techniques such as milling or attrition, laser ablation, inert-gas evaporation and vapor condensation. Bottom-up approaches it uses atoms, molecules, and nanoparticles which assemble themselves as the building blocks for the creation of nanostructures. They build up nanostructure materials from the bottom: atom by atom, molecule by molecule or cluster by cluster. The properties and functionalities of nanostructured materials produced maybe assisted by changing the size of building blocks, controlling their surface and assembly organization. Commonly used techniques are sol-gel methods, colloidal dispersion method, chemical vapor deposition and hydrothermal routes.

1.6.1 Colloidal routes

The colloidal route was the first reported method used to synthesize small particles and involves controlled precipitation reaction in a homogeneous solution. Colloidal semiconductor nanocrystals are synthesized from precursor compounds dissolved in solutions, much like the traditional chemical processes. The synthesis of colloidal semiconductor nanocrystals is based on a three-component system composed of the precursor, organic surfactants, and solvents. The synthesis of highly monodispersed colloidal was explained in the 1940’s by (La Mer & Dinegar, 1950; Johnson & La Mer, 1946), who suggested that if the seed (nuclei) could be made to grow in concert into larger particles, monodispersed sols could be formed. However, if nucleation and grow are properly controlled particles with a dimension of the order of nanometers can be reproducibly synthesized. The small crystals which are less stable, dissolve and then re-crystallize on larger more stable crystals, a process is known as Ostwald ripening. However, quantum dots have low solubility, which can be achieved by the correct choice of solvent, pH, temperature and a passivating agent. Highly monodispersed samples are obtained if the processes of nucleation and growth are distinctly separated, fast nucleation and slow growth. The colloidal stability of these

crystals has been improved by using solvents with low dielectric constants or stabilizers such as styrene/maleic acid copolymer (Henglein, 1984; Rossetti *et al.*, 1984; Rossetti *et al.*, 1985). Controlling of the size of nanocrystalline CdS was achieved by altering nucleation kinetics using pH (Rossetti *et al.*, 1984). Although these methods can be effective, some important semiconductors cannot easily be synthesized such as CdSe, GaAs, InP, and InAs. Annealing of amorphous colloidal particles is also a problem as these tend to be low-temperature processes producing poorly crystalline material. Such aqueously prepared nanoparticles are not sufficiently stable at higher temperatures for annealing without agglomeration. CdS and ZnS have also been produced from methanolic media without the use of an organic ligand for stabilization using the repulsion of the electrostatic double layer to prevent agglomeration (Rossetti *et al.*, 1985). Previous studies on organically capped nanocrystals have reported that the temperature may induce a phase transition in the capping organic layer, which may significantly affect the PL of QDs dispersed in organic solution (Wuister, Donega, *et al.*, 2004; Wuister, Houselt, *et al.*, 2004), but very few studies have addressed the temperature-dependence of the functionalized QDs properties in aqueous solution (Liu *et al.*, 2006).

The synthesis of colloidal quantum dots is often performed from toxic organometallic precursors through high-temperatures (Peng & Peng, 2002), which can be avoided by using different organic ligands (Murray *et al.*, 2000; Peng & Peng, 2001). The most widely used surface-capping materials possess hydroxyl (-COH), carboxyl (-COOH), thiol (-SH) or amine (-NH₂) functions which are ready to conjugate with a metal source without further modification. These ligands render QDs soluble in aqueous media, preventing aggregation while maintaining their small size and photoluminescence (PL) properties (Mohamed *et al.*, 2014). In the past two decades, great efforts have been made for synthesis of QDs with high photoluminescence quantum yield. Highly fluorescent QDs are readily synthesized through organometallic routes mostly capped with trioctylphosphine oxide (Qu & Peng, 2002). Nevertheless, to meet the requirement of bio-applications, such hydrophobic QDs need to be transferred from organic phase to aqueous solution which they lose both quantum yield and stability (Osaki *et al.*, 2004; Wuister *et al.*, 2003). An alternative approach is to directly synthesize QDs in water, which avoids phase transfer of QDs and the use of organic solvents. This method is regarded simple, cheaper and more environmentally friendly than the organometallic route (Gaponik *et al.*, 2002). Li *et al.* reported a

facile one-step route to synthesize CdS nanocrystals using 3-mercaptopropionic acid as the capping agent (Li *et al.*, 2007). Saunders et al. successfully fabricated CdS nanorods with tunable photoluminescence via surface treatments, such as ligand exchange, surface passivation, and defect formation (Saunders *et al.*, 2008).

1.6.2 Hot injection routes

The “hot injection method” relying on the rapid injection of precursors into the hot reaction medium, fulfills this requirement and is extensively used. It consists of mixing all components at low/room temperature and subsequent heating to reflux. The absence of the pyrolytic event, which characterizes hot-injection approaches, strongly improves the reproducibility and possibility of large-scale nanoparticle production. Nevertheless, similar synthetic procedures for semiconductor NCs are scarce and essentially restricted to cadmium chalcogenides (Li & Reiss, 2008). The synthesis begins with the rapid injection of organometallic reagents into a hot coordinating solvent to produce a temporally discrete homogeneous nucleation, slow growth, and annealing in the coordinating solvent results in uniform surface derivatization and regularity in core structure (Murray, Norris, *et al.*, 1993). The precursor solution consisted of CdMe₂ and Se in trioctylphosphine (TOP). The injection leads to the instantaneous formation of nuclei of CdSe, the formation of new nuclei is prevented due to a drop in temperature. The results are a suspension of reasonably monodisperse nuclei together with considerable amounts of Cd and Se precursors, increasing the temperature leads to the slow growth of the existing nuclei but not to new nucleation.

However, increasing growth temperature the size of the resulting CdSe nanocrystals increases and TOPO molecules slow down the growth considerably by coordinating the surface of Cd atoms, therefore forming a steric barrier for reactants. The slow growth at relatively high temperatures allows the nanocrystals to anneal to form nearly defect-free wurtzite lattices, which are identical to the bulk lattice (Mahajan *et al.*, 2013). Talapin and co-workers described highly monodispersed CdSe nanocrystals which were prepared in a three-component hexadecylamine-trioctylphosphine oxide-trioctylphosphine (HDA-TOPO-TOP) mixture. The modification of the conventional organometallic synthesis of CdSe nanocrystals in TOPO-TOP provides much better control over growth dynamics, resulting in the absence of defocusing of the particle size distribution during

growth (Talapin *et al.*, 2001). Reiss and co-workers synthesized high-quality CdSe/ZnSe core/shell nanocrystals without the use of any pyrophoric organometallic precursors, the effective surface passivation of monodisperse CdSe nanocrystals is achieved by overcoating them with a ZnSe shell. The resulting core/shell nanocrystals exhibit high room temperature photoluminescence efficiencies in both organic and water solvents after functionalization with mercaptoundecanoic acid (Reiss & Pron, 2002). The technique is environmentally friendly, inexpensive, involving the use of relatively non-toxic reagents and has a short reaction time.

1.6.3 Single-molecule precursors

Nanocrystallites have been prepared by a wide range of synthetic methods in which many approaches involve aqueous solutions and classical techniques of colloidal chemistry. However, for some technological important semiconductors metal chalcogenides, such synthetic methodologies have limitations including the use of noxious compounds, such as H₂Se or H₂S and a potential for the adventitious incorporation of oxide. The problem was overcome using molecular compounds, containing both elements of the semiconductor to produce the final nanodispersed materials (Trindade & O' Brien, 1996). In preliminary work, high-quality CdSe nanocrystallites were obtained by the thermolysis, in hot tri-n-octylphosphine oxide (TOPO) as dispersing medium of the single molecule precursor [CH₃CdSe₂CN(C₂H₅)₂]₂. This synthetic approach is an extension of TOPO method developed by (Murray, Norris, *et al.*, 1993). The advantage of using the single-source approach is that hazardous and volatile compounds such as (CH₃)₂Cd are not involved in the high-temperatures procedures used to produce the semiconductor materials. Furthermore, the method opens a way of obtaining a wide range of nanodispersed semiconductors with specific properties by tailoring the precursor (Matijevic, 1986; Trindade *et al.*, 1994). Much work has been done to evolve efficient routes for high-quality monodispersed quantum dots, produced a good quality CdSe nanoparticles passivated with tri-n-octylphosphine oxide (TOPO) using volatile metal alkyls and a chalcogen source (Murray, Norris, *et al.*, 1993).

Alivisatos and co-workers synthesized CdSe quantum dots by adapting Murray's method with the principle difference being the higher temperature (350 °C) of injection of the precursors. The formation of nanoparticles by both these methods was explained with an analogy to classical

colloidal chemistry. Instantaneous nucleation after the injection of the reactants into the coordinating solvent at elevated temperatures is followed by controlled growth and annealing, which is consistency with Ostwald ripening (Alivisatos, 1996). The use of single-source molecular precursors, as initially reported by Trindade and O'Brien, has proven to be an efficient route to high-quality crystalline monodispersed nanoparticles semiconducting materials (Trindade & O'Brien, 1996; Trindade & O'Brien, 1997). O'Brien and co-workers have demonstrated the use of pyrolyzable single-source molecular precursors based on metal dithio and diseleno carbamate complexes for the preparation of CdS, ZnS, ZnSe, and CdSe. The use of single-source precursors with preformed metal-chalcogenide bonds provides a convenient reactive intermediate for growth under lyothermal conditions, allowing for the preparation of large quantities of materials from relatively innocuous reagents (Trindade & O'Brien, 1996). Yin *et al.* have reported the morphology controlled synthesis of ZnS nanoparticles which enhance photocatalytic activity (Yin *et al.*, 2016). Tian *et al.* have carried out starch assisted synthesis of ZnS nanoparticles (Tian *et al.*, 2016). In generally the use of single-source precursors have distinct advantages over other methods, these include low toxicity, no or limited pre-reactions, choice of ligand which can influence volatility.

1.7 Application of nanotechnology

The benefits of this technology derived from the ability to tailor essential structures of materials at the nanoscale levels to achieve specific properties such as chemical, physical, electronic and mechanical which can be used for wide variety of applications. Some of the nanoparticles synthesized in this present study may find applications in light-emitting devices, biomarkers, and dual-modality probes.

1.7.1 Light-emitting devices

Light-emitting-diode (LED) technology was originally developed from the high-efficiency electroluminescence of semiconductor devices in early 1962 (Black *et al.*, 1963). The high brightness, high efficiency and long durability of LEDs render them ideal for displays and solid-state lighting (Craford, 1992). Among the basic colors, LEDs covering green to violet light are still under intensive development due to the low efficiency of the available devices. Weak blue LEDs

fabricated from semiconducting SiC have been produced, but they are orders of magnitude less efficient than their red and yellow counterparts (Suzuki *et al.*, 1977). In recent year, with the development of metal organic chemical vapor deposition (MOCVD), gallium nitride (GaN) has become the most important building block for LEDs operation in the green to ultraviolet light range (Zhong *et al.*, 2003; Kobayashi *et al.*, 2007; Naoi *et al.*, 2007). However, is difficult to grow to align nanowire arrays. Attempts have been made to find substitutes to replace GaN nanowires (Zhou *et al.*, 2007). To overcome the limited availability of GaN nanowires and take advantage of their ideal blue-light emission, development has begun of so-called hybrid p-n heterojunction LEDs, which are composed of heterojunctions between oxide-semiconductor nanowires and GaN p-type thin layers (Won *et al.*, 2004; Gao *et al.*, 2007; Chan *et al.*, 2007). The p-type organic heterostructure has also been studied (Ko *et al.*, 2005; Sun *et al.*, 2008). Among all of the known oxide semiconductors, ZnO nanowires are the top choice for blue emission not only due to their superior properties, with a wide band-gap and large exciton-binding energy, but also due to their easy growth via chemical and physical vapor-phase approaches (Xu *et al.*, 2008; Gan *et al.*, 2005). Hence, it is known that ZnO nanowires can be grown following a designed pattern into aligned arrays on almost any substrate in any shapes (Qin *et al.*, 2008). Sun *et al.* described a heterostructure lighting-emitting diode made of *N,N*-di(naphtha-2yl)-*N,N'*-diphenyl-benzidine and ZnO nanorods fabricated by aqueous thermal deposition. An excitonic ultraviolet emission at 342 nm was observed in the electroluminescence spectrum of the heterostructure light-emitting diode (Zhou *et al.*, 2007).

1.7.2 Biomarkers

To fully understand the basic biological functions in a living system one needs a sophisticated detection system. Luminescence technique has been widely used as a sensitive tool for many years in many areas of sciences and technologies. The organic dyes were widely used to detect biological components in the living systems. To a large extent, the use of these dye molecules has greatly helped the understanding of many biological problems. However, the photo bleaching of these dye molecules has some limitations which are sensitive detection and real-time monitoring of important biological processes it requires continuous exposure of an intense excitation source under which makes organic fluorophores unsuitable. Therefore, there are a demand to develop

nonisotopic, highly photostable and sensitive luminescent probes (Bruchez *et al.*, 1998; Chan *et al.*, 1998; Chumanov *et al.*, 1999; Elghanian *et al.*, 1997; Mucic *et al.*, 1998). Recently, the use of semiconductor quantum dots has shown great promises due to their unique properties such as size-tunable luminescent properties and functionalizability to couple biomolecules (Mitchell *et al.*, 1999; Chan *et al.*, 1998; Bruchez *et al.*, 1998). The development of new generation of biomarkers has been suggested to be better than organic dyes. Nonetheless, they have not been used extensively because of their poor solubility in water, agglutination, blinking properties and moderate quantum yields (Adler *et al.*, 1999; Harma *et al.*, 1999; Giunchedi *et al.*, 1999). Nie *et al.* functionalized gold nanorods with hydrophilic CTAB ligands grafted along the rod sides with hydrophobic polystyrene on the rods end which assembled into either discrete chains or spherical bundles depending on the water concentration in mixed DMF or THF solvent (Nie *et al.*, 2007).

Zhuang *et al.* achieved water dispersible disc-shaped CdS-CdSe nanorod assemblies in a two-stage process by further coordinating individual alkyl capped nanorods with a dual interaction ligands (dithiol-functionalized Tween-20, Tween-SH) followed by annealing in ethylene glycol at 80 °C (Zhuang *et al.*, 2009). Sanyal *et al.* demonstrated the formation of water dispersed nanorod assemblies by phase transfer of semiconductor (CdS, CdSe, CdTe) nanorods from the organic to aqueous using pluronic triblock copolymers, which resulted on randomly dispersed nanorods in the organic medium to form discs encapsulation hydrophobic core of water-dispersible micelles. The assemblies showed excellent cellular uptake exhibiting membrane and cell-specific fluorescence (Sanyal *et al.*, 2009).

1.7.3 Dual-modality probes

Optical imaging is highly sensitive, but its applications in vivo and in human are hindered by a limited penetration depth in tissue and the lack of anatomic resolution and spatial information. Although near-infrared wavelengths can be used to improve the penetration depth, and 3-D fluorescence tomography can be used to provide spatial information (Ntziachristos *et al.*, 2004; Ntziachristos *et al.*, 2003), other imaging modalities, such as magnetic resonance imaging (MRI), are much better for tomography and 3-D imaging. Thus, there has been considerable interest in developing dual-modality contrast agents for combined optical and MRI, which has exceptional

tissue contrast and spatial resolution and has been widely used in the clinical setting. This was achieved by reacting superparamagnetic iron oxide nanoparticles with the fluorescent dye (Kircher *et al.*, 2004). Schellenberger *et al.* have developed dual magneto-optical probes that are able to bind to apoptotic cells and are detectable by both fluorescence and MRI. Similarly, dual magnetic and optical imaging probes have been used to yield highly detailed anatomic and molecular information in living organisms (Schellenberger *et al.*, 2004). These probes are prepared by conjugation of peptides to cross-linked iron oxide amine (amino-CLIO), either by a disulfide linkage or a thioether linker, followed by the attachment of the dye Cy5 or Cy7. Fluorescence quenching of the attached fluorochrome occurs by interaction with the iron oxide core, and by electronic coupling among the dye chromophores (self-quenching). This class of dual-modality probes provides the basis for “smart” nanoparticles, capable of pinpointing their position through their magnetic properties while providing information on their environment by optical imaging. Therefore, research has shown that QDs can be linked with Fe_2O_3 and FePt to generate dual-function nanoparticles (Wang *et al.*, 2004; Gu *et al.*, 2004).

Zhang *et al.* synthesized GdS coated CdTe nanoparticles as an excellent agent for FL and T_1 -weighted MR dual-modality imaging by a facile aqueous route at room temperature. The prepared GdS coated CdTe NPs exhibit small particle size, high quantum yield, and outstanding longitudinal relaxation rate. The coating of GdS shell on the surface of CdTe core not only provide both prominent fluorescent and paramagnetic properties but also reduce toxicity and increase the biocompatibility of NPs (Zhang *et al.*, 2016). Zhao *et al.* have developed a folic acid-conjugated silica-coated gold nanorod quantum dots probe for dual-modality, fluorescence imaging and photothermal therapy (Yan *et al.*, 2014). The results have shown that the probe composed of QDs and AuNR exhibited great potential for target tumor imaging and therapy.

1.8 Problem Statement

Traditionally, colloidal synthetic methods for producing semiconductor nanoparticles have been based on the use of organic stabilizers to cap the surface of nanoparticles in order to control the growth process. These methods generally use surfactants such as trioctylphosphine oxide, long-chain amines or long-chain carboxylic acid as capping agents, which produce hydrophobic nanoparticles which are not bio-compatible with the biological environment. So, we propose the direct preparation of bio-compatible quantum (QDs) as an alternative route to surface modification of organically capped nanoparticles using the hydrophilic stabilizer.

1.9 Aims and Objectives

The aim of this research work was to synthesize water-soluble, amino acid-based semiconductor nanoparticles and study the influence of some parameters on the physical and chemical properties of such nanoparticles. To fulfill the above-mentioned aim, the following objectives were identified:

- To synthesize water-soluble (L-cysteine, L-glutamic, and L-phenylalanine) capped metal selenide (CdSe , Cu_xSe_y and Fe_xSe_y) nanoparticles.
- To characterize nanoparticles using UV Visible and PL spectroscopy, XRD and microscopic technique (TEM).
- To study the influence of reaction temperature (55, 75 and 95°C), pH 11 and capping agents on the morphology of the synthesized nanoparticles.
- To determine magnetic properties of Cu_xSe_y and Fe_xSe_y nanoparticle using vibration sample magnetometer (VSM).

CHAPTER 2

EXPERIMENTAL SECTION

2.1 Chemical reagents used

Chemical	Molecular Formula	Manufacturer
L-cysteine	C ₃ H ₇ NO ₂ S	Sigma-Aldrich (≥97.00 %)
L-glutamic acid	C ₅ H ₉ NO ₄	Sigma-Aldrich (≥99.00 %)
L-phenylalanine	C ₉ H ₁₁ NO ₂	Sigma-Aldrich (≥98.00 %)
Iron(II) chloride tetrahydrate	FeCl ₂ ·4H ₂ O	Sigma-Aldrich (≥99.00 %)
Copper(II) chloride	CuCl ₂	Sigma-Aldrich (97.00 %)
Cadmium(II) chloride	CdCl ₂ ·2.5H ₂ O	Sigma-Aldrich (81.00 %)
Sodium selenite	Na ₂ SeO ₃	Sigma-Aldrich (99 %)
Sodium borohydride	NaBH ₄	Riedel-de Haen (95%)
Sodium hydroxide	NaOH	Promark chemicals (99.86 %)

2.2 Materials and Apparatus

Centrifuge, magnetic hotplate stirrer, 250 mL 3-necked round bottom flask and 50 mL beakers, thermometer, magnetic stirrer bars, centrifuge tubes, spatula, micropipettes and sample bottles.

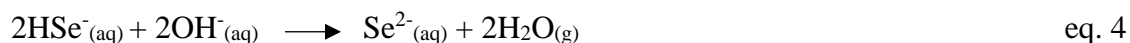
2.3 Synthesis

2.3.1 Preparation of Selenium Source

Selenium source was prepared by dissolving 0.05 M of Na₂SeO₃ (0.5g) with 2.0 M NaBH₄ (0.3783g) in 50 mL distilled water which is taken in 100 mL beaker. The solution was stirred for 20 minutes until the brown solution forms that indicates the reduction of selenium.

2.3.2 Preparation of L-cysteine-capped CdSe nanoparticles

Cysteine-capped CdSe nanoparticles were synthesized using one-pot synthetic approach directly in an aqueous medium. In a typical room temperature reaction, 20 mL of 0.1 M solution of CdCl₂·2.5H₂O in distilled water (0.5g) was made. Added slowly by continuous stirring 30 ml of 0.2 M solution of L-Cysteine into the CdCl₂·2.5H₂O solution. The solution became turbid white. Adjusted the pH of the solution to 11 by adding freshly prepared 1 M NaOH solution, which turned the solution transparent again. Added the desired quantity of the prepared Se source (here Cd²⁺: Se²⁻ is maintained 1:1) into it dropwise. The solution has been refluxed for 1 h at different temperatures (i.e. 55, 75 and 95 °C) yellow to orange coloured solution indicated the formation of CdSe nanoparticles. The particles can be separated from the unreacted chemicals and bi-products by adding acetone and filtering out the material, after several washing it can be again dissolved in water. The reaction equations (Eq. 1 – 5) are shown below:



2.3.3 Preparation of L-cysteine-capped Cu_xSe_y nanoparticles

Following the same procedure described above, 20 mL of 0.2 M solution of CuCl_2 in distilled water (0.5g) was made. Added slowly by continuous stirring 30 ml of 0.2 M solution of L-Cysteine into the CuCl_2 solution. The solution became turbid white. Adjusted the pH of the solution to 11 by adding freshly prepared 1 M NaOH solution, which turned the solution transparent again. Added the desired quantity of the prepared Se source (here Cu^{2+} : Se^{2-} is maintained 1:1) into it dropwise. The solution has been refluxed for 1 h at different temperatures (55, 75 and 95 °C). Blue to black coloured solution indicated the formation of Cu_xSe_y nanoparticles. The particles can be separated from the unreacted chemicals and bi-products by adding acetone and filtering out the material, after several washing it can be again dissolved in water.

2.3.4 Preparation of L-cysteine-capped Fe_xSe_y nanoparticles

The reactions were carried out following the procedure described above, 20 mL of 0.1 M solution of $\text{FeCl}_2 \cdot 4\text{H}_2\text{O}$ in distilled water (0.5g) was made. Added slowly by continuous stirring 30 ml of 0.2 M solution of L-Cysteine into the $\text{FeCl}_2 \cdot 4\text{H}_2\text{O}$ solution. The solution became turbid white. Adjusted the pH of the solution to 11 by adding freshly prepared 1 M NaOH solution, which turned the solution transparent again. Added the desired quantity of the prepared Se source (here Fe^{2+} : Se^{2-} is maintained 1:1) into it dropwise. The solution has been refluxed for 1 h at different temperatures (55, 75 and 95 °C). Brown to black coloured solution indicated the formation of Fe_xSe_y nanoparticles. The particles can be separated from the unreacted chemicals and bi-products by adding acetone and filtering out the material, after several washing it can be again dissolved in water.

2.3.5 Preparation of nanoparticles capped with L-glutamic acid and L-phenylalanine

The reactions were carried out following the procedure described in section 2.3.2, 2.3.3 and 2.3.4 for the synthesis of metal selenide nanoparticles using different amino acid as capping agents.

2.4 Characterization techniques

2.3.2 Infrared spectrometer

Infrared spectra of the nanoparticles were recorded on PerkinElmer spectrum 400 FT-IR spectrometer ranging from 500 to 4000 cm^{-1} . The samples were placed onto the universal ATR sample holder and pressed on top by gauge force arm.

2.3.3 Optical characterization

The optical properties of the materials were determined by placing the water dispersion of the nanoparticles into quartz cuvettes (1 cm path length) PG Instruments Ltd T80+ UV-Vis spectrometer were used to carry out the optical measurements. Emission spectra of the particles were recorded on a JASCO spectrofluorometer FP-8600 spectrometer with a xenon lamp at room temperature. The samples were placed in glass cuvettes (1 cm) with distilled water as a solvent.

2.3.4 X-ray diffraction analysis

X-ray diffraction (XRD) patterns of powdered samples were carried out on Bruker D8 advance using a Co (1.78898 nm) radiation source operating at 40 kV, for 2θ values over $20^\circ - 60^\circ$ with a scan speed of $0.01^\circ 2\theta \cdot \text{s}^{-1}$.

2.3.5 Electron microscopy

The morphology of nanoparticles was determined by Technai G² TEM spirit operated at 200 kV. Transmission electron microscopy (TEM) samples were prepared by drop-casting the nanocrystal dispersion in distilled water onto the carbon-coated copper grids and allowed to dry at room temperature.

CHAPTER 3

RESULTS AND DISCUSSION

SYNTHESIS, CHARACTERIZATION OF L-CYSTEINE, L-GLUTAMIC ACID AND L-PHENYLANILINE CAPPED METAL SELENIDE NANOPARTICLES

The colloidal method is employed in this work to synthesize metal selenide nanoparticles with the selected amino acids, L-cysteine, L-glutamic acid and L-phenylalanine. In the preparation of the selenide ion source, a dark brown colour solution appeared which confirmed the reduction of the selenium source to Se^{2-} after mixing all the solutions. The reducing solution contained sodium borohydride, NaBH_4 . It is a strong soluble hydride reducing agent and is capable of reducing the Na_2SeO_3 source to Se^{2-} . The reducing agent was added to the solution under stirring condition was about 15 minutes. The solution also contained the surfactant molecules, hydrophilic amino acids, acting as the stabilizer for the synthesis of nanoparticles. During the reaction, the mixture was stirred vigorously by using hot-plate to ensure a completed reaction and to stabilize the reaction system. With stirring, the stability can be achieved, and agglomeration of particles can be prevented. The surfactants L-cysteine, L-glutamic acid and L-phenylalanine contains the hydrophilic carboxylate groups faced outwards, making nanocrystals water-soluble and stable due to the negative charge on the surface. The presence of surfactants affected the growth and particles characteristics significantly. It is very important in the particle formation due to its ability for compartmentalization. In this research, the metals of choice are cadmium, copper and iron as they have significant chemical properties that can be useful to understand the behavior of nanoparticles in an amino acid surfactant environment. The samples of metal selenide nanoparticles are synthesized at different temperatures were characterized by using Fourier transform infrared spectroscopy (FT-IR), Ultraviolet visible spectrophotometer (UV-Vis), Photoluminescence spectrophotometer (PL), X-ray powder diffraction (XRD), Transmission electron microscopy (TEM) and Vibrating sample magnetometer (VSM). This characterization was carried out under room temperature condition.

3.1 L-Cysteine-capped metal selenide nanoparticles

3.1.1 FTIR spectral analysis of metal selenide nanoparticles capped with L-cysteine

The surface modification of the metal selenide nanoparticles with cysteine was confirmed by FT-IR spectra as shown in Fig 3.1. Shows the FT-IR spectra of (a) free L-cysteine and (b-d) L-cysteine-capped metal selenide nanoparticles. The IR absorption band around 1550-1600 cm^{-1} (sv COO^- , 1400 cm^{-1} (mv COO^- , 3500-3000 cm^{-1} (mv OH, COOH), indicate the $-\text{COO}^-$ group. The peak at 2900-3420 cm^{-1} (mv N-H) indicates $-\text{NH}_2$ group, while the peak at 2550-2750 cm^{-1} (mv S-H) represents $-\text{S-H}$ group. There are coexisting IR absorption bands of $-\text{COO}^-$, $-\text{NH}_2$ observed on both L-cysteine and L-cysteine-capped metal selenide QDs. Therefore, carboxylic acid and the amino group are present on the surface of the metal selenide QDs, while the S-H group vibration (2550-2670 cm^{-1} wv S-H) is absent on the surface of the L-cysteine-capped metal selenide QDs. The reason for the disappearance of S-H group vibration on the surface of metal selenide nanoparticles is due to the formation of covalent bonds between thiols and the surface of metal selenide.

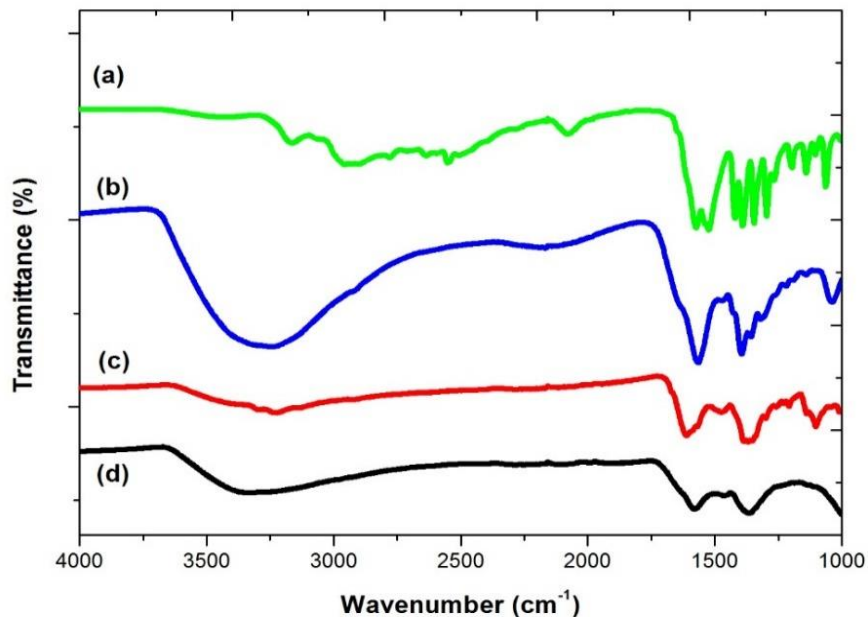


Fig. 3. 1 FT-IR spectra of (a) free L-cysteine, (b) L-cysteine-capped CdSe, (c) L-cysteine-capped Cu_xSe and (d) L-cysteine-capped Fe_xSe_y

3.1.2 Cadmium selenide nanoparticles capped with L-cysteine

(a) Optical properties

Absorption spectroscopy can be used to characterize the size and distribution of semiconductor nanocrystals. Semiconductor nanocrystals are known to have an absorption edge, which is shifted with respect to the bulk material towards shorter wavelengths. This blue-shift is thus taken as an indication of the presence of such nanocrystals and can be used to evaluate the crystallite size (Sheng *et al.*, 2006). The absorption spectra of synthesized cadmium selenide nanoparticles are shown in Fig. 3.2(i). A large blue-shift absorption from their bulk materials was observed for synthesized cadmium selenide nanoparticles. This was also confirmed by the band gap estimation from the energy curves shown in Fig. 3.2(ii). This is an indication of a decrease in particle size resulting in quantum confinement effect. The absorption spectra revealed that the band edges are located at approximately 596 nm, 626 nm and 633 nm for the temperatures of 55° C, 75° C, and 95° C respectively. The band-edges suggest that the particle size increases with an increase in reaction temperature. It was suggested that at a higher temperature, the smaller particles diminished while the larger ones grew due to the Oswald ripening (Lubyshev *et al.*, 1996). The emission spectra of synthesized CdSe nanoparticles are shown in Fig.3.3. The emission maxima were found to be at 562 nm, 576 nm and 593 nm for the temperatures of 55° C, 75° C, and 95° C respectively. All the samples show a well-defined emission band with monodispersed particle distributions. However, as the reaction temperature has increased a red-shift observed in the PL emission peak. This red-shift indicated growth of the nanoparticles as the temperature increases.

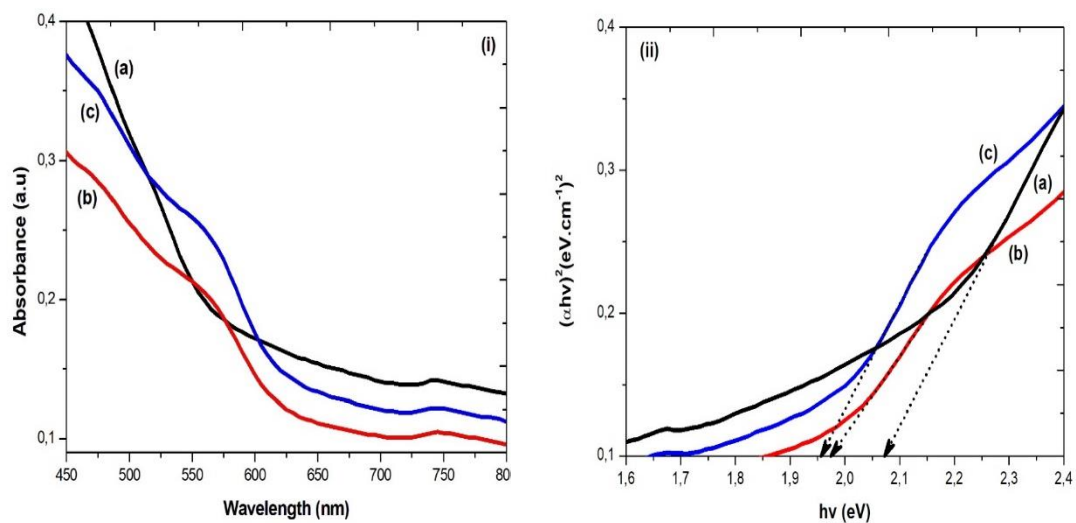


Fig. 3. 2 Absorption spectra (i) and Tauc's plot (ii) of L-cysteine-capped CdSe nanoparticles prepared at (a) 55° C, (b) 75° C and (c) 95° C

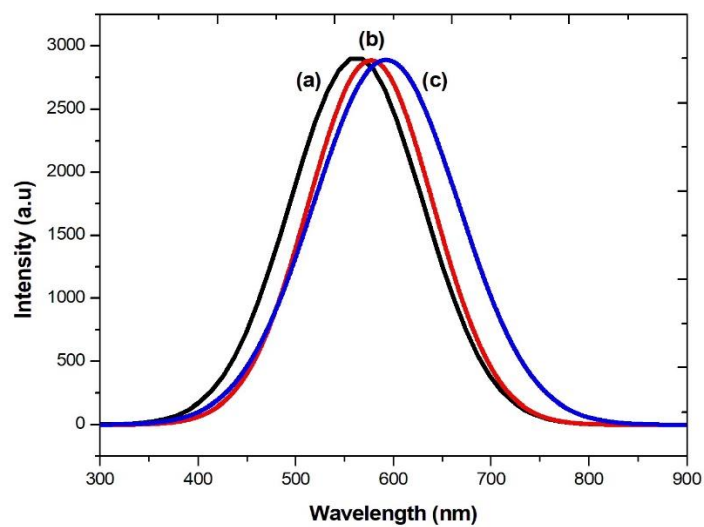


Fig. 3. 3 Emission spectra of L-cysteine-capped CdSe nanoparticles prepared at (a) 55° C, (b) 75° C and (c) 95° C

(b) Structural characterization

XRD patterns and TEM images were undertaken to determine the structural properties of synthesized cadmium selenide nanoparticles. The XRD patterns of synthesized CdSe nanoparticles are shown in Fig. 3.4. The diffraction peaks indicate the nanocrystalline nature. These peaks at angles (2θ) of 29° , 49° , and 58° correspond to the reflection from (111), (220) and (311) crystal planes respectively. The XRD pattern is identical to the cubic phase of CdSe (JCPDS No.: 03-065-3415). However, it was compared with the standard diffraction pattern, and no peaks of impurities were detected, indicating the high purity of the products. In these samples (111) plane is very clear and abundant which indicated preferential growth of crystallites in this particular direction which implies that the growth of the CdSe particles can be controlled by the temperature (Mahmoud *et al.*, 2012). There is generally an increase in crystallinity in the nanoparticles as the temperature is increased as evident from more pronounced peaks at higher temperature compared to amorphous peaks appearing at 55°C . The TEM images of cadmium selenide nanoparticles Fig. 3.5, generally revealed that the particles were spherical in shape. The average particle diameter was 4.12 ± 0.321 nm, 5.02 ± 0.234 nm and 5.53 nm for the temperature of 55°C , 75°C , and 95°C respectively. The synthesized nanoparticles confirming the optical properties yield from UV-Vis absorption and PL emission spectra as well the XRD data are in an agreement with the TEM analysis. Furthermore, the size distribution was homogeneous of the synthesized nanoparticles as proved by the emission spectra, one can note that the increase in temperature results in an increase in the average particle size of cadmium selenide quantum dots. This confirms that the temperature controls the size and distribution of cadmium selenide nanoparticles.

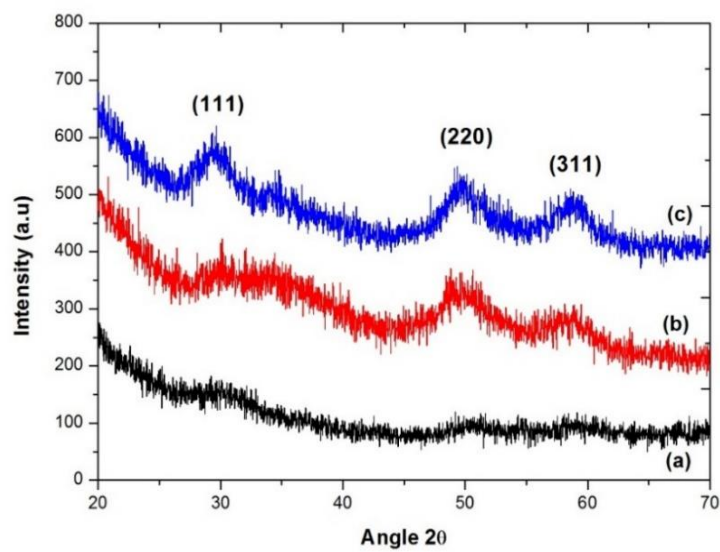


Fig. 3. 4 XRD patterns of *L*-cysteine-capped CdSe nanoparticles prepared at (a) 55° C, (b) 75° C and (c) 95° C

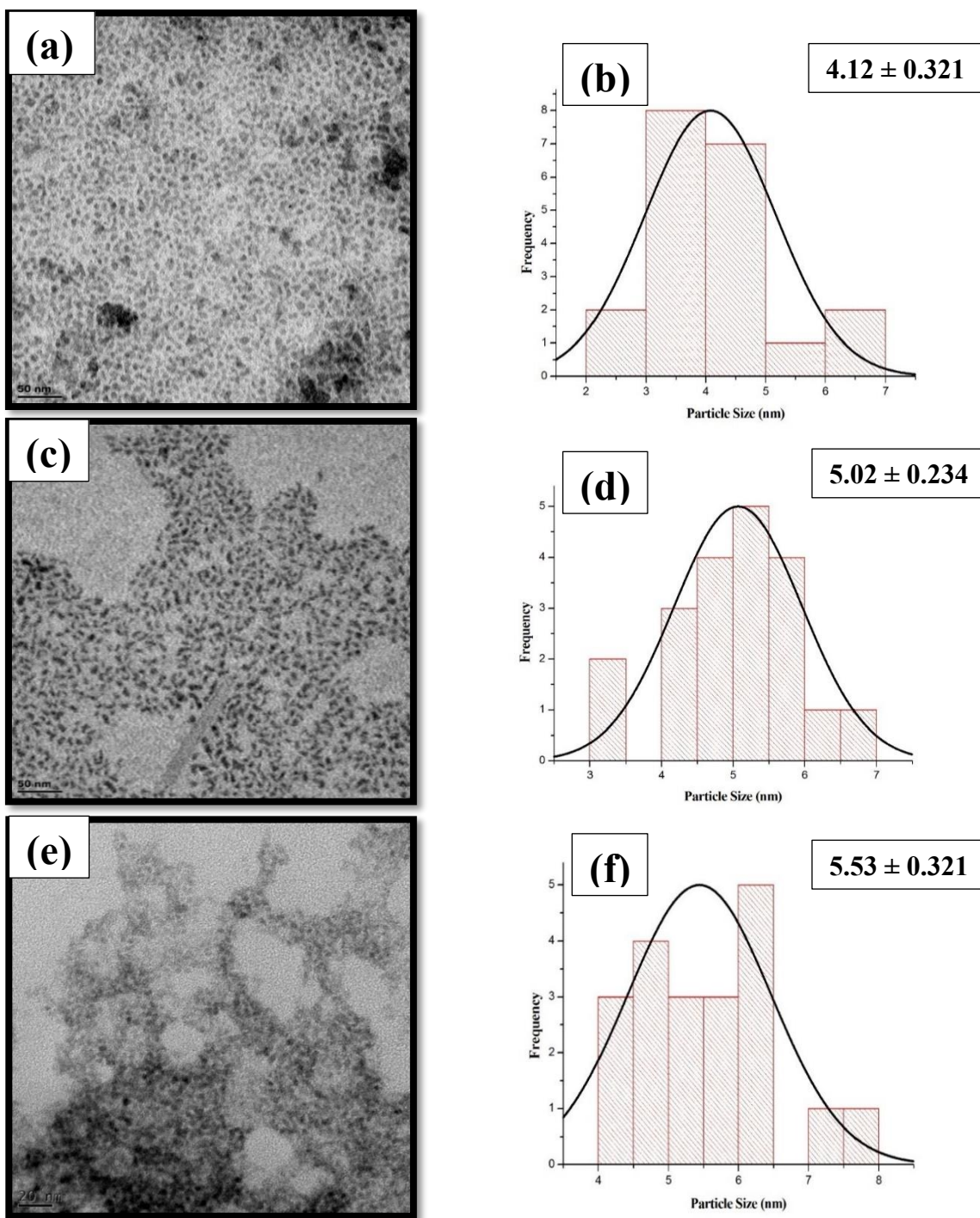


Fig. 3. 5 TEM images and size distribution curves of L-cysteine-capped CdSe nanoparticles prepared at (a and b) 55° C, (c and d) 75° C and (e and f) 95° C.

3.1.3 Copper selenide nanoparticles capped with L-cysteine

(a) Optical properties

The UV-Vis absorption spectra of synthesized copper selenide nanoparticles are shown in Fig. 3.6(i). The absorption band edges were blue-shifted from the bulk absorption band edge of 1180 nm (Kamar *et al.*, 2011). However, the band edge seemed to be less dependent upon the reaction temperature of the synthesis. The band edges were estimated using Tauc's relation shown in Fig. 3.6(ii). The absorption spectra revealed the band edges are located at approximately 571 nm, 620 nm and 577 nm for the temperature of 55° C, 75° C, and 95° C respectively. The absorption band edges of nanocrystals obtained at 55° C and 75° C are dependent on the reaction temperature. However, the one obtained at 95° C revealed a different trend which could be attributed to a change in morphology or polydispersed particles. The broad peaks observed on PL spectra at 55° C and 75° C suggest the sample are monodispersed. However, the sample synthesized at 95° C shows that the particles obtained approach polydispersity which means they consist of different morphology. This observation agrees with the UV-Vis absorption spectra as observed at 55° C and 75° C which could be composed of similar properties, while sample synthesized at 95° C poses different features. The emission maximum for samples Fig. 3.7(a and b) was located at about 435 nm, this maximum is allocated at the same position which suggesting similarities of the properties. However, sample Fig. 3.7(c) shows the maximum at 421 nm and full width at half maximum (FWHM) is reduced which could be attributed to the polydispersed distribution.

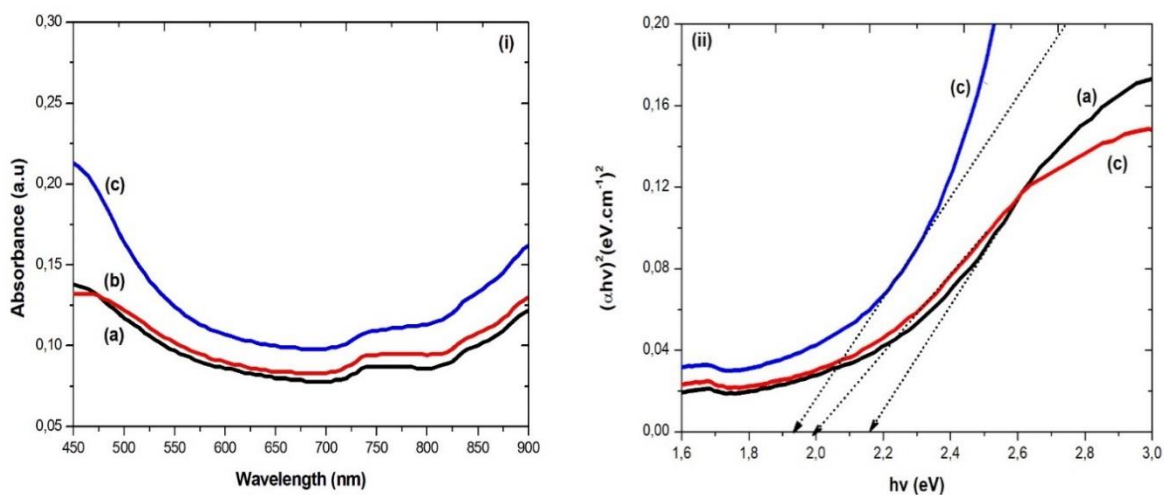


Fig. 3. 6 Absorption spectra (i) and Tauc's plot (ii) of L-cysteine-capped Cu_xSe nanoparticles prepared at (a) 55° C, (b) 75° C and (c) 95° C

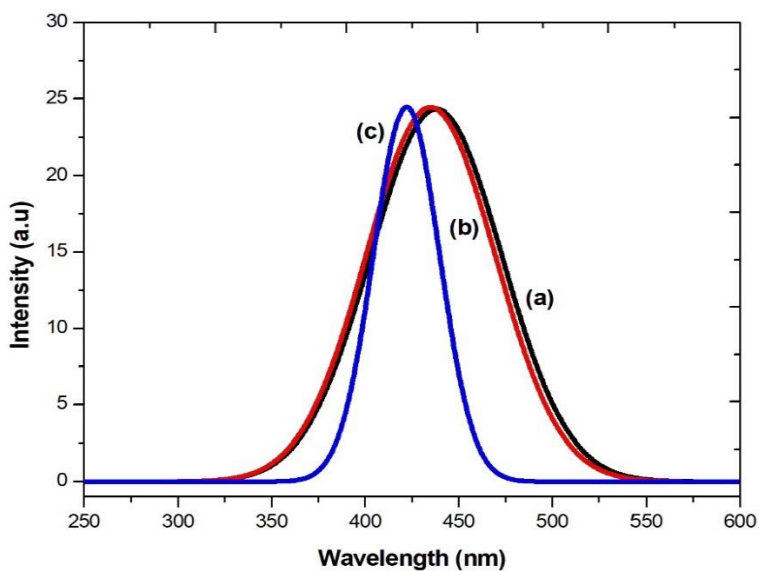


Fig. 3. 7 Emission spectra of L-cysteine-capped Cu_xSe nanoparticles prepared at (a) 55° C, (b) 75° C and (c) 95° C

(b) Structural characterization

The XRD patterns of synthesized materials from different reaction temperatures are shown in Fig. 3.8. The XRD patterns showed that the particles yielded were indeed copper selenide with mainly a cubic Cu_2Se phase (JCPDS No.: 01-088-2045). The sharpness of the peaks observed in Fig. 3.8(b and c) suggests that the particles synthesized gave more crystalline nanoparticles compare to the one at Fig. 3.8(a) and the position of the peaks matched perfectly with the Cu_2Se with no detection of impurities. The TEM images of all synthesized copper selenide nanoparticles and the corresponding size distributions are shown in Fig. 3.9. The nanoparticles were in various shapes dominated by rods phase. The diameters of 1.33 ± 0.367 nm, 4.79 ± 0.78 nm and 4.95 ± 0.718 nm for the temperatures of 55°C , 75°C , and 95°C respectively. The particles synthesized at 55°C Fig. 3.9(a) were smaller with a better Gaussian curve and narrower size distribution (standard deviation of 0.367) than those synthesized at higher temperatures. It was observed that when the temperature was increased the morphology changes from spherical nanorods. This confirms that the temperature had an influence on the morphology. The XRD patterns also generally crystalline nanoparticles as compared to L-cysteine capped cadmium selenide, indicating that influence of the amino acid to different metals.

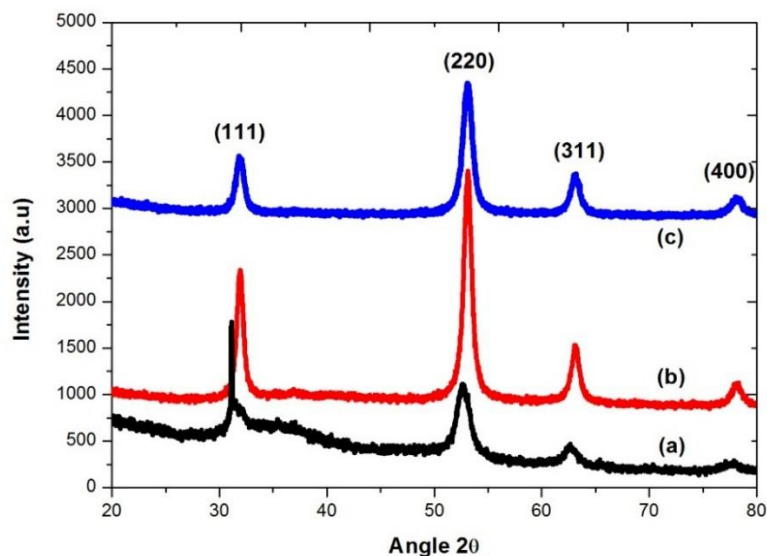


Fig. 3. 8 XRD patterns of L-cysteine-capped Cu_xSe nanoparticles prepared at (a) 55°C , (b) 75°C and (c) 95°C

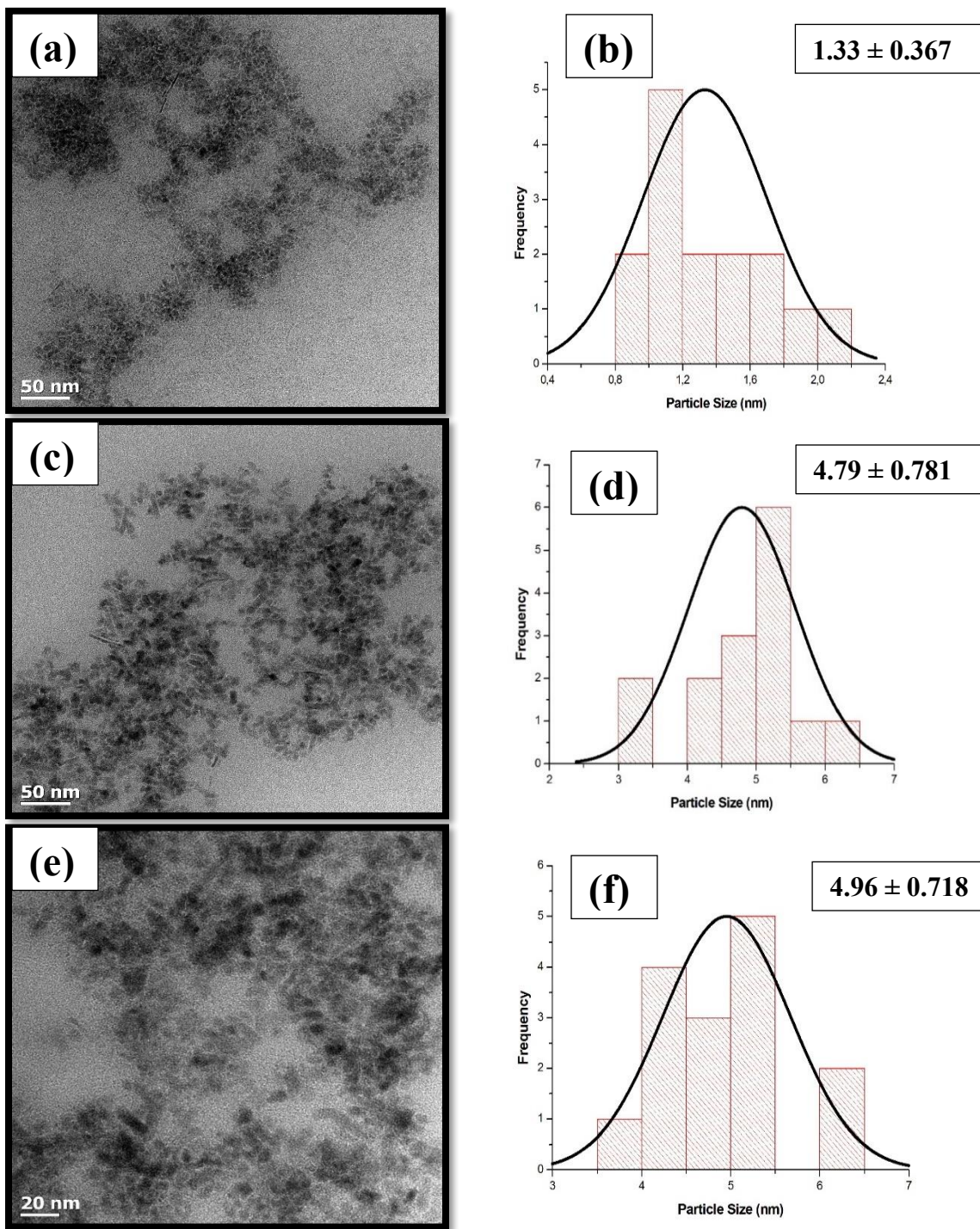


Fig. 3. 9 TEM images and size distribution curves of L-cysteine-capped Cu_xSe nanoparticles prepared at (a and b) 55° C, (c and d) 75° C and (e and f) 95° C

(c) Magnetic properties

Magnetic properties of nanoparticles bearing such as copper and iron have shown with previous studies (Liu *et al.*, 2006). That there is as relationship between increased magnetic behavior with particle size. Ferromagnets (permanent magnets) can retain a memory of an applied field once it is removed, this behavior is called hysteresis. The hysteresis loop illustrates the technical magnetic properties of a ferromagnetic material. Saturation magnetization (M_s) is determined from the extrapolation of the curve of H/M (M = magnetization and H = applied field) versus H and is the maximum induced magnetic moment that can be obtained in a magnetic field, beyond this field no further increase in magnetization occurs. Coercivity (H_c) is a measure of the width of a hysteresis loop and permanence of the magnetic moment. The various hysteresis parameters are not solely intrinsic properties but are dependent on grain size, domain state, stresses, and temperature. Fig. 3.10 shows that almost linear without any hysteresis loop, indicating the absence of magnetism and exhibit paramagnetic nature at room temperature. However, hysteresis loop has remanent magnetization (M_s) and H_c values of 2.0177 emu/g and 25.403 G respectively.

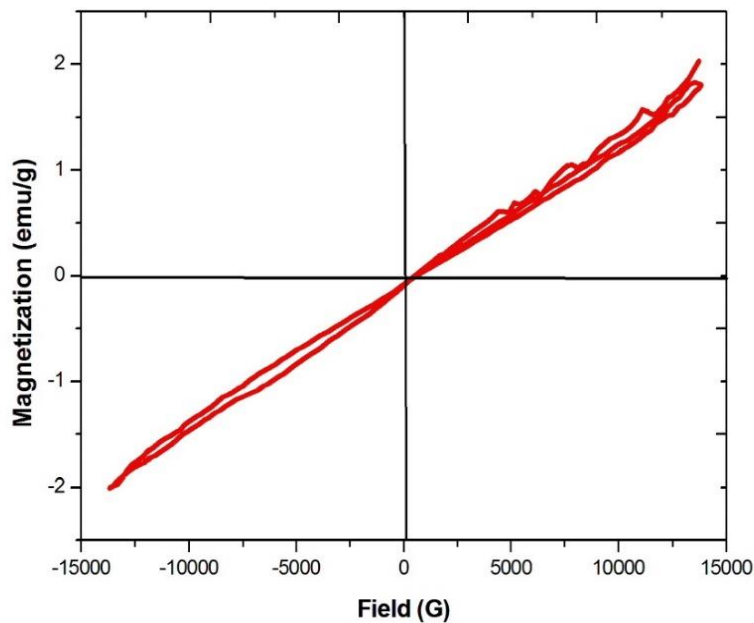


Fig. 3. 10 VSM spectra of *L*-cysteine-capped Cu_xSe nanoparticles prepared at 75° C

3.1.4 Iron selenide nanoparticles capped with L-cysteine

(a) Optical properties

The UV-Vis absorption spectra of iron selenide nanoparticles are shown in Fig. 3.11. The absorption band edges were blue-shifted from the bulk absorption band edge of iron selenide. However, it is evident from the absorption spectra of L-cysteine-capped iron selenide nanoparticles synthesized at different temperature were featureless. The shape of the absorption spectra gives no information about the shape of the nanoparticles obtained.

The PL spectra are shown in Fig. 3.12. The broad peaks observed in the PL spectra suggest the samples are polydispersed particles that are well passivated. The presence of a smooth single peak is also indicative of the existence of predominantly simple morphology. The emission maximum is located at 454 nm, 456 nm and 459 nm for iron selenide obtained at 55° C, 75° C, and 95° C respectively. They were slightly different on the emission maximum which suggests comparable properties of the materials obtained.

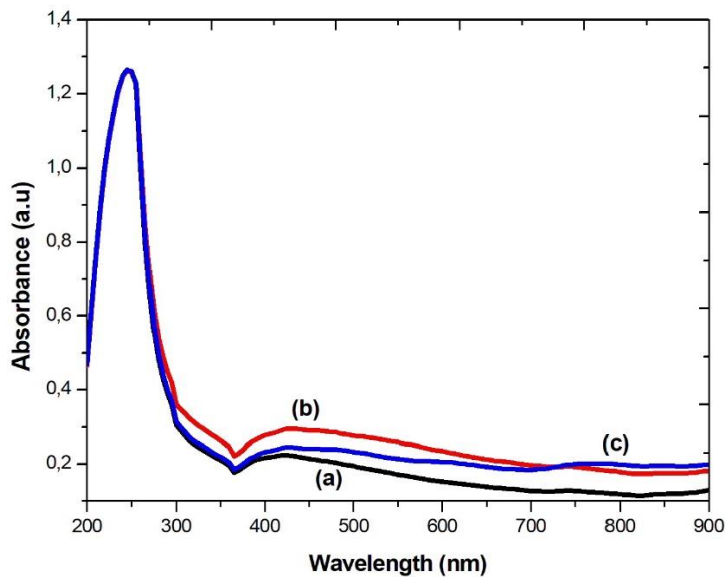


Fig. 3. 11 Absorption spectra of L-cysteine-capped Fe_xSe_y nanoparticles (a) 55° C, (b) 75° C and (c) 95° C

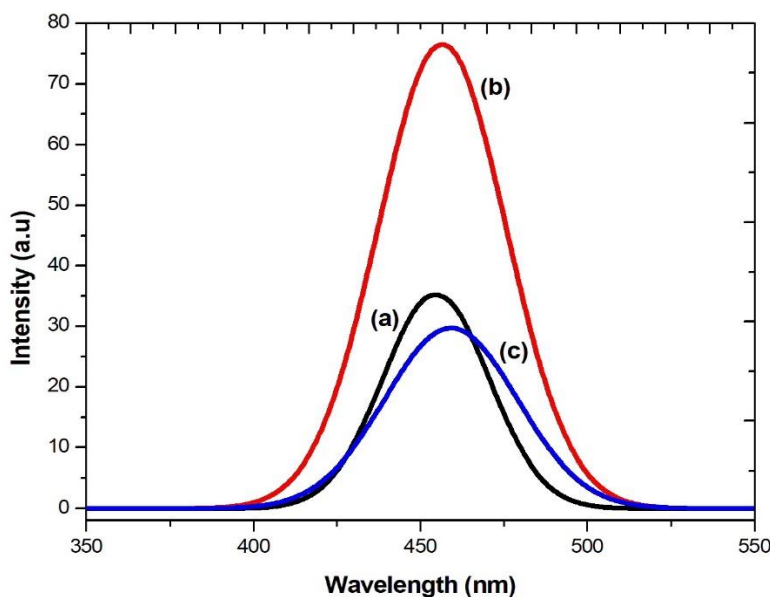


Fig. 3. 12 Emission spectra of L-cysteine-capped Fe_xSe_y nanoparticles (a) $55^\circ C$, (b) $75^\circ C$ and (c) $95^\circ C$

(b) Structural characterization

Fig. 3.13 shows the XRD patterns of the iron selenide nanoparticles synthesized at different temperatures. The observed diffraction peaks of hexagonal FeSe are found at 2θ values of 27.89, 35.13, 41.52, 49.09, 53.83, 61.40, 73.43, and 78.03 corresponding to the lattice planes (100), (002), (102), (110), (103), (112), (202) and (203), (JCPDS.: 03-065-9125) respectively. The (022) plane becomes broad and pronounced as the reaction temperature increases this is an indication of the particle growth. The TEM images of all synthesized iron selenide nanoparticles and the corresponding size distributions are shown in Fig. 3.14. The nanoparticles were dominated by spherical phase. The diameters of 5.37 ± 0.858 nm, 6.12 ± 1.262 nm and 3.77 ± 0.777 nm for the temperatures of $55^\circ C$, $75^\circ C$, and $95^\circ C$ respectively. The particles synthesized in [(Fig. 3.14(a and b))] were increasing in diameter as the reaction temperature was increased. However, the particles obtained at $95^\circ C$ (Fig. 3.14(c)) contradictory to the XRD results where the plane (022) showed a broader peak suggesting the particles obtained are bigger in size. This could be attributed to fact that powder X-ray diffraction techniques are a bulk technique that analyses the entire sample and

not individual particles; this, therefore, implies that a more monodispersed sample can result in a smaller particle size average thus a broader peak compared to a polydispersed sample.

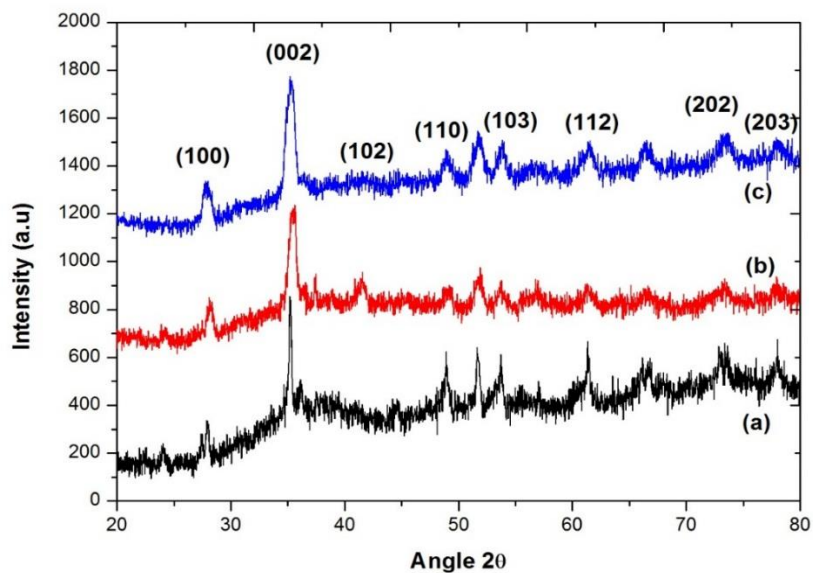


Fig. 3. 13 XRD patterns of L-cysteine-capped Fe_xSe_y nanoparticles (a) 55° C, (b) 75° C and (c) 95° C

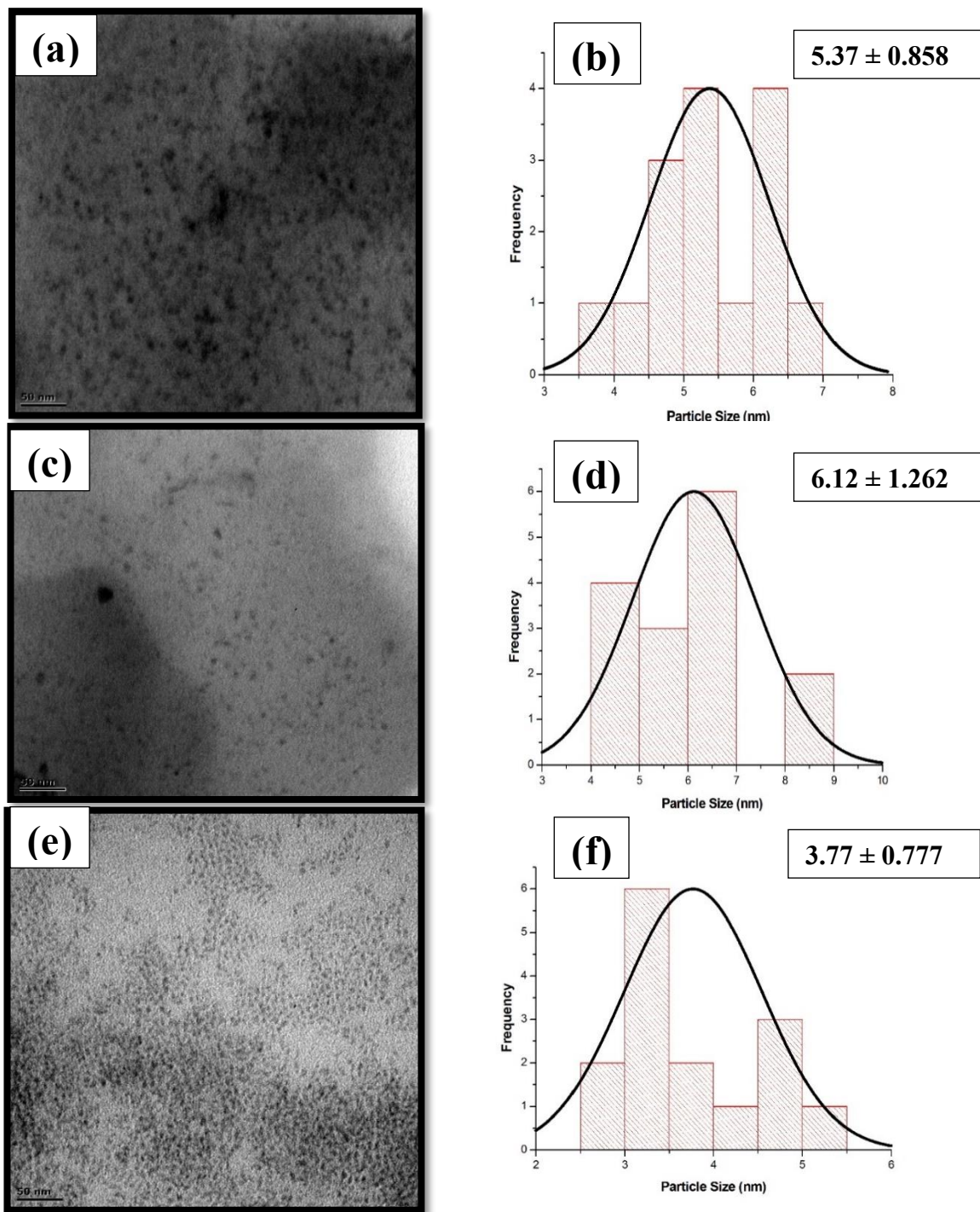


Fig. 3. 14 TEM images and size distribution curves of L-cysteine-capped Fe_xSe_y nanoparticles (a and b) 55° C, (c and d) 75° C and (e and f) 95° C

(c) Magnetic properties

The vibrating sample magnetometer (VSM) spectra of synthesized iron selenide nanoparticles are shown in Fig. 3.15. The figure shows magnetic hysteresis curve for the sample measured at room temperature. The obtained results show almost linear without any hysteresis loop, indicating the absence of magnetism and exhibit paramagnetic nature at room temperature. However, hysteresis loop has remanent magnetization (M_s) and H_c values of 2.3406 emu/g and 20.863 G respectively.

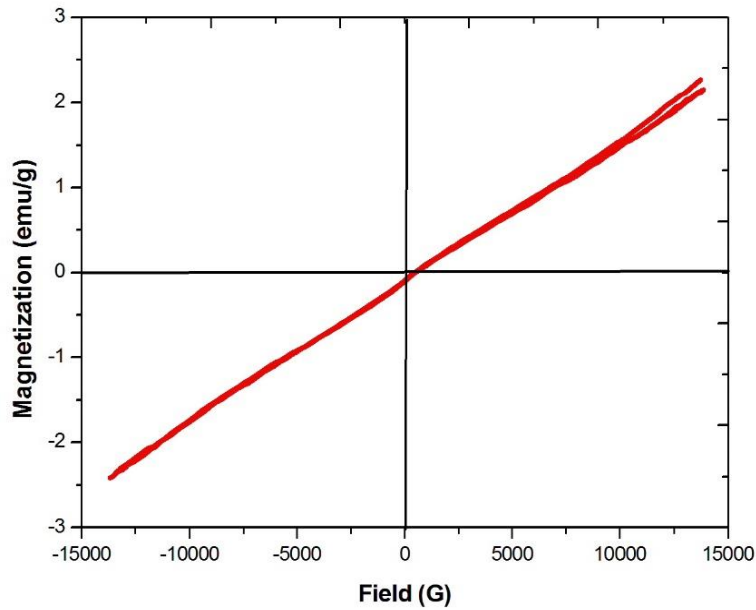


Fig. 3. 15 VSM spectra of *L*-cysteine-capped Fe_xSe_y nanoparticles at 75° C

3.2 L-Glutamic acid capped metal selenide nanoparticles

3.2.1 FTIR spectral analysis of metal selenide nanoparticles capped with L-glutamic acid

The FT-IR spectra were taken to study the interaction of the capping molecules with the surface of the nanocrystals. In Fig. 3.16 pure glutamic acid shows characteristic peaks appearing at 2966 cm^{-1} (O-H stretching), 2853 cm^{-1} (C-H stretching), 1690 cm^{-1} (C=O group) and 1523 cm^{-1} (N-H stretching of the amino group). These bands between the regions of $2750\text{--}3100\text{ cm}^{-1}$ from the carboxyl groups disappear when glutamic acid is bonded to the nanocrystals surface. This implies that the nanocrystals interact with the glutamic acid through the COO^- moiety on the carboxylic group. Upon interaction with the nanocrystal, the metal selenide draws the electron density towards itself resulting in the weakening of the other bonds and thus their disappearance in the spectra.

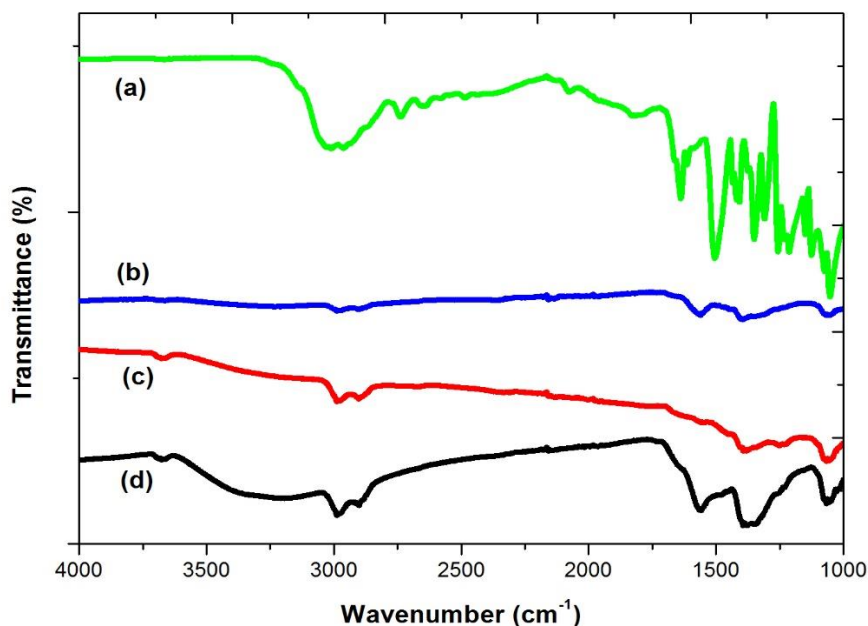


Fig. 3. 16 FT-IR spectra of (a) free L-glutamic acid, (b) L-glutamic acid-capped CdSe, (c) L-glutamic acid-capped Cu_xSe and (d) L-glutamic acid-capped Fe_xSe_y

3.2.2 Cadmium selenide nanoparticles capped with L-glutamic acid

(a) Optical properties

The UV-Vis absorption spectra of synthesized cadmium selenide nanoparticles are shown in Fig. 3.17. The absorption band edges were blue-shifted from the bulk absorption band edge of 713 nm. This is due to the quantum confinement effect, where more discrete energy state is formed, resulting in change of the band gap of the nanoparticles (Malik *et al.*, 2001). However, the band edge seemed to be less dependent upon the reaction temperature of the synthesis and show some high degree of tailing, possibly because of agglomeration of the particles which make it to be difficult to estimate the band edges. Fig. 3.18 shows typical room temperature luminescence spectra of cadmium selenide nanoparticles. The emission maximum, which appears at 400 nm, 387 nm and 385 nm for the temperatures of 55 °C, 75 °C and 95 °C respectively, which are red shifted to the absorption spectrum. This red shift in relation to the absorption band edge was generally observed in II-VI semiconductor nanoparticles (Malik *et al.*, 2000; Green & O'Brien, 1999). However, the photoluminescence spectrum is broad. The relatively broad emission spectrum has also been reported previously for semiconductor nanoparticles (Chatterjee *et al.*, 2006). The broad emission could be attributed to a polydispersed distribution of the nanoparticles.

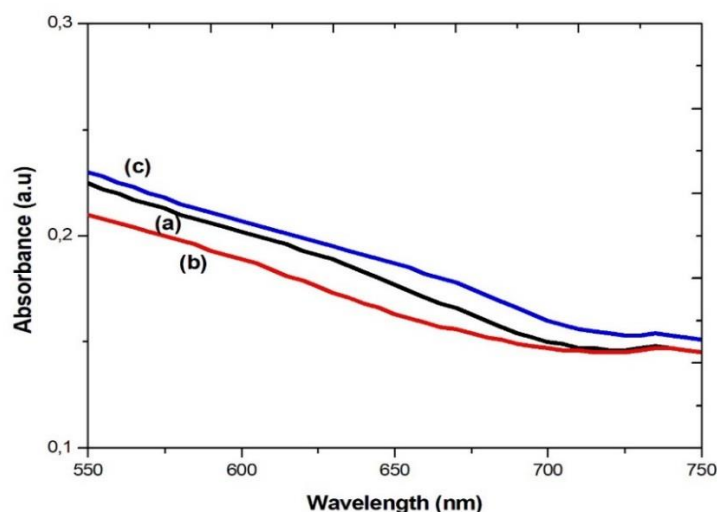


Fig. 3. 17 Absorption spectra of L-glutamic acid-capped CdSe nanoparticles prepared at (a) 55 °C, (b) 75 °C and (c) 95 °C

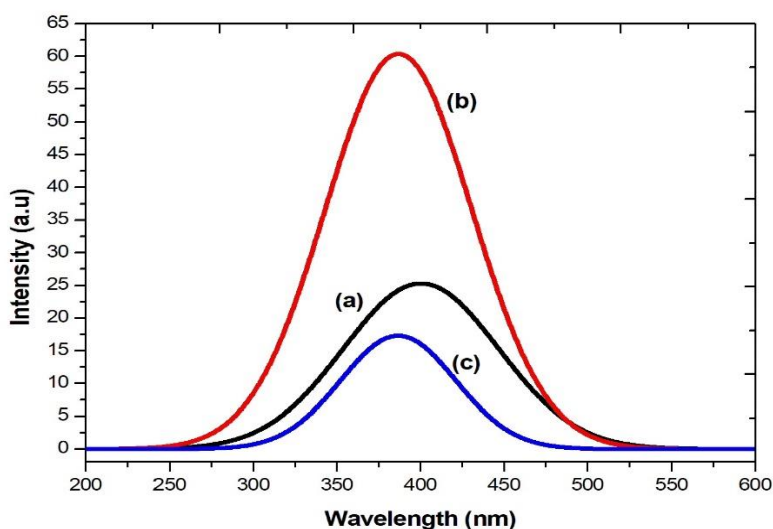


Fig. 3. 18 Emission spectra of *L*-glutamic acid-capped CdSe nanoparticles prepared at (a) 55 °C, (b) 75 °C and (c) 95 °C

(b) Structural characterization

The XRD patterns of synthesized materials from different reaction temperatures are shown in Fig. 3.19. They were found to crystallize in a predominant cubic CdSe phase (JCPDS No.: 00-010-0454) and encountered another minor impurity which could be attributed to the unreacted materials or secondary products such as additional phase of cadmium selenide, elemental cadmium or selenium.

The TEM images of all synthesized cadmium selenide nanoparticles and the corresponding size distributions are shown in Fig. 3.20. The particles obtained were spherical in shape. The average diameters of 1.92 ± 0.316 nm, 3.14 ± 0.482 nm and 4.37 ± 0.725 nm for the temperatures of 55 °C, 75 °C and 95 °C respectively. Thus, the size of the produced CdSe nanoparticles increased with the reaction temperature. It is due to the fact that higher temperature favors the fusion of smaller particles into larger ones. From the images, it was observed that some of those spherical particles were fused together to form clusters/aggregates which was also reported by (Kaur & Tripathi, 2014).

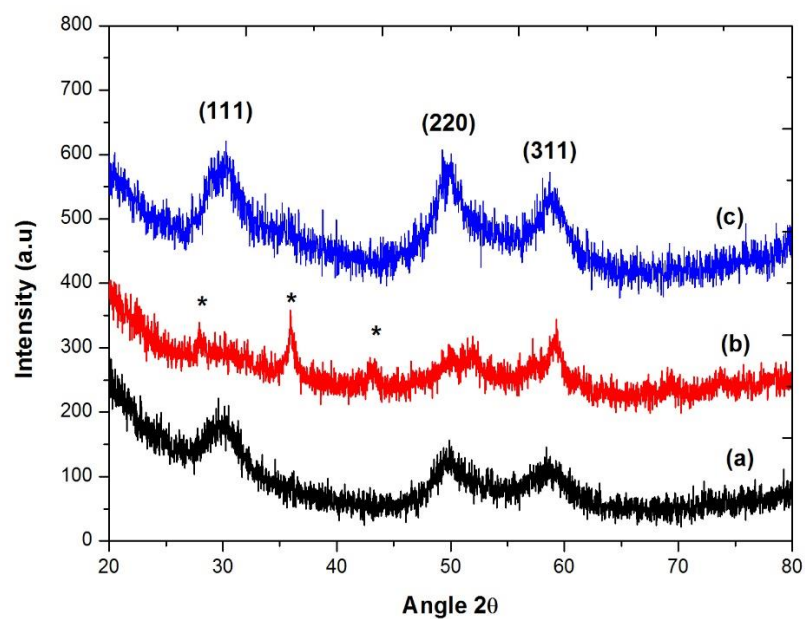


Fig. 3. 19 XRD patterns of (cubic) and (* impurities) phase of L-glutamic acid-capped CdSe nanoparticles prepared at (a) 55 °C, (b) 75 °C and (c) 95 °C

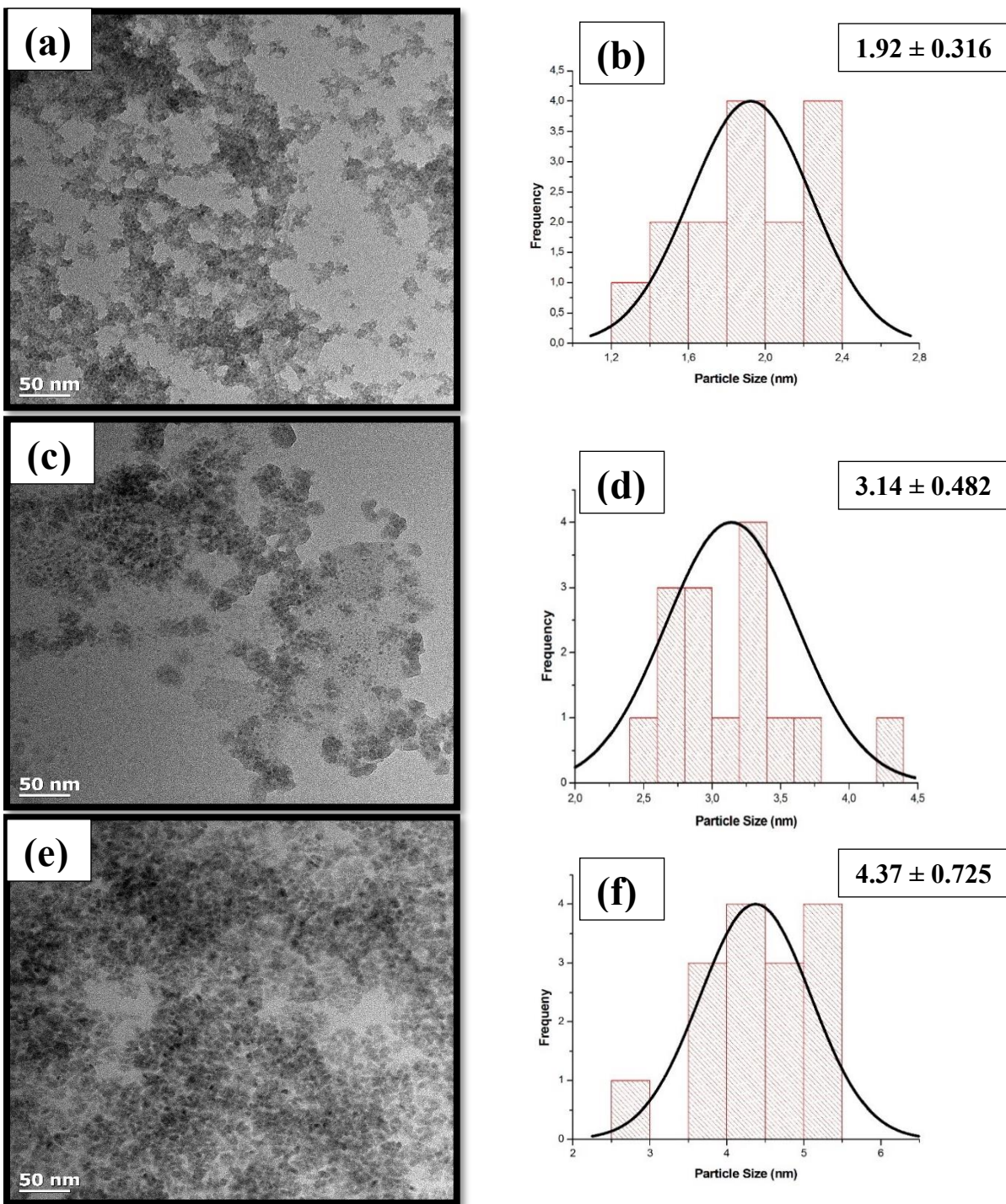


Fig. 3. 20 TEM images and size distribution curves of *L*-glutamic acid-capped CdSe nanoparticles prepared at (a and b) 55 °C, (c and d) 75 °C and (e and f) 95 °C

3.2.3 Copper selenide nanoparticles capped with L-glutamic acid

(a) Optical properties

The UV-Vis absorption spectra of copper selenide nanoparticles are shown in Fig. 3.21(i) and the extracted band edges are shown in Fig. 3.21(ii). The large blue-shifted band edges are observed, from the counter bulk absorption band edge of copper selenide. The absorption spectra revealed the band edges are located at approximately 603 nm, 599 nm and 624 nm for the temperature of 55 °C, 75 °C, and 95 °C respectively. The absorption band edges of copper selenide show that the nanocrystals obtained at different temperature revealed comparable properties according to the absorption analysis. However, as the temperature is increased, there is a slight red-shift of the band edge suggesting an increase in particle size. Furthermore, there is a decrease in wavelength for particles synthesized at 75 °C. This suggest a slight decrease in particles size of the synthesized material. Fig. 3.22 shows the emission spectra of copper selenide nanoparticles synthesized at 55, 75 and 75 °C. The photoluminescence spectra showed a broad peak which suggest the samples are polydispersed. However, the samples synthesized at 75 °C and 95 °C shows less polydispersity. The emission maximum is located at 390 nm, 395 nm and 398 nm for temperatures of 55 °C, 75 °C, and 95 °C, respectively.

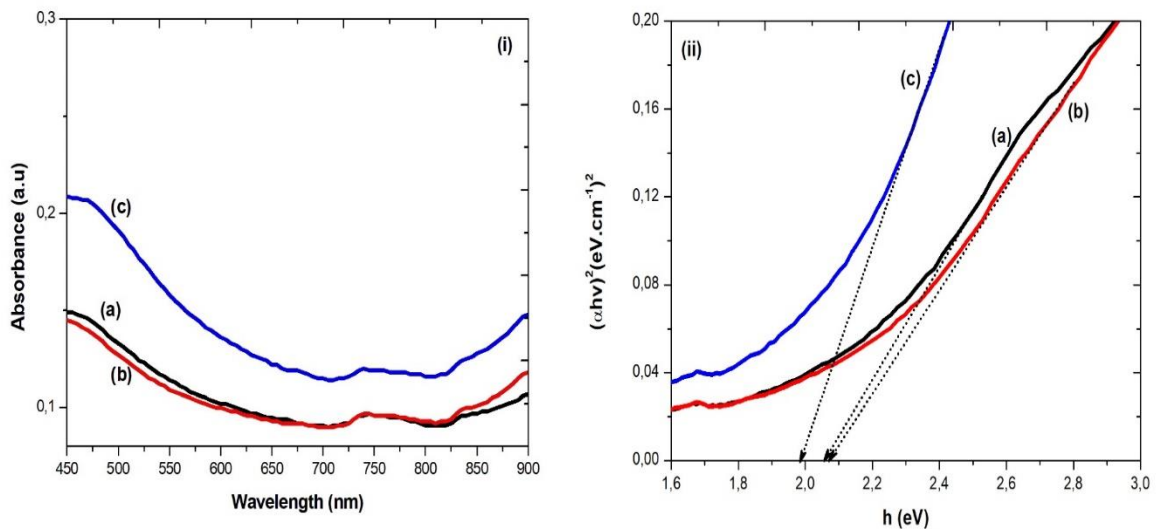


Fig. 3. 21 Absorption spectra (i) and Tauc's plot (ii) of L-glutamic acid-capped Cu_xSe nanoparticles prepared at (a) 55 °C, (b) 75 °C and (c) 95 °C

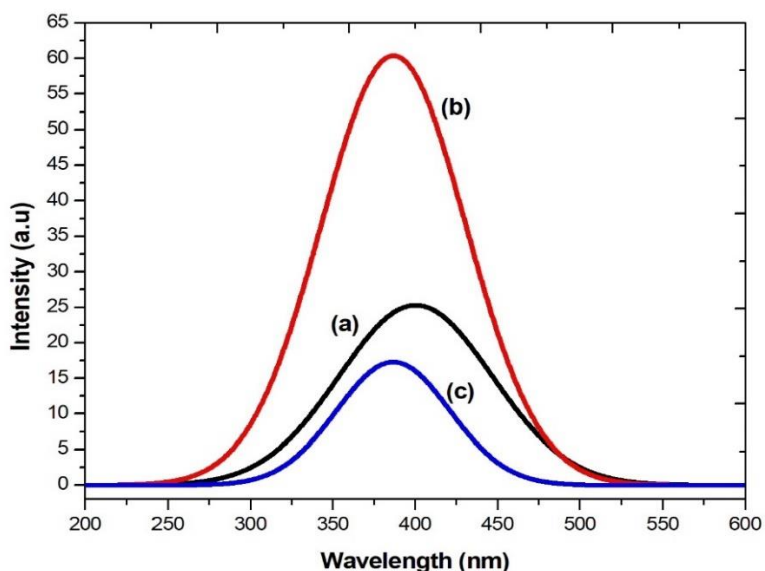


Fig. 3. 22 Emission spectra of L-glutamic acid-capped Cu_xSe nanoparticles prepared at (a) 55 °C, (b) 75 °C and (c) 95 °C

(b) Structural characterization

Fig. 3.23 shows the XRD patterns of copper selenide particles synthesized at 55, 75 and 95 °C. The materials synthesized at all three temperatures had a unit cell of the crystals appearing in cubic face-centered attributed to Cu_2Se (JCPDS No.: 01-088-2045) since the Miller indices of the main peaks appeared at the same 2θ values. The peaks at angles 2θ of 32°, 53°, 63° and 78° correspond to the reflection from (111), (220), (311) and (400) crystal planes respectively. The diffraction peaks are relatively broad signifying small size nanoparticles and no peaks of impurities were detected, indicating the high purity of the products. The shape and size distribution of the nanoparticles obtained from TEM are shown in Fig. 3.24. The diameters of 5.44 ± 0.901 nm, 19.46 ± 3.608 nm and 9.34 ± 1.270 nm for the temperatures of 55 °C, 75 °C, and 95 °C respectively. The TEM images of the synthesized particles shows spherical shapes, and small degree of agglomeration was also observed. The mean diameter for nanoparticles synthesized at 75 °C is larger than that of particles at 95 °C, which is not in agreement with the results from UV-Vis absorption spectra (band edge of 395 nm at 75 °C compared to 398 nm at 95 °C). This discrepancy

may be due to the degree of agglomeration in sample from 75 °C synthesis as observed from the corresponding TEM image of the materials.

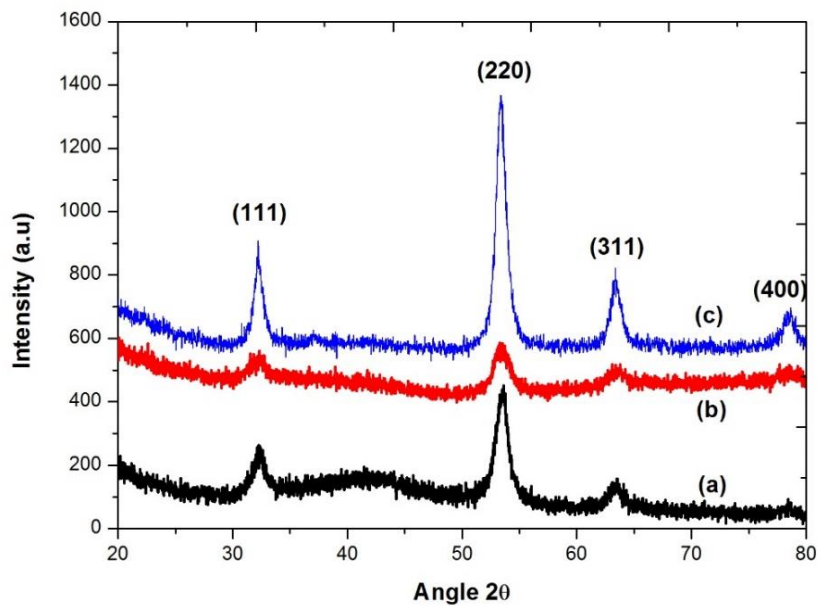


Fig. 3. 23 XRD patterns of L-glutamic acid-capped Cu_xSe nanoparticles prepared at (a) 55 °C, (b) 75 °C and (c) 95 °C

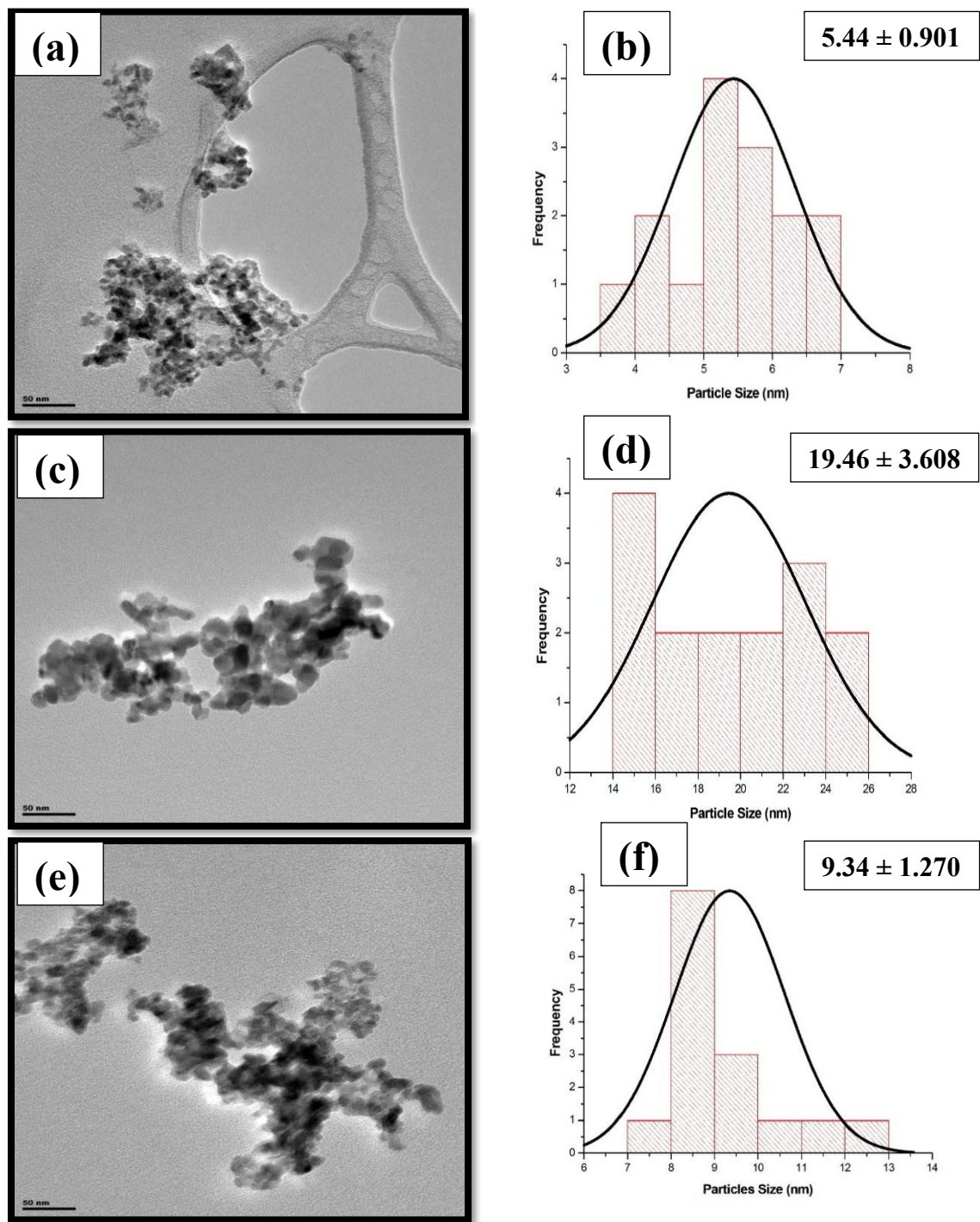


Fig. 3. 24 TEM images and size distribution curves of L-glutamic acid-capped Cu_xSe nanoparticles prepared at (a and b) 55 °C, (c and d) 75 °C and (e and f) 95 °C

(c) Magnetic properties

The vibrating sample magnetometer (VSM) spectra of synthesized iron selenide nanoparticles are shown in Fig. 3.25. The Figure shows magnetic hysteresis curve for the sample measured at room temperature. The obtained results show almost linear without any hysteresis loop, indicating the absence of magnetism and exhibit paramagnetic nature at room temperature. However, hysteresis loop has remanent magnetization (M_s) and H_c values of 1.7351 emu/g and 76.753 G respectively.

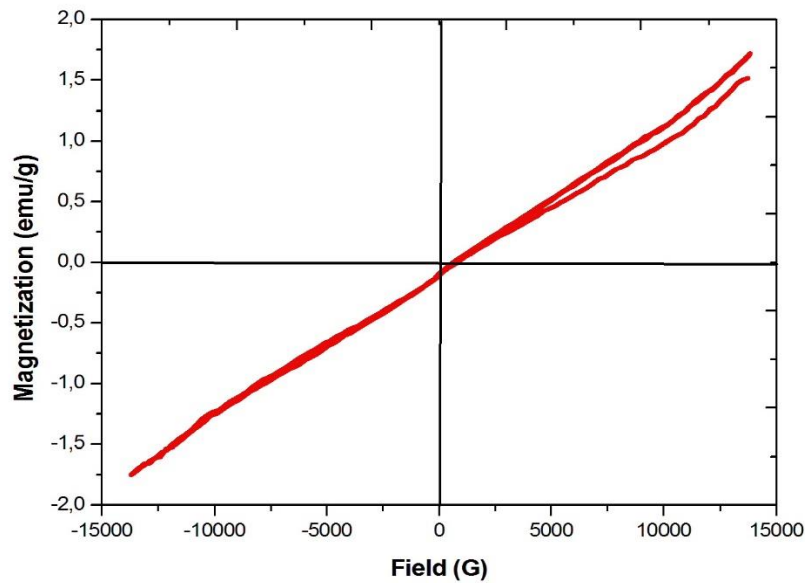


Fig. 3. 25 VSM spectra of *L*-glutamic acid-capped Cu_xSe nanoparticles prepared at 75 °C

3.2.4 Iron selenide capped with L-glutamic acid

(a) Optical properties

The UV-Vis absorption spectra of iron selenide nanoparticles are shown in Fig. 3.26. The absorption band edges were blue-shifted from the bulk absorption band edge of iron selenide. Nevertheless, the blue-shift of all the band edges results from quantum confinement effects. However, it is evident from the absorption spectra of L-glutamic acid-capped iron selenide nanoparticles synthesized at different temperature were featureless. Furthermore, the absorption spectra also showed some degree of tailing signifying polydispersed samples.

The PL spectra are shown in Fig. 3.27. The photoluminescence spectra are red-shifted from their corresponding absorption band edges. A broad peak observed on PL spectra suggest the samples are polydispersed particles that are well passivated. The emission maximum is located at 489 nm, 490 nm and 492 nm for iron selenide nanoparticles obtained at 55° C, 75° C, and 95° C respectively. More important to note is the broadness of the peaks. The FWHM increases as the temperature increases. This suggest that the particle size distribution is become less mono-dispersed as the temperature is increasing.

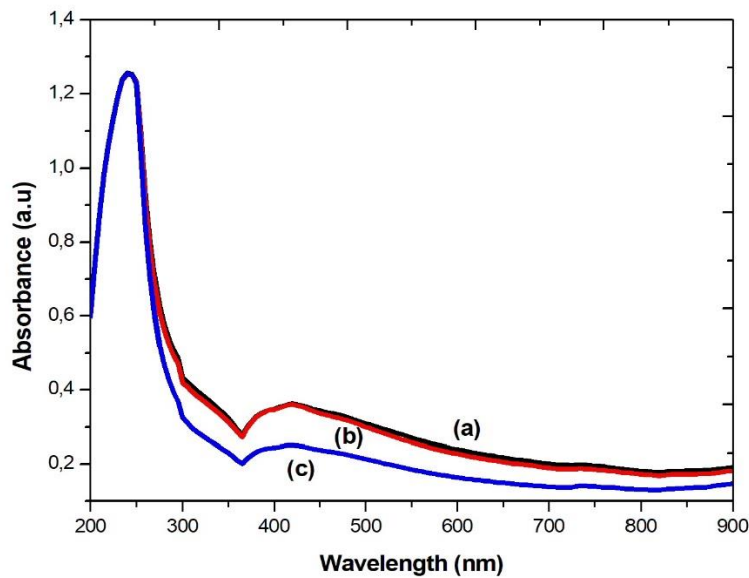


Fig. 3. 26 Absorption spectra of L-glutamic acid-capped Fe_xSe_y nanoparticles prepared at (a) 55 °C, (b) 75°C and (c) 95 °C

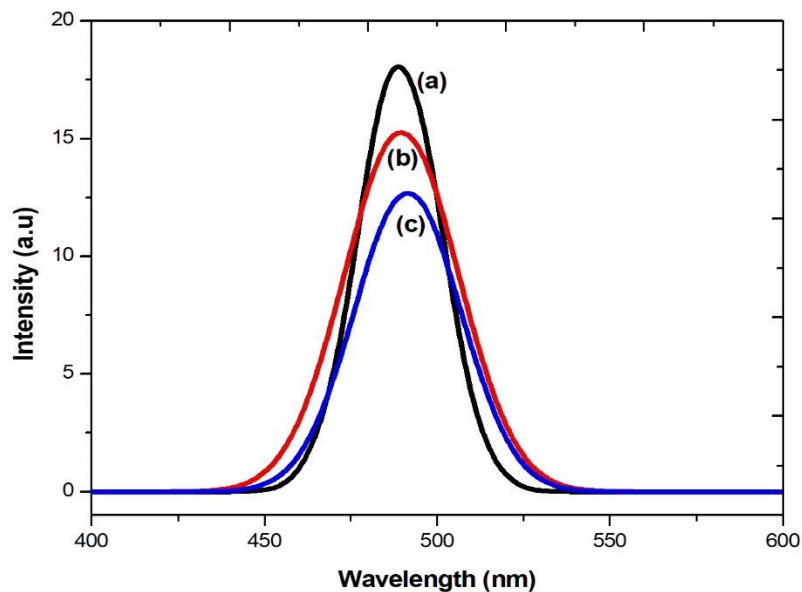


Fig. 3. 27 Emission spectra of L-glutamic acid-capped Fe_xSe_y nanoparticles prepared at (a) 55 °C, (b) 75 °C and (c) 95 °C

(b) Structural characterization

The X-ray diffraction patterns were taken to confirm the crystal phase and check the purity of the samples. Fig. 3.28 shows the XRD patterns of the iron selenide nanoparticles synthesized at different temperatures. The patterns show obvious nearly narrow diffraction peaks, indicating that the particles are in the nanosized regime or well distributed. The observed diffraction peaks of hexagonal FeSe are found at 2θ values of 27.89, 35.13, 41.52, 49.09, 53.83, 61.40, 73.43, and 78.03 corresponding to the lattice planes (100), (002), (102), (110), (103), (112), (202) and (203) respectively. As the temperature was increased to 95 °C, no change in phase was observed. Hexagonal phase of FeSe (JCPDS.: 03-065-9125) with characteristic (100), (002), (102), (110), (103), (112), (202) and (203) peaks was still maintained. This showed that temperature did not affect the phase of FeSe nanoparticles.

The morphologies of the functionalized FeSe nanoparticles are depicted in Fig. 3.29. The nanoparticles were dominated by spherical phase with minor agglomeration. The diameters of 10.97 ± 2.428 nm, 10.66 ± 1.356 nm and 11.83 ± 2.177 nm for the temperatures of 55°C , 75°C , and 95°C respectively. The TEM images shows spherical particles that are agglomerated. The agglomeration in this case does not distort the morphology into chain-like structures rather the particles maintain their spherical nature. This observation is consistent with the broader XRD peak observed at the elevated temperature. However, the particles prepared at 95°C showed some mixed morphology predominated by spherical shape particle, thus change in morphology could be attributed to the reaction temperature used.

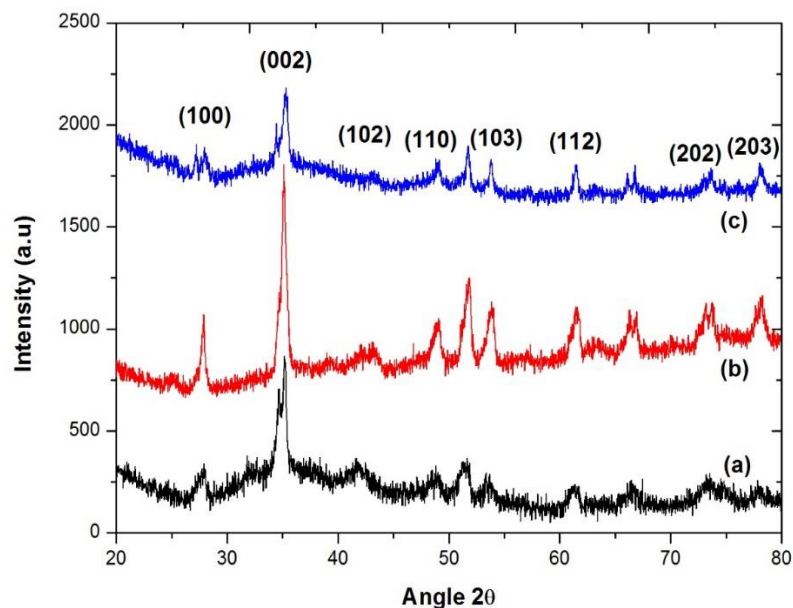


Fig. 3. 28 XRD patterns of *L*-glutamic acid-capped Fe_xSe_y nanoparticles prepared at (a) 55°C , (b) 75°C and (c) 95°C

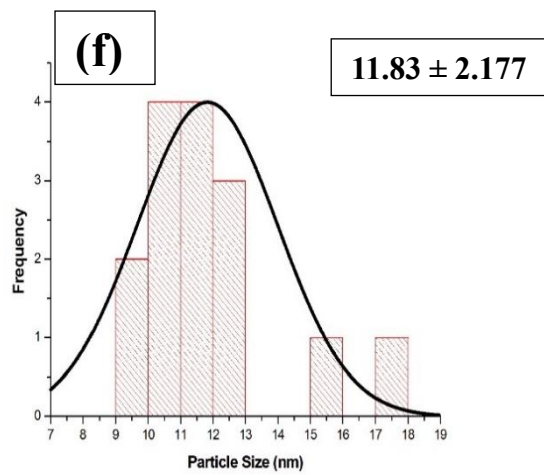
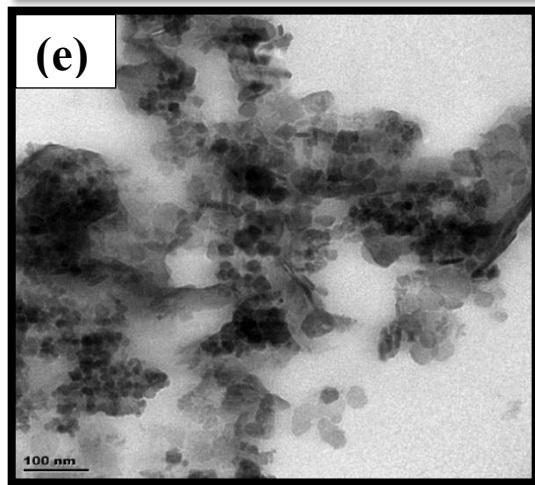
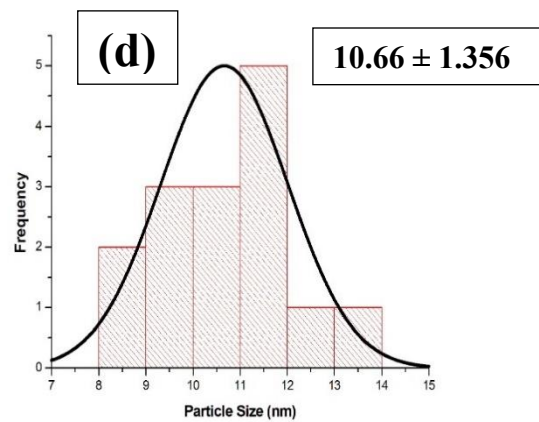
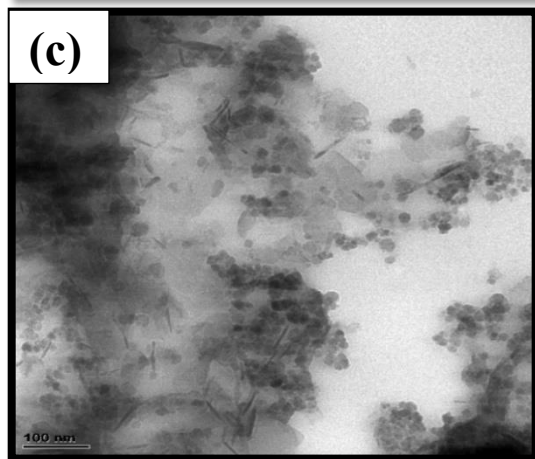
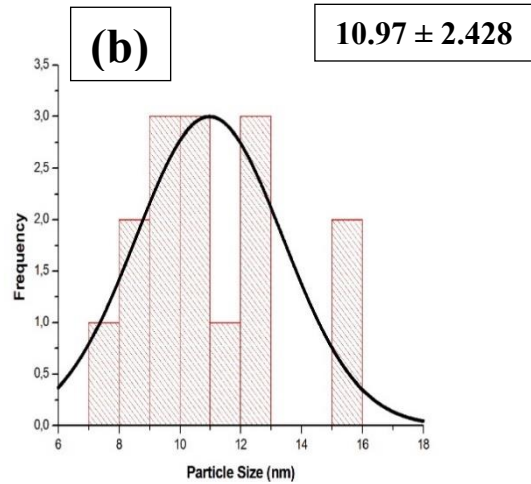
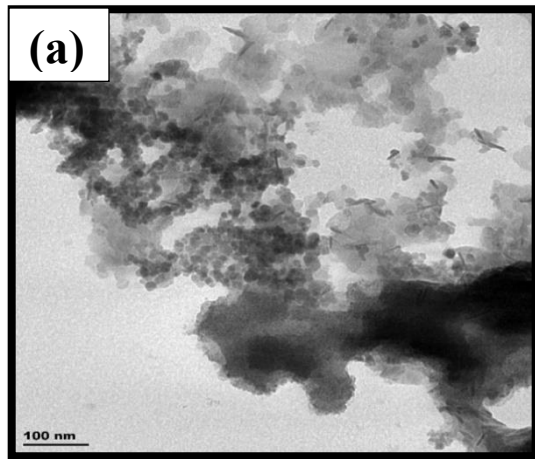


Fig. 3. 29 TEM images and size distribution curves of *L*-glutamic acid-capped Fe_xSe_y nanoparticles prepared at (a and b) 55 °C, (c and d) 75 °C and (e and f) 95 °C

(c) Magnetic properties

The vibrating sample magnetometer (VSM) spectra of synthesized iron selenide nanoparticles are shown in Fig. 3.30. The Figure depicts magnetic hysteresis curve for the sample measured at room temperature. The figure shows a twofold behavior for FeSe nanoparticles, ferromagnetic behavior in low fields and paramagnetic behavior in up fields. The hysteresis loop has remanent magnetization (M_s) and H_c values of 5.8292 emu/g and 14.538 G respectively.

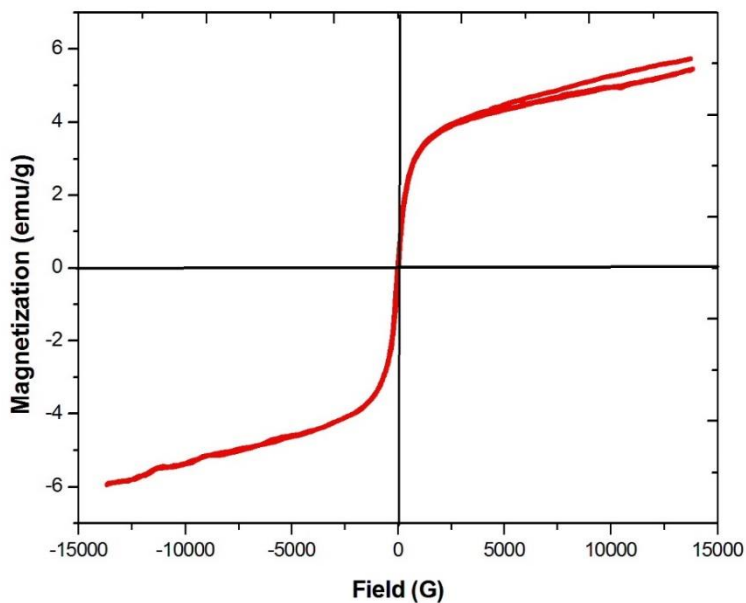


Fig. 3. 30 VSM spectra of L-glutamic acid-capped Fe_xSe_y nanoparticles at 75 °C

3.3 L-Phenylalanine capped metal selenide nanoparticles

3.3.1 FT-IR analysis of L-phenylalanine capped metal selenide nanoparticles

The surface modification of the metal selenide nanoparticles with L-phenylalanine was confirmed by FT-IR spectra as shown in Fig. 3.31. Pure L-phenylalanine shows characteristic peaks appearing at 3095 cm^{-1} (O-H and N-H stretching), 2917 cm^{-1} (C-H group aliphatic stretching), 1621 cm^{-1} (C=C bending vibration of aromatic ring), 1464 cm^{-1} (C-H aliphatic group), and 1374 cm^{-1} (O-H bending of the phenolic and carboxylic groups). These bonds between the regions of $2946\text{--}3095\text{ cm}^{-1}$ from the carboxyl group disappear when L-phenylalanine is bonded to the nanocrystals surface. This implies that the nanocrystals interact with the L-phenylalanine through the COO^- moiety of the carboxylic group.

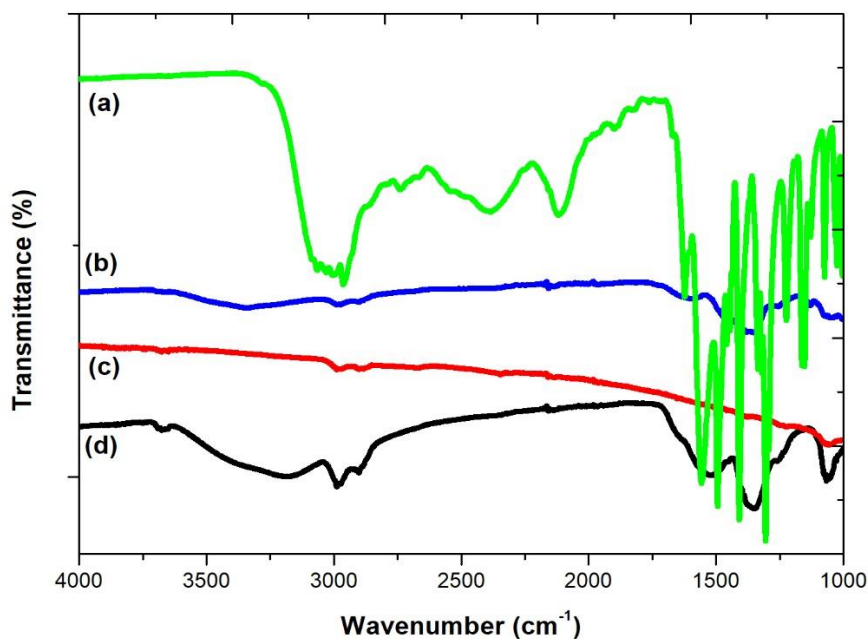


Fig. 3. 31 FT-IR spectra of (a) free L-phenylalanine, (b) L-phenylalanine-capped CdSe, (c) L-phenylalanine-capped Cu_xSe and (d) L-phenylalanine-capped Fe_xSe_y

3.3.2 Cadmium selenide nanoparticles capped with L-phenylalanine

(a) Optical properties

The band gap energy in nanoparticles could be obtained from the absorption maxima. Electrons in the conduction band and holes in the valence band are spatially confined by the potential barrier of the surface according to quantum confinement theory. Due to confinement of both electrons and holes, the lowest energy optical transition from the valence to conduction band will increase in energy, effectively increasing the band gap. The shoulder or peak of the spectra corresponds to the fundamental absorption edges in the nanoparticles and could be used to estimate the band gap of the nanomaterial (Moloto *et al.*, 2009). The absorption and photoluminescence spectra of an aqueous solution of phenylalanine-capped cadmium selenide at different temperature are shown in Fig. 3.32. The absorption band-edges are all blue-shifted in relation to the bulk band gap indicating quantum confinement. The absorption band-edges as calculated using the direct band gap method (Lippens & Lannoo, 1989). It is evident from the absorption spectra of phenylalanine-CdSe nanoparticles synthesized at three different temperature were featureless. The shape of the absorption spectra gives no information about the shape. Therefore, it was difficult to extrapolate their band-edges due to the degree of tailoring of the absorption spectra. The emission spectra of synthesized CdSe nanoparticles are shown in Fig. 3.33. The emission maxima were found to be at 391 nm, 389 nm and 394 nm for the temperatures of 55° C, 75° C, and 95° C respectively. The broader emission spectra observed of nanoparticles prepared at 55° C, shows a broad emission peak which is an indication of polydispersed of the particles compared to those prepared at 75° C and 95° C which approaches monodispersity.

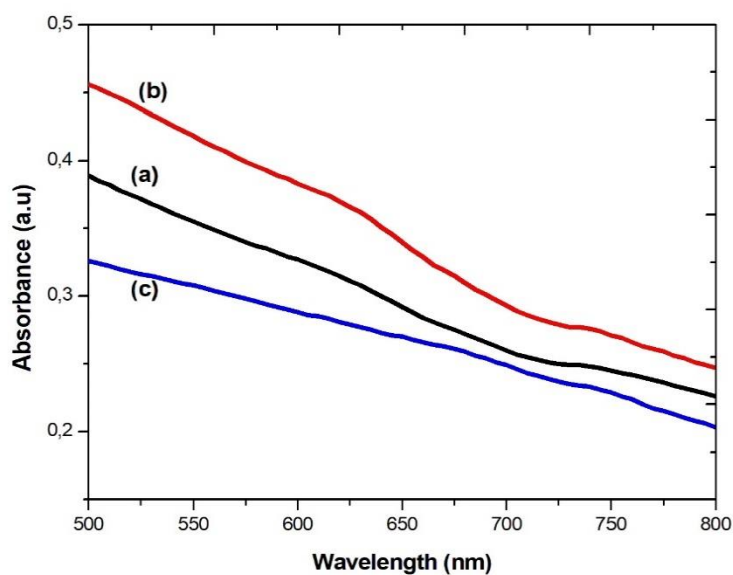


Fig. 3. 32 Absorption spectra of L-phenylalanine-capped CdSe nanoparticles prepared at (a) 55 °C, (b) 75 °C and (c) 95 °C

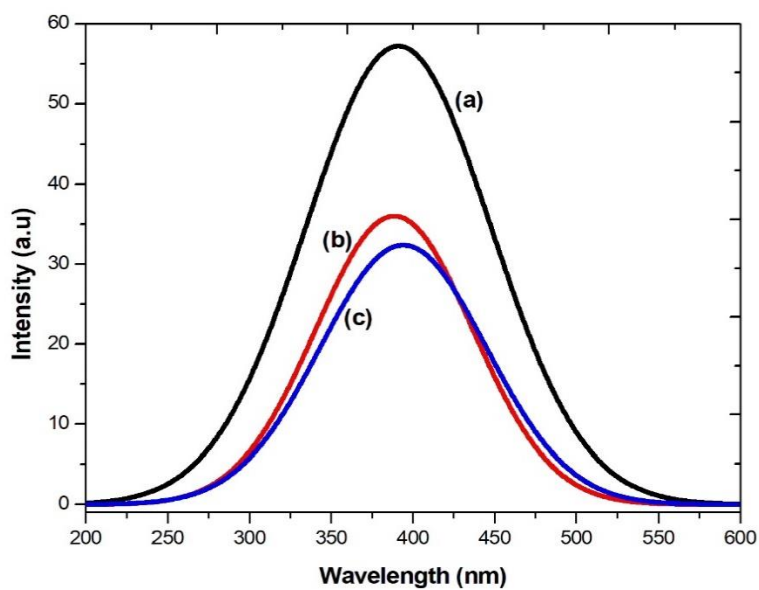


Fig. 3. 33 Emission spectra of L-phenylalanine-capped CdSe nanoparticles prepared at (a) 55 °C, (b) 75 °C and (c) 95 °C

(b) Structural characterization

XRD patterns and TEM images were undertaken to determine the structural properties of synthesized cadmium selenide nanoparticles. The XRD patterns of synthesized cadmium selenide nanoparticles are shown in Fig. 3.34. The diffraction peaks indicate the nanocrystalline nature. These peaks at angles (2θ) of 29° , 49° , and 58° correspond to the reflection from (111), (220) and (311) crystal planes respectively which is identical to the cubic phase of cadmium selenide (JCPDS No.: 01-075-5680). Therefore, it was compared with the standard diffraction pattern, and no peaks of impurities were detected, indicating the high purity of the products. The plane (111) becomes broader as the reaction temperature is increased which indicates small particles or narrow size distribution and the crystallinity of the peaks is improved as a function of temperature. The similar observation was also reported by (Mahmoud *et al.*, 2012).

The TEM images of all synthesized cadmium selenide nanoparticles and the corresponding size distributions are shown in Fig. 3.35. The particles obtained were very small and spherical in shape with a minor agglomeration which could be attributed to the capping molecule used. The average diameters of 4.020 ± 0.870 nm and 3.429 ± 0.482 nm for the temperatures of 55°C and 75°C respectively. However, for the sample prepared at 95°C , we couldn't calculate the size distribution of nanoparticles were not well passivated with L-phenylalanine this could be attributed to its structure, the phenyl ring creates steric hindrance which makes it difficult to bind to the surface of nanoparticles while maintaining stability. It is observed that a more linear structure is preferable as compared to cysteine amino acid.

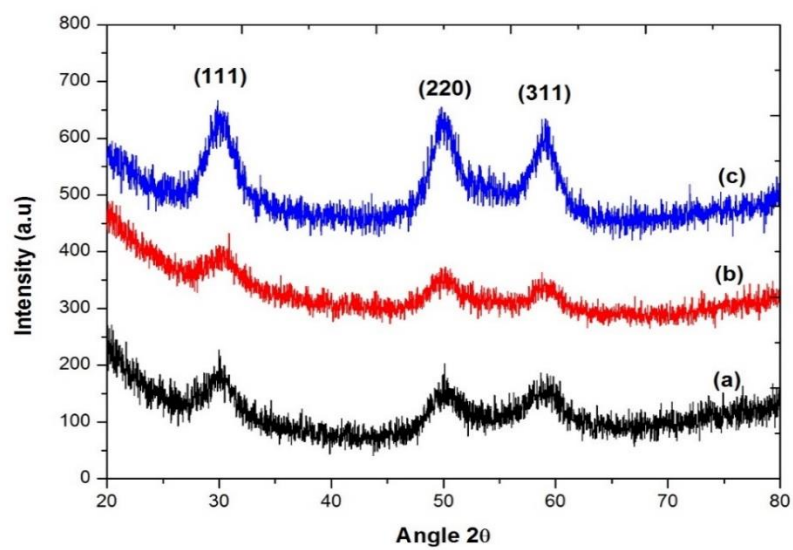


Fig. 3. 34 XRD patterns of L-phenylalanine-capped CdSe nanoparticles prepared at (a) 55 °C, (b) 75 °C and (c) 95 °C

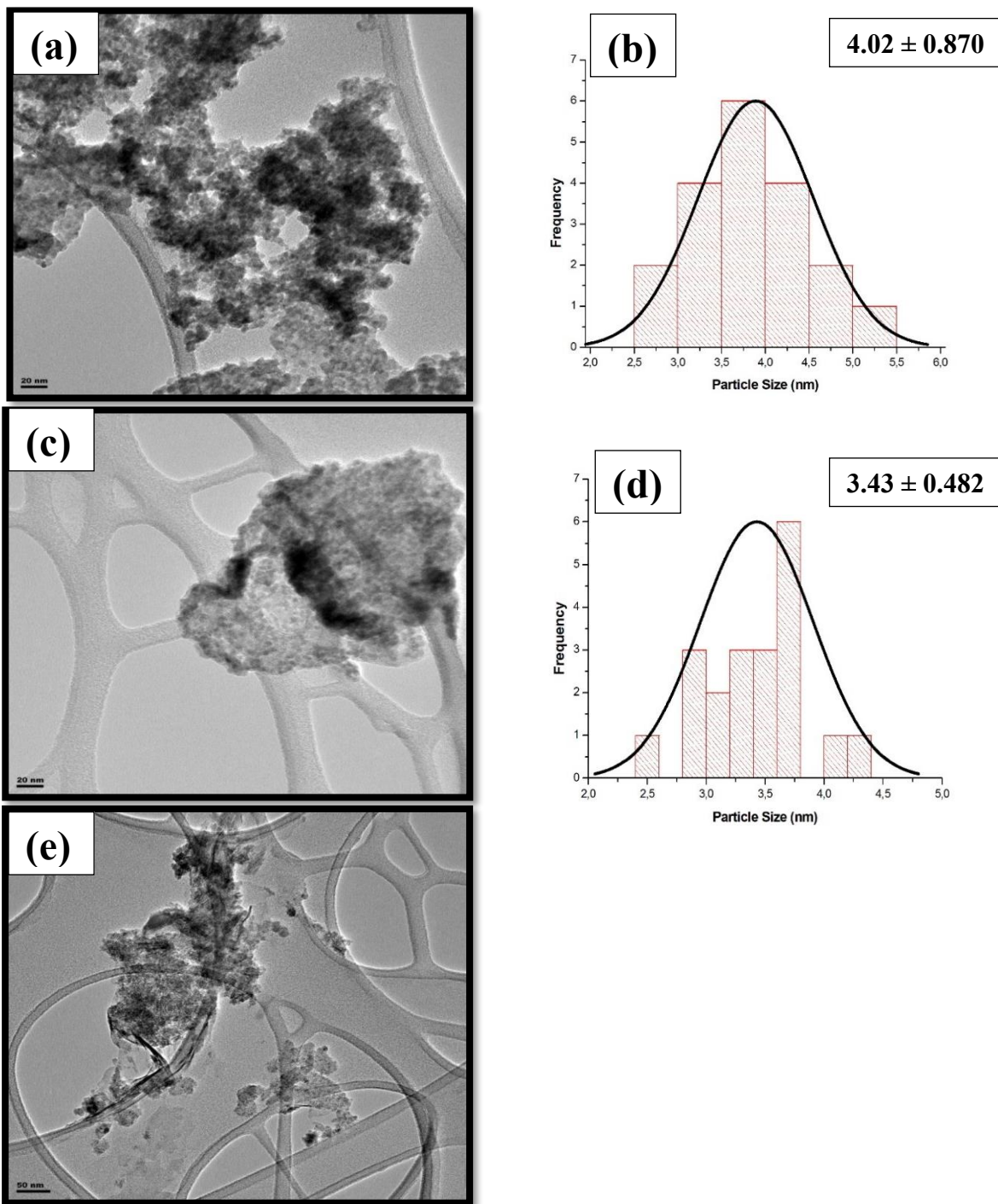


Fig. 3. 35 TEM images and size distribution curves of L-phenylalanine-capped CdSe nanoparticles prepared at (a and b) 55 °C, (c and d) 75 °C and (e) 95 °C

3.3.3 Copper selenide nanoparticles capped with L-phenylalanine

(a) Optical properties

Absorption spectroscopy can be used to characterize the size and size distribution of semiconductor nanocrystals. The changes of optical absorption of semiconductor nanoparticles with size or compared with bulk semiconductors are known to be one of the main exponents of quantum confinement effect. A familiar blue-shift of the fundamental absorption edge and excitonic maximum is observed for direct gap semiconductors. Fig. 3.36 shows the absorption spectra of the L-phenylalanine functionalized copper selenide nanoparticles. The unusual spectra are typical of Cu_2Se nanocrystals, given the shape of the spectra it is impossible to extract the absorption band edges using the extrapolation method, but the size and size distribution of nanocrystals can be inferred from the fluorescence spectra. However, the absorption spectra show some degree of tailing, possibly as results of the agglomeration of the nanoparticles.

The spectra in Fig. 3.37 show fluorescence peaks of the as-prepared nanocrystals at different temperatures. Fig. 3.37(a-b) were found to have a narrow emission peaks which is an indication of monodispersity of the particles and the emission maximum was located at 428 nm and 435 nm, which implies the growth of the nanocrystals as the reaction temperature was increased. Furthermore, the emission wavelength of particles synthesized at 75 °C is red-shifted from the one at 55 °C nanocrystals suggesting that the previous has bigger particle size. However, the broad emission peak at Fig. 3.37(c) suggest a polydispersed sample distribution with emission maximum at 433 nm which indicates a decrease in size particle as compare to the ones prepared at low temperature.

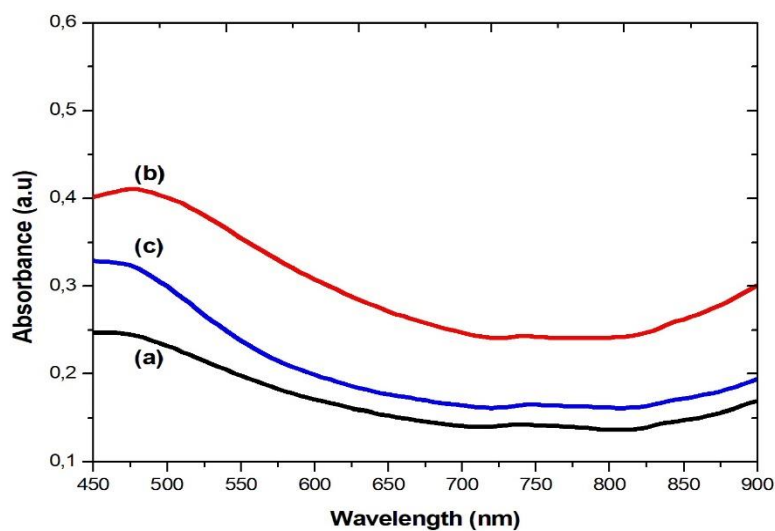


Fig. 3. 36 Absorption spectra of L-phenylalanine-capped Cu_xSe nanoparticles prepared at (a) 55 °C, (b) 75 °C and (c) 95 °C

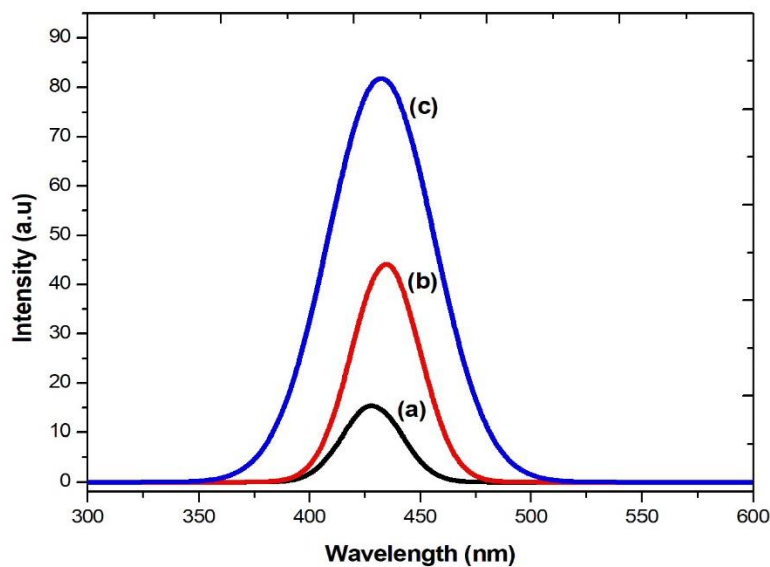


Fig. 3. 37 Emission spectra of L-phenylalanine-capped Cu_xSe nanoparticles prepared at (a) 55 °C, (b) 75 °C and (c) 95 °C

(b) Structural characterization

The morphology and size of Cu₂Se nanoparticles were investigated by powder XRD and TEM. The X-ray diffraction pattern were taken to confirm the crystal phases and check the purity of the samples. The diffractograms in Fig. 3.38 were indexed to a cubic phase of Cu₂Se nanocrystals (JPCDS card no.: 00-027-0158) and encountered another minor impurity which could be attributed to the unreacted materials. The narrowness of the peaks signifies the bigger size and crystallinity of these nanoparticles. As the temperature increased it was observed that the crystallinity and the broadness of the diffractograms decreased. However, the observation of only the cubic phase at different temperatures is not surprising since it was reported that hexagonal phase nanoparticles are easily obtained at extremely high temperatures and cubic phase are more prevalent at low temperatures.

The TEM images in Fig. 3.39 demonstrate the morphology and size of Cu₂Se nanoparticles. The morphology was found to be the same as the temperature was increased. Therefore, TEM images of the synthesized particles shows spherical shapes, and degree of agglomeration was also observed. As the temperature is increased, the reaction approaches a critical temperature where one type of morphology dominates. Due to agglomeration it was impossible to determine the size distribution of the synthesized nanoparticles. The TEM corroborates the obtained results from absorption and emission spectra which shows some tailoring at low reaction temperature.

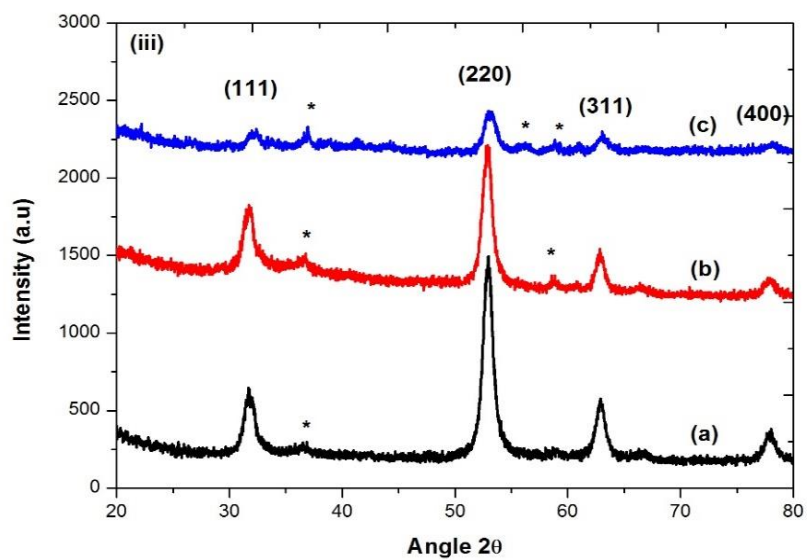


Fig. 3. 38 XRD patterns of L-phenylalanine-capped Cu_xSe nanoparticles prepared at (a) 55 °C, (b) 75 °C and (c) 95 °C

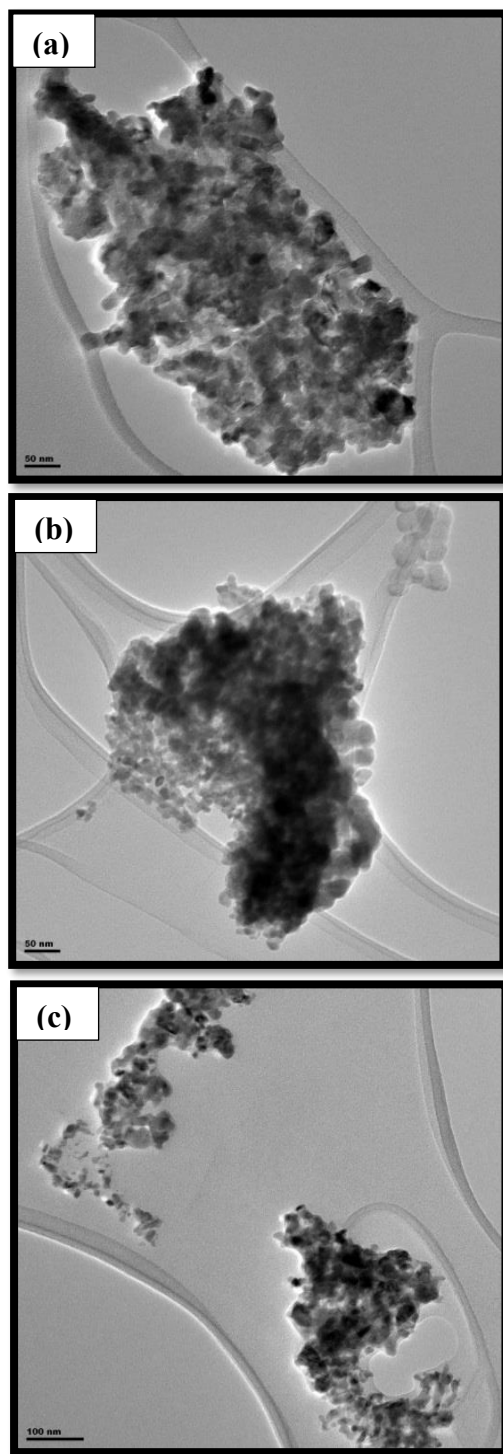


Fig. 3. 39 TEM images of *L*-phenylalanine-capped Cu_xSe nanoparticles prepared at (a) 55 °C, (b) 75 °C and (c) 95 °C

(c) Magnetic properties

The vibrating sample magnetometer (VSM) spectra of synthesized iron selenide nanoparticles are shown in Fig. 3.40. The Figure shows magnetic hysteresis curve for the sample measured at room temperature. The obtained results show almost linear without any hysteresis loop, indicating the absence of magnetism and exhibit paramagnetic nature at room temperature. However, hysteresis loop has remanent magnetization (M_s) and H_c values of 1.0088 emu/g and 42.678 G respectively.

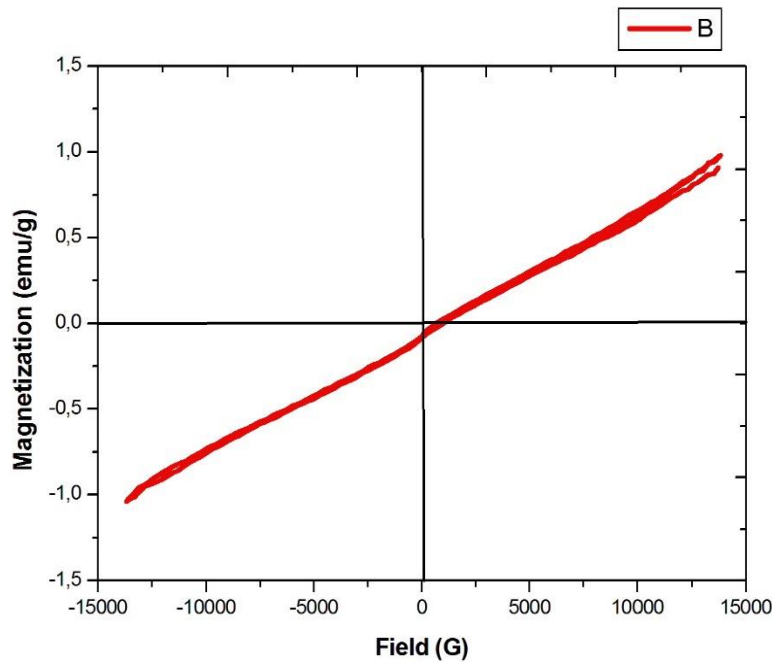


Fig. 3. 40 VSM spectra of L-phenylalanine-capped Cu_xSe nanoparticles at 75 °C

3.3.4 Iron selenide capped with L-phenylalanine

(a) Optical properties

The UV-Vis absorption spectra of iron selenide nanoparticles are shown in Fig. 3.41. The absorption band edges were blue-shifted from the bulk absorption band edge of iron selenide. However, the absorption spectra of iron selenide nanoparticles synthesized at different reaction temperature were featureless and tailoring which could be attributed to agglomerated or bigger size nanoparticles that are formed. It was difficult to extrapolate the band-edges due to the tailoring nature of the absorption spectra. Furthermore, the absorption properties were less dependent to the reaction temperature in which no trend was observed. The emission spectrum of the nanoparticles depends on their surface state, size and surface passivation. The photoluminescence spectra in Fig. 3.42(a-c) of phenylalanine-capped FeSe nanoparticles showed a broad emission peaks under an excitation wavelength of 300 nm for particles synthesized at 55 °C, 75 °C and 95 °C. The broadness of the emission peaks with increased temperature suggest that the size and shape of the nanoparticles was approaching polydispersity.

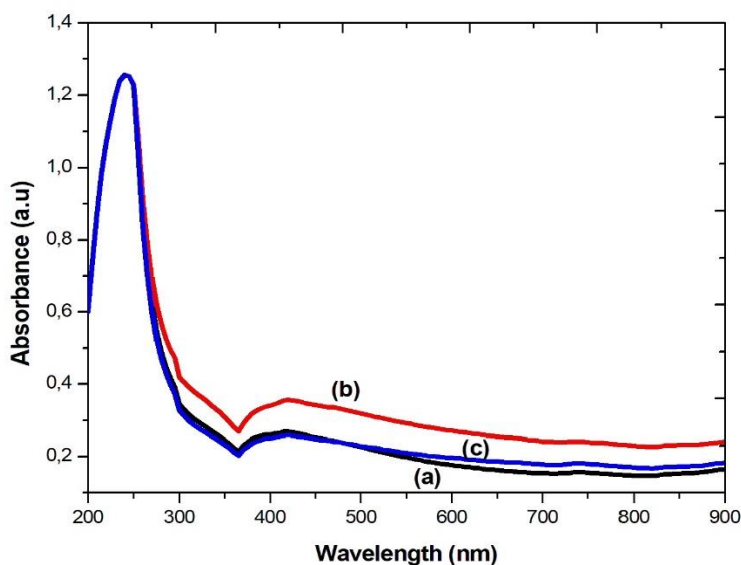


Fig. 3. 41 Absorption spectra of L-phenylalanine-capped Fe_xSe_y nanoparticles prepared at (a) 55 °C, (b) 75 °C and (c) 95 °C

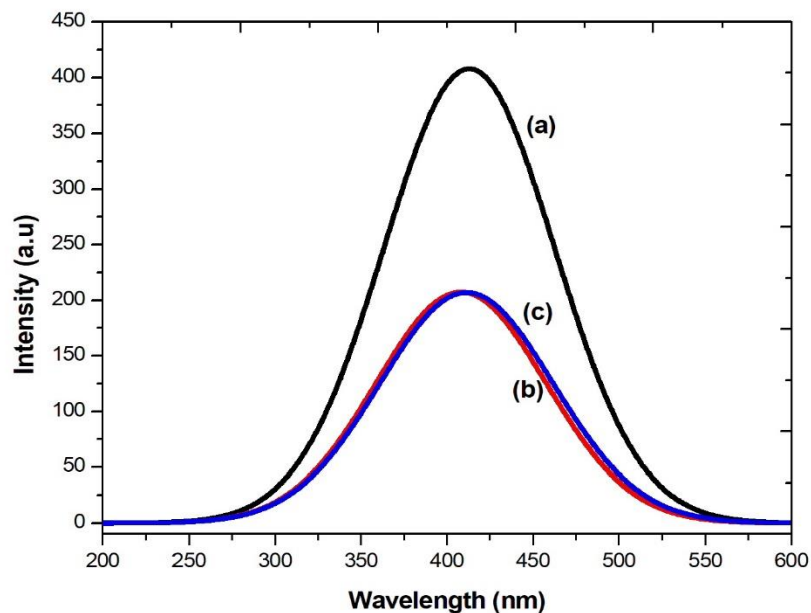


Fig. 3. 42 Emission spectra of L-phenylalanine-capped Fe_xSe_y nanoparticles prepared at (a) 55 °C, (b) 75 °C and (c) 95 °C

(b) Structural characterization

The purity and crystallinity of as prepared L-phenylalanine-capped FeSe nanoparticles were characterized by using powder XRD. Fig. 3.43 shows that all samples prepared at different temperatures 55 °C, 75 °C and 95 °C are indexed to hexagonal phase of FeSe nanoparticles with characteristic peaks of (100), (002), (102), (110), (103), (112), (202) and (203) corresponding to 2θ values of 27.89, 35.13, 41.52, 49.09, 53.83, 61.40, 73.43, and 78.03 respectively. The narrowness of the peaks signifies bigger size of nanoparticles. As the temperature increased it was observed that the broadness of the diffractograms decreased. However, the broad peak observed in Fig. 3.43(c) shows an amorphous FeSe which could be attributed to the low temperature that is used in the preparation.

The morphologies of the synthesized FeSe nanoparticles are depicted in Fig. 3.44. The TEM image of L-phenylalanine-capped FeSe nanoparticles shows cluster-like structure with spherical particles.

The observed agglomeration of the particles is consistency with the photoluminescence results where a broad peak was observed. This observation is consistency with the broader XRD peak observed for nanoparticles synthesized at 55 °C which depicts an amorphous structure of FeSe nanoparticles. Furthermore, this observation is in agreement with the optical properties obtained.

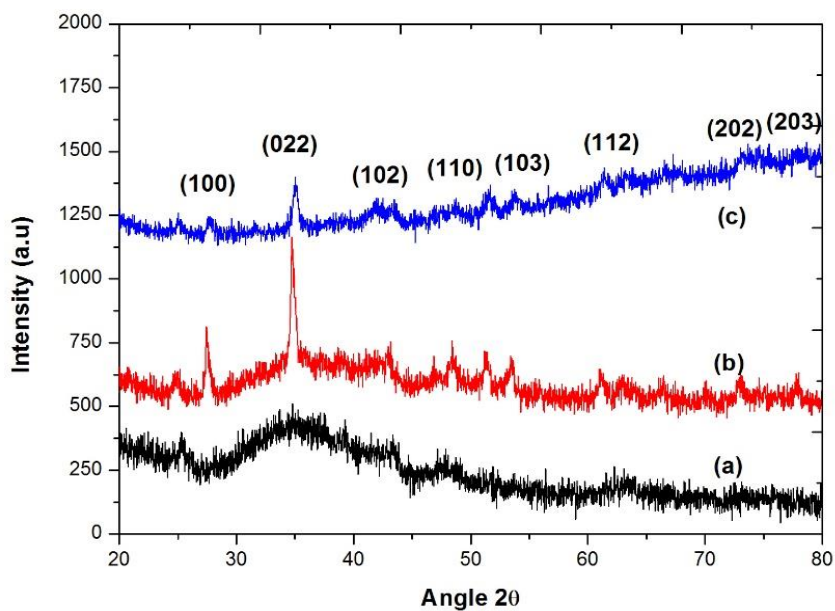


Fig. 3. 43 XRD patterns of L-phenylalanine-capped Fe_xSe_y nanoparticles prepared at (a) 55 °C, (b) 75 °C and (c) 95 °C

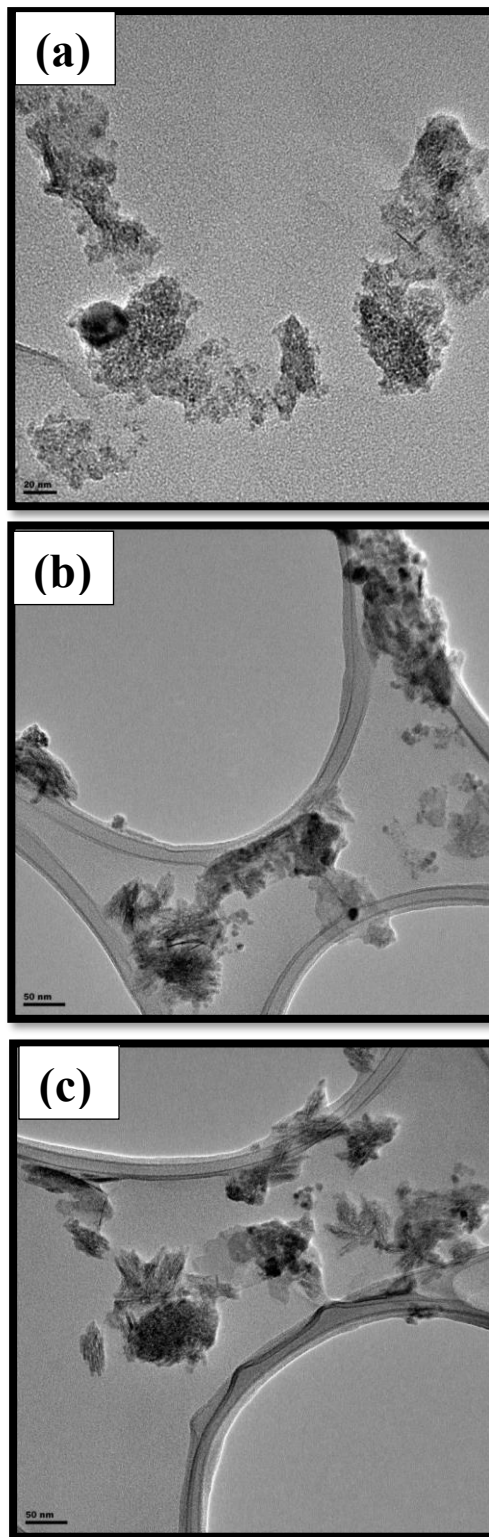


Fig. 3. 44 TEM images of L-phenylalanine-capped Fe_xSe_y nanoparticles prepared at (a) 55 °C, (b) 75 °C and (c) 95 °C

(c) Magnetic properties

To provide additional evidence for this, magnetization measurements were also performed. Fig. 3.45 shows the magnetic hysteresis curve for FeSe nanoparticles measured at room temperature. The Figure shows a twofold behavior for FeSe nanoparticles, ferromagnetic behavior in low fields and paramagnetic behavior in up fields. The hysteresis loop has remanent magnetization (M_s) and H_c values of 7.0315 emu/g and 11.654 G respectively

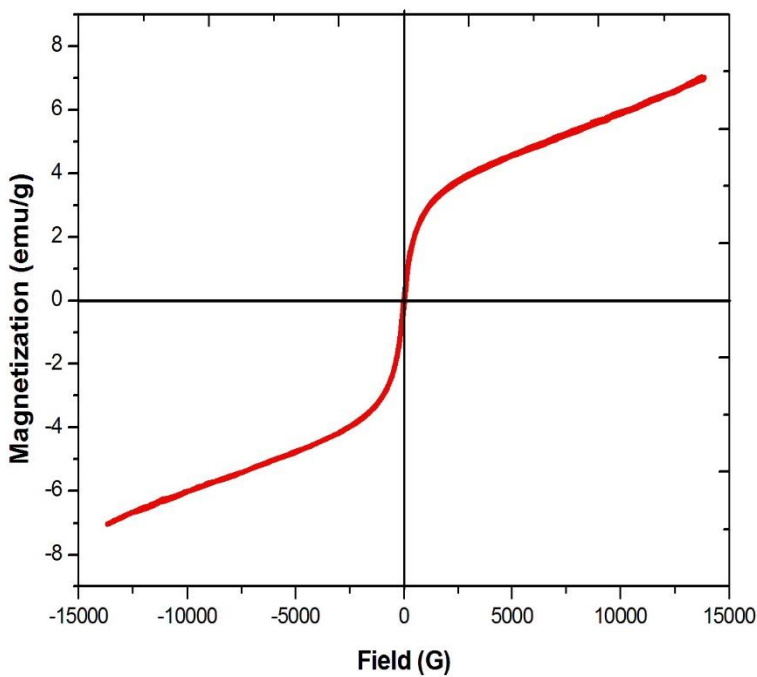


Fig. 3. 45 VSM spectra of L-phenylalanine-capped Fe_xSe_y nanoparticles prepared at 75 °C

CONCLUSIONS AND FUTURE WORK

3.4 Conclusions

Development of new synthetic protocols for nanomaterials over a range of composition, size and shapes constitutes a steadily evolving branch of nanotechnology. Chemical methodologies for the synthesis of inorganic nanoparticles are most popular and extensively practiced. However, use of corrosive chemicals and ecologically hazardous non-polar organic solvents may cause environmental damage due to their excessive use. Therefore, it has become necessary to develop alternative, environmentally friendly, “green chemistry” based methods for the synthesis of nanoparticles. Furthermore, some semiconductor nanoparticles are made water-soluble through ligand exchange and silica encapsulation. This approach results in the nanocrystals being partially soluble and have large particle sizes. In this project, we propose the direct use of hydrophilic multi-functional ligands because of its simplicity and it eliminates the possibility of having competing hydrophobic ligands on the surface of the nanocrystal and their particles sizes are comparable to conventional particles. The semiconductor nanoparticles reported in this work are water-soluble which can have potential in biological application. Different capping molecules that are water-soluble have been used to synthesize cadmium selenide, copper selenide and iron selenide nanoparticles. The capping molecules used are L-cysteine, L-glutamic acid and L-phenylalanine.

L-cysteine-capped CdSe, Cu₂Se and FeSe nanoparticles have been synthesized by the aqueous medium through a simple, non-toxic and environmentally friendly colloidal route. The use of cysteine as a stabilizing agent and the temperature of the reaction mixture are important parameters that determined the final morphology of cysteine capped metal selenide nanoparticles. The TEM results show that spherical to nanorods shaped metal selenide nanoparticles were obtained at the different reaction temperatures and the size of the nanoparticle formed were increasing as the temperature increases. A large blue-shift absorption from their bulk materials was observed for synthesized metal selenide nanoparticles. This is an indication of a decrease in particle size resulting in quantum confinement effect. The band-edges suggest that the particle size increases with an increase in reaction temperature. It was suggested that at higher temperature, the smaller

particles diminished while the larger ones grew due to the Oswald ripening. It was also observed from the experimental results that effective balance between the binding of cysteine molecule and the growth rates determine the size of the nanoparticles formed. The smaller particle size is mainly caused by the slow growth rate of cysteine at temperature 75° C or 95° C. The vibrating sample magnetometer (VSM) shows almost linear without any hysteresis loop, which indicated the absence of magnetism and exhibits paramagnetic nature than diamagnetic properties. X-ray diffraction measurement confirms the structure, single cubic for CdSe and Cu₂Se while FeSe revealed a hexagonal phase for the synthesized nanoparticles.

L-glutamic acid-capped metal nanoparticles showed moderately good capping ability, for the nanoparticles. However, CdSe nanoparticles were found to be well dispersed as compared to Cu₂Se and FeSe nanoparticles capped with L-glutamic acid molecule. The optical properties of L-glutamic acid capped metal selenide nanoparticles were blue-shifted from their bulk materials. The narrow emission peaks obtained from the photoluminescence suggests that the nanoparticles were very small and uniform which was confirmed by results obtained from TEM analysis. The morphologies of the L-phenylalanine-capped metal selenide showed a higher degree of agglomeration thought to be results of the interaction between the OH group. The L-phenylalanine ligand was less effective this could be attributed to the aromatic ring present which can create steric effect. Nevertheless, both the Cu₂Se and CdSe capped nanoparticles showed nanoparticles with improved morphology than FeSe nanoparticles

3.5 Future work and recommendations

High-quality monodispersed water-soluble semiconductor nanoparticles were successfully synthesized but there is a great need for *in vitro* and *in vivo* toxicity studies to be carried out on these particles to fully understand their potential biological applications. Furthermore, synthetic strategies of making semiconductor nanoparticles water-soluble should be employed by varying certain parameters such as reaction time, pH and precursor ratio when using amino acids as capping molecules.

3.6 References

- ADLER, J., JAYAN, A. & MELIA, C. 1999. A method for quantifying differential expansion within hydrating hydrophilic matrices by tracking embedded fluorescent microspheres. *J. Pharm. Sci.* **88** (3) pp. 371–377.
- ALIVISATOS, A.P. 1996. Semiconductor clusters nanocrystals and quantum dots. *Science* **271** p. 933.
- ALONSO, M.J., CALVO, P. & REMUN, C. 1997. Novel hydrophilic chitosan – polyethylene oxide nanoparticles as protein carriers. *J. Appl. Polym. Sci.* **63** pp. 125–132.
- ARICO, A.S., ANTONUCCI, V., GIORDANO, N., CREA, F. & ANTONUCCI, P.L. 1991. photoelectrochemical behavior of thermally activated natural pyrite-based photoelectrodes. *Mater. Chem. Phys.* **28** pp. 75–87.
- BAWENDI, M.G., CARROLL, P.J., WILSON, W.L. & BRUS, L.E. 1992. Luminescence properties of CdSe quantum crystallites : Interior and surface localized states Resonance between. *J. Phys. Chem.* **15** pp. 946–953.
- BLACK, J., LOCKWOOD, H. & MAYBURG, S. 1963. Recombination radiation in GaAs radiative recombination of GaInNP alloys lattice matched to GaAs recombination radiation in GaAs. *J. Appl. Phys.* **34** (1) p. 178.
- BRUCHEZ, M., MORONNE, M., GIN, P., WEISS, S., ALIVISATOS, A.P., ROEDERER, M., SCHRÖCK, E., WAGGONER, A., JU, J.Y., RUAN, C.C., ET AL. 1998. Semiconductor nanocrystals as fluorescent biological labels. *Science* **281** pp. 2013–6.
- BURGIN, J., LIU, M., GUYOT-SIONNEST, P., BURGIN, J., LIU, M. & GUYOT-SIONNEST, P. 2008. Dielectric sensing with deposited gold bipyramids dielectric sensing with deposited gold bipyramids. **112** pp. 19279–19282.
- CAMPOS, C.E.M., LIMA, J.C. DE, GRANDI, T.A. & MACHADO, K.D. 2004. XRD , DSC , MS and RS studies of Fe 75 Se 25 iron selenide prepared by mechano-synthesis. *J. Magn. Magn. Mater.* **270** pp. 89–98.
- CAMPOS, C.E.M., LIMA, J.C. DE, GRANDI, T.A., MACHADO, K.D. & PIZANI, P.S. 2003. GaSe formation by mechanical alloying Ga 50 Se 50 mixture. *Solid State Commun.* **126** pp. 611–615.
- CAO, M., CAO, C., LIU, M., WANG, P. & ZHU, C. 2009. Selective fluorometry of cytochrome c using glutathione-capped CdTe quantum dots in weakly basic medium. *Microchim. Acta* **165** (3–4) pp. 341–346.
- CHAN, D., SUK, W., HYUN, B., KOUN, H. & HEE, C. 2007. Fabrication of the hybrid ZnO LED structure grown on p-type GaN by metal organic chemical vapor deposition. *Phys. B* **402** pp. 386–390.

- CHAN, W.C.W., NIE, S., CHAN, W.C.W. & NIE, S. 1998. Quantum dot bioconjugates for ultrasensitive nonisotopic detection. *Science* **281** (2016–2018).
- CHATTERJEE, A., PRIYAM, A., DAS, S.K. & SAHA, J.A. 2006. Size tunable synthesis of cysteine-capped CdS nanoparticles by γ -irradiation. *Colloid Interface Sci.* **294** pp. 334–342.
- CHUMANOV, G., SOKOLOV, K., GREGORY, B., OSIFCHIN, R.G., REIFENBERGER, R., AL-, M.M., SHENTON, B.W., DAVIS, S.A. & MANN, S. 1999. Directed self-assembly of nanoparticles into macroscopic materials using antibody-antigen recognition. *Adv. Mater.* **11** (6) pp. 449–452.
- CLAPP, A.R., MEDINTZ, I.L., MAURO, J.M., FISHER, B.R., BAWENDI, M.G. & MATTOUSSI, H. 2004. Fluorescence resonance energy transfer between quantum dot donors and dye-labeled protein acceptors. *J. Am. Chem. Soc.* **126** (126) pp. 301–310.
- CRAFORD, M.G. 1992. LEDs Challenge the Incandescents. *IEEE Circuits Devices* **8** p. 25.
- DABBOUSI, B.O., MIKULEC, F. V, HEINE, J.R., MATTOUSSI, H., OBER, R., JENSEN, K.F. & BAWENDI, M.G. 1997. (CdSe) ZnS core - shell quantum dots : synthesis and characterization of a size series of highly luminescent nanocrystallites. *J. Phys. Chem. B.* **9463** (97) pp. 9463–9475.
- DE, M., GHOSH, P.S. & ROTELLO, V.M. 2008. Applications of nanoparticles in biology. *Adv. Mater.* **20** (22) pp. 4225–4241.
- DENG, D.W., YU, J.S. & PAN, Y. 2006. Water-soluble CdSe and CdSe/CdS nanocrystals: A greener synthetic route. *J. Colloid Interface Sci.* **299** (1) pp. 225–232.
- DUBERTRET, B., DUBERTRET, B., SKOURIDES, P. & NORRIS, D.J. 2002. *In Vivo* imaging of quantum dots encapsulated in phospholipid micelles. *Science* **298** pp. 1759–1762.
- ELGHANIAN, R., STORHOFF, J.J., MUCIC, R.C., LETSINGER, R.L. & MIRKIN, C.A. 1997. Selective colorimetric detection of polynucleotides based on the distance-dependent optical properties of gold nanoparticles. *Science* **277** pp. 1078–1081.
- ENNAOUI, A., FIECHTER, S., PETTENKOFER, C., BILKER, K., BRONOLD, M., CH, H. & TRIBUTSCH, H. 1993. Iron disulfide for solar energy conversion. *Sol. Energy Mater. Sol. Cells* **29** pp. 289–370.
- FILANKEMBO, A., GIORGIO, S., LISIECKI, I., PILENI, M.P., JUSSIEU, P., CEDEX, F.-P. & LUMINY, C. DE. 2003. Is the anion the major parameter in the shape control of nanocrystals. *J Phys Chem B* pp. 7492–7500.
- GAN, A., SUBSTRATES, A.G.N., WANG, X., SONG, J., LI, P., RYOU, J.H., DUPUIS, R.D., SUMMERS, C.J. & WANG, Z.L. 2005. Growth of uniformly aligned ZnO nanowire heterojunction arrays on GaN, AlN, and Al_{0.5}Ga_{0.5}N substrates. *J. Am. Chem. Soc.* **127** pp. 7920–7923.
- GAO, H., YAN, F., LI, J. & ZENG, Y. 2007. Synthesis and characterization of ZnO nanorods and

- nanoflowers grown on GaN-based LED epiwafer using a solution. *J. Phys. D: Appl. Phys* **40** (3654).
- GAPONIK, N., TALAPIN, D. V., ROGACH, A.L., HOPPE, K., SHEVCHENKO, V., KORNOWSKI, A., EYCHMILLER, A., WELLER, H., SHEVCHENKO, E. V & EYCHMU, A. 2002. Thiol-capping of CdTe nanocrystals : An alternative to organometallic synthetic routes. *J Phys Chem B* pp. 7177–7185.
- GARCÍA, V., NAIR, P.. & NAIR, M.T. 1999. Copper selenide thin films by chemical bath deposition. *J. Cryst. Growth* **203** (1–2) pp. 113–124.
- GERION, D., PINAUD, F., WILLIAMS, S.C., PARAK, W.J., ZANCHET, D., WEISS, S. & ALIVISATOS, A.P. 2001. Synthesis and properties of biocompatible water-soluble silica-coated CdSe / ZnS semiconductor quantum dots. *J. Phys. Chem. B* **105** pp. 8861–8871.
- GIUNCHEDI, P., CONTE, U., CHETONI, P. & SAETTONE, M.F. 1999. Pectin microspheres as ophthalmic carriers for piroxicam : Evaluation *in vitro* and *in vivo* in albino rabbits. *Eur. J. Pharm. Sci.* **9** pp. 1–7.
- GU, H., ZHENG, R., ZHANG, X. & XU, B. 2004. Facile one-pot synthesis of bifunctional heterodimers of nanoparticles : A conjugate of quantum dot and magnetic nanoparticles. *J Phys Chem B* **126** pp. 5664–5665.
- GREEN, M. & O'BRIEN, P. 1999. Recent advances in the preparation of semiconductors as isolated nanometric particles: New routes to quantum dots. *Chem. Commun.* (22) pp. 2235–2241.
- HAN, H., SHENG, Z. & LIANG, J. 2006. A novel method for the preparation of water-soluble and small-size CdSe quantum dots. *Mater. Lett.* **60** pp. 3782–3785.
- HARAM, S.K. & SANTHANAM, K.S. V. 1992. Electroless deposition on copper substrates and characterization of thin films of copper (I) selenide. *Mater. Res. Bull.* **27** (10) pp. 1185–1191.
- HARMA, H., LEHTINEN, P., TAKALO, H. & LOVGREN, T. 1999. Immunoassay on a single microparticle : The effect of particle size and number on a miniaturized time-resolved fluorometric assay of free prostate-specific antigen. *Anal. Chim. Acta* **387** pp. 11–19.
- HENGLEIN, A. 1984. Catalysis of photochemical reactions by colloidal semiconductors. *Pure Appl. Chem* **56** (9) pp. 1215–1224.
- HEYDING, R.D.. 1966. The copper/selenium system. *Can. J. Chem.* **44** pp. 1233–1236.
- HINES, M. A & GUYOTSIONNEST, P. 1996. Synthesis and characterization of strongly luminescing ZnS- capped CdSe nanocrystals. *J. Phys. Chem.* **100** (2) pp. 468–471.
- HSU, F., LUO, J., YEH, K., CHEN, T., HUANG, T., WU, P.M., LEE, Y., HUANG, Y., CHU, Y., YAN, D., ET AL. 2008. Superconductivity in the PbO-type structure -FeSe. **105** pp. 14262–14264.

- JOHNSON, I. & LA MER, V. 1946. The Determination of the particle size of monodispersed systems by the scattering of light. *J. Am. Chem. Soc.* **69** (15) pp. 1184–1192.
- JUNGWIRTH, T., MACDONALD, A.H. & ZIESE, M. 2002. Ferromagnetic semiconductors. *Semicond. Sci. Technol.* **17** pp. 377–392.
- KAITO, C., NONAKA, A., KIMURA, S., SUZUKI, N. & SAITO, Y. 1998. Size effect on solid-solid reaction growth between Cu film and Se particles. *J. Cryst. Growth* **186** (3) pp. 386–392.
- KARAMI, Z. & SHEIKHSHOAIE, I. 2017. rGO/ZnO Nanocomposite Modified Carbon Paste Electrode as Sensor for Tyrosine Analysis. *Anal. Bioanal. Electrochem* **9** (7) pp. 834–840.
- KAVIYARASU, K., AYESHAMARIAM, A., MANIKANDAN, E., KENNEDY, J., LADCHUMANANANDASIVAM, R., UMBELINO GOMES, U., JAYACHANDRAN, M. & MAAZA, M. 2016. Solution processing of CuSe quantum dots: Photocatalytic activity under RhB for UV and visible-light solar irradiation. *Mater. Sci. Eng. B Solid-State Mater. Adv. Technol.* **210** pp. 1–9.
- KEMMLER, M., LAZELL, M., BRIEN, P.O., OTWAY, D.J. & PARK, J. 2002. The growth of thin films of copper chalcogenide films by MOCVD and AACVD using novel single-molecule precursors. *J. Mater. Sci. Mater. Electron.* **13** pp. 531–535.
- KIM, E.C., KANG, S.G., CHO, I.H., HWANG, Y.S., GOOK, H. & KIM, J.G. 1997. Crystallographic and magnetic structures of Fe₇Se₈ at low temperature (4 – 78 K). *Am. Inst. Phys.* **81** (8) pp. 4131–4133.
- KIM, J.Y., HIRAMATSU, H. & OSTERLOH, F.E. 2005. Planar polarized light emission from CdSe nanoparticle clusters. *J. Am. Chem. Soc.* **127** (44) pp. 15556–15561.
- KIM, S. & BAWENDI, M.G. 2003. Oligomeric ligands for luminescent and stable nanocrystal quantum dots. *J. Am. Chem. Soc.* **125** pp. 14652–14653.
- KIRCHER, M.F., WEISSLEDER, R. & JOSEPHSON, L. 2004. A dual fluorochrome probe for imaging proteases. *Bioconjugate Chem* **15** pp. 242–248.
- KO, R., WORD, R.C. & GODINEZ, M. 2005. Ultraviolet electroluminescence from ZnO/polymer heterojunction light-emitting diodes. *Nano Lett.* **5** (10) pp. 2005–2008.
- KOBAYASHI, T., EGAWA, S., SAWADA, M. & HONDA, T. 2007. GaN-based Schottky-type UV light-emitting diodes and their integration for flat-panel displays. *Phys. Status Sol. C* **4** (1) pp. 61–64.
- KONESWARAN, M. & NARAYANASWAMY, R. 2009. Sensors and actuators B : Chemical l - cysteine-capped ZnS quantum dots based fluorescence sensor for Cu²⁺ ion. *Sensors Actuators B* **139** pp. 104–109.
- KUMAR, P. & SINGH, K. 2009. Element directed aqueous solution synthesis of copper telluride nanoparticles, characterization, and optical properties. *Cryst. Growth Des.* **9** (7) pp. 3089–

3094.

- KUMAR, P. & SINGH, K. 2010. Structural, optical and raman studies of template-free solvothermally synthesized ZnSe/ZnSe: Ce³⁺ nanoparticles. *Curr. Nanosci.* **6** (4) pp. 402–407.
- KUMAR, P. & SINGH, K. 2011. Synthesis, characterizations, and optical properties of copper selenide quantum dots. *Struct. Chem.* **22** (1) pp. 103–110.
- KUMAR, P. & SINGH, K. 2010. Synthesis of CdSe Nanoparticles at 50 °C by Wet Chemical Method. *Curr. Nanosci.* **6** (1) pp. 89–93.
- KUMAR, P., SINGH, K. & SRIVASTAVA, O.N. 2010. Template free-solvothermally synthesized copper selenide (CuSe, Cu_{2-x}Se, Cu₂Se and Cu₂Se) hexagonal nanoplates from different precursors at low temperature. *J. Cryst. Growth* **312** (19) pp. 2804–2813.
- KUNKEL, R., POELSEMA, B., VERHEIJ, L.K. & COMSA, G. 1990. Reentrant layer-by-layer growth during molecular-beam epitaxy of metal-on-metal substrates. *Phys. Rev. Lett.* **65** (6) pp. 733–736.
- KUNO, M. 2003. Modeling distributed kinetics in isolated semiconductor quantum dots. *Phys. Rev. B* **67** pp. 1–15.
- LAKSHMI, M., BINDU, K., BINI, S., VIJAYAKUMAR, K.P., KARTHA, C.S., ABE, T. & KASHIWABA, Y. 2001. Reversible Cu_{2-x}Se Cu₃Se₂ phase transformation in copper selenide thin films prepared by chemical bath deposition. *Thin Solid Films* **386** (1) pp. 127–132.
- LAKSHMI, M., BINDU, K., BINI, S., VIJAYAKUMAR, K.P., SUDHA KARTHA, C., ABE, T. & KASHIWABA, Y. 2000. Chemical bath deposition of different phases of copper selenide thin films by controlling bath parameters. *Thin Solid Films* **370** (1) pp. 89–95.
- LAKSHMIKUMAR, S.T. & RASTOGI, A.C. 1994. Selenization of Cu and in thin-films for the preparation of selenide photo-absorber layers in solar-cells using Se vapor source. *Sol. Energy Mater. Sol. Cells* **32** (1) pp. 7–19.
- LANDIN, L., MILLER, M., PISTOL, M., PRYOR, C. & SAMUELSON, L. 1998. Optical studies of individual InAs quantum dots in GaAs few particle effects. *Science* **280** pp. 262–264.
- LEE, B.S., CHO, S. & CHEON, J. 2003. Anisotropic shape control of colloidal inorganic nanocrystals. *Adv. Mater.* **15** (5) pp. 441–444.
- LI, H., SHIH, W. & SHIH, W. 2007. Synthesis and characterization of aqueous carboxyl-capped CdS quantum dots for bioapplications. *Ind. Eng. Chem. Res.* **46** pp. 2013–2019.
- LI, L. & REISS, P. 2008. One-pot synthesis of highly luminescent InP/ZnS nanocrystals without precursor injection. *J. Am. Chem. Soc.* **130** pp. 11588–11589.
- LI, L., REISS, P. & PROTIE, M. 2009. Reviews Core/Shell semiconductor nanocrystals. *Nano-*

- micro small.* (2) pp. 154–168.
- LI, Y., WANG, J., DENG, Z., WU, Y., SUN, X., YU, D. & YANG, P.. 2001. Bismuth nanotubes: A rational low-temperature synthetic route. *J. Am. Chem. Soc.* **123** (40) pp. 9904–9905.
- LI, Y.D., DING, Y., QIAN, Y.T., ZHANG, Y. & YANG, L. 1998. A solvothermal elemental reaction to produce nanocrystalline ZnSe. *Inorg. Chem.* **37** (12) pp. 2844–2845.
- LI, Y.D., DING, Y. & WANG, Z.Y. 1999. A novel chemical route to ZnTe semiconductor nanorods. *Adv. Mater.* **11** (10) p. 847–851.
- LIEBER, C.M. 1998. One-dimensional nanostructures: Chemistry, physics & applications. *Solid State Commun.* **107** (11) pp. 607–616.
- LIPPENS, P. & LANNOO, M. 1989. Calculation of the band gap for small CdS and ZnS crystallites. *Am. Phys. Soc.* **39** (15) pp. 10935–10942.
- LIU, I., LO, H., CHIEN, C., LIN, Y., CHEN, C., CHEN, Y., SU, W. & LIOU, S. 2008. Enhancing photoluminescence quenching and photoelectric properties of CdSe quantum dots with hole accepting ligands. *J. Mater. Chem.* pp. 675–682.
- LIU, K., LIU, H., WANG, J. & SHI, L. 2009. Synthesis and characterization of Cu₂Se prepared by hydrothermal co-reduction. *J. Alloys Compd.* **484** pp. 674–676.
- LIU, T., HUANG, Z., WANG, H., WANG, J., LI, X., ZHAO, Y. & LUO, Q. 2006. Temperature-dependent photoluminescence of water-soluble quantum dots for a bioprobe. *Anal. Chim. Acta* **559** pp. 120–123.
- LIU, Y., KIM, M., WANG, Y. & WANG, Y.A. 2006. Highly luminescent, stable, and water-soluble CdSe/CdS core-shell dendron nanocrystals with carboxylate anchoring groups. *Langmuir.* (12) pp. 6341–6345.
- LIU, Y., YAO, D., SHEN, L., ZHANG, H., ZHANG, X. & YANG, B. 2012. Alkylthiol-enabled Se powder dissolution in oleylamine at room temperature for the phosphine-free synthesis of copper-based quaternary selenide nanocrystals. *J. Am. Chem. Soc.* **134** (17) pp. 7207–7210.
- LUCCARDINI, C., TRIBET, C., VIAL, F. & DAHAN, M. 2006. Size, charge, and interactions with giant lipid vesicles of quantum dots coated with an amphiphilic macromolecule. *Langmuir.* **22** (5) pp. 2304–2310.
- LUBYSHEV, D.I., GONZÁLEZBORRERO, P.P., MAREGA, E., PETITPREZ, E. & SCALA, N. LA. 1996. exciton localization and temperature stability in self-organized InAs quantum dots. *Appl. Phys. Lett.* **68** (2) pp. 205–207.
- MAHAJAN, S., RANI, M., DUBEY, R.B. & MAHAJAN, J. 2013. synthesis of cdse crystal using hot injection method. *Int. J. Latest Res. Sci. Technol.* **2** (1) pp. 518–521.
- MALIK, M.A., BRIEN, P.O. & REVAPRASADU, N. 2000. Semiconductor nanoparticles: their

- properties, synthesis and potential for application. *S. Afr. J. Sci.* **96** pp. 55–60.
- MALIK, M.A., REVAPRASADU, N. & O'BRIEN, P. 2001. Air-stable single-source precursors for the synthesis of chalcogenide semiconductor nanoparticles. *Chem. Mater.* **13** (3) pp. 913–920.
- MANNA, L., SCHER, E.C. & ALIVISATOS, A. P. 2000. Synthesis of soluble and processable rod-, arrow-, teardrop-, and tetrapod-shaped CdSe nanocrystals. *J. Am. Chem. Soc.* **122** (51) pp. 12700–12706.
- MANNA, L., SCHER, E.C., LI, L., ALIVISATOS, A.P., SCIENCES, M., DI, V. & BERKELEY, L. 2002. Epitaxial growth and photochemical annealing of graded CdS/ZnS shells on colloidal CdSe nanorods. *J. Am. Chem. Soc.* **124** (24) pp. 7136–7145.
- MATIJEVIE, E. 1986. Monodispersed colloids : Art and science. *Langmuir.* **2** pp. 12–20.
- MATTOUSSI, H., MAURO, J.M., GOLDMAN, E.R., ANDERSON, G.P., SUNDAR, V.C., MIKULEC, F. V & BAWENDI, M.G. 2000. Self-assembly of CdSe-ZnS quantum dot bioconjugates using an engineered recombinant protein. *J. Am. Chem. Soc.* **122** pp. 12142–12150.
- MEIXNER, M., SCHÖLL, E., SHCHUKIN, V. & BIMBERG, D. 2002. Erratum: self-assembled quantum dots: Crossover from kinetically controlled to thermodynamically limited growth. *Phys. Rev. Lett.* **88** (5) p. 59901.
- LA MER, V.. & DINEGAR, R. 1950. Theory, production and mechanism of formation of monodispersed hydrosols. *J. Am. Chem. Soc.* **72** (8) pp. 4847–4854.
- MITCHELL, G.P., MIRKIN, C.A. & LETSINGER, R.L. 1999. Programmed assembly of DNA functionalized quantum dots. *J. Am. Chem. Soc.* **121** pp. 8122–8123.
- MITZI, B.D.B., YUAN, M., LIU, W., KELLOCK, A.J., CHEY, S.J., DELINE, V. & SCHROTT, A.G. 2008. A high-efficiency solution-deposited thin-film photovoltaic device. *Adv. Mater.* **20** pp. 3657–3662.
- MOHAMED, N.B.H., HAOUARI, M., ZAABOUB, Z., NAFOUTTI, M., HASSEN, F., MAAREF, H. & OUADA, H. BEN. 2014. Time resolved and temperature dependence of the radiative properties of thiol-capped CdS nanoparticles films. *J Nanopart Res* **16** p. 2242.
- MAHMOUD, W.E., AL-AMRI, A.M. & YAGHMOUR, S.J. 2012. Low temperature synthesis of CdSe capped 2-mercaptoethanol quantum dots. *Opt. Mater. (Amst).* **34** (7) pp. 1082–1086.
- MOLOTO, N., REVAPRASADU, N., MOLOTO, M.J., BRIEN, P.O. & RAFTERY, J. 2009. N , N '-diisopropylthiourea and N, N '-dicyclohexyl-thiourea zinc (II) complexes as precursors for the synthesis of ZnS nanoparticles. *S. Afr. J. Sci.* **105** pp. 258–263.
- MUCIC, R.C., STORHOFF, J.J., MIRKIN, C.A. & LETSINGER, R.L. 1998. DNA-directed synthesis of binary nanoparticle network materials. *J. Am. Chem. Soc.* **120** pp. 12674–12675.

- MURRAY, C., KAGAN, C. & BAWENDI, M. 2000. Synthesis and characterization of monodisperse nanocrystals and close-packed nanocrystal assemblies. *Annu. Rev. Mater. Sci* **30** pp. 545–610.
- MURRAY, C.B., NORRIS, D.J. & BAWENDI, M.G. 1993. Synthesis and characterization of nearly monodisperse CdE (E = S, Se, Te) Semiconductor Nanocrystallites. *J. Am. Chem. Soc.* **115** pp. 8706–8715.
- NAKAYAMA, H., WADA, N. & TSUHAKE, M. 2004. Intercalation of amino acids and peptides into Mg-Al layered double hydroxide by reconstruction method. *Int. J. Pharm.* **269** pp. 469–478.
- NAOI, Y., IKEDA, K., HAMA, T., ONO, K., CHOI, R., FUKUMOTO, T. & NISHINO, K. 2007. Blue light emitting diode fabricated on a-plane GaN film over r-sapphire substrate and on a-plane bulk GaN substrate. *Phys. Status Solid C* **4** (7) p. 2810.
- NAYAK, N.C. & SHIN, K. 2006. Synthesis of L-phenylalanine stabilized gold nanoparticles and their thermal stability. *J. Nanosci. Nanotechnol.* **6** (11) pp. 3512–3516.
- NIE, Z., FAVA, D., KUMACHEVA, E., ZOU, S., WALKER, G.C. & RUBINSTEIN, M. 2007. Self-assembly of metal–polymer analogues of amphiphilic triblock copolymers. *Nat. Mater.* **6** p. 609.
- NIRMAL, M., NORRIS, D.J., KUNO, M., BAWENDI, M.G., EFROS, A.L. & ROSEN, M. 1995. Observation of the “dark exciton” in CdSe quantum dots. *Phys. Rev. Lett.* **75** (20) pp. 3728–3731.
- NTZIACHRISTOS, V., BREMER, C. & WEISSLEDER, R. 2003. Fluorescence imaging with near-infrared light : New technological advances that enable in vivo molecular imaging. *Eur. Radiol* **13** pp. 195–208.
- NTZIACHRISTOS, V., SCHELLENBERGER, E.A., RIPOLL, J., YESSAYAN, D., GRAVES, E., BOGDANOV, A., JOSEPHSON, L. & WEISSLEDER, R. 2004. Visualization of antitumor treatment by means of fluorescence molecular tomography with an annexin V–Cy5.5 conjugate. *Proc. Natl. Acad. Sci* **101** pp. 12294–12299.
- O' BRIEN, P.O. & MALIK, M.A. 2005. Precursor routes to semiconductor quantum dots. *Phosphorus, Sulfur, and Silicon.* **180** pp. 689–712.
- OSAKI, F., KANAMORI, T., SANDO, S., SERA, T. & AOYAMA, Y. 2004. A quantum dot conjugated sugar ball and its cellular uptake: On the size effects of endocytosis in the subviral region. *J. Am. Chem. Soc.* **126** pp. 6520–6521.
- OUERTANI, B., OUERFELLI, J., SAADOUN, M., BESSA, B.R., HAJJI, M. & KANZARI, M. 2005. Transformation of amorphous iron oxide films pre-deposited by spray pyrolysis into FeS₂-pyrite films. *Mater. Lett.* **59** pp. 734–739.
- OUERTANI, B., OUERFELLI, J., SAADOUN, M. & BESSAI, B. 2005. Transformation of amorphous iron oxide thin films predeposited by spray pyrolysis into a single FeSe₂-phase by

- selenisation. *Sol. Energy Mater. Sol. Cells* **87** pp. 501–511.
- PACHOLSKI, C., KORNOWSKI, A. & WELLER, H. 2002. Self-assembly of ZnO: From nanodots to nanorods. *Angew. Chemie - Int. Ed.* **41** (7) pp. 1188–1191.
- PAN, D., WANG, Q., JIANG, S., JI, X. & AN, L. 2007. Low-temperature synthesis of oil-soluble CdSe, CdS, and CdSe/CdS core-shell nanocrystals by using various water-soluble anion precursors. *J. Phys. Chem. C* **111** (15) pp. 5661–5666.
- PARK, S., KIM, S. & LEE, S. 2000. Synthesis and magnetic studies of uniform iron nanorods and nanospheres. *J. Am. Chem. Soc.* **122** (35) pp. 8581–8582.
- PATHAK, S., CHOI, S. & ARNHEIM, N. 2001. Hydroxylated quantum dots as luminescent probes for in situ hybridization. *J. Am. Chem. Soc.* **123** pp. 4103–4104.
- PAWAR, S.M., MOHOLKAR, A. V, SURYAVANSHI, U.B., RAJPURE, K.Y. & BHOSALE, C.H. 2007. Electrosynthesis and characterization of iron selenide thin films. *Sol. Energy Mater. Sol. Cells* **91** pp. 560–565.
- PENG, X., MANNA, L., YANG, W., WICKHAM, J., SCHER, E., KADAVANICH, A. & ALIVISATOS, A.P. 2000. Shape control of CdSe nanocrystals. *Nature* **404** (6773) pp. 59–61.
- PENG, Z.A. & PENG, X. 2001. Formation of high-quality CdTe, CdSe, and CdS nanocrystals using CdO as precursor. *J. Am. Chem. Soc.* **123** pp. 183–184.
- PENG, Z.A. & PENG, X. 2002. Nearly monodisperse and shape-controlled CdSe nanocrystals via alternative routes: Nucleation and growth. *J. Am. Chem. Soc.* **124** pp. 3343–3353.
- PINNA, N., WEISS, K., URBAN, J. & PILENI, M. 2001. Triangular CdS nanocrystals: Structural and optical studies. *Adv. Mater.* **13** (4) pp. 261–264.
- POUDEL, B., HAO, Q., MA, Y., LAN, Y., MINNICH, A., YU, B., YAN, X., DRESSELHAUS, M.S., CHEN, G. & REN, Z. 2008. High-thermoelectric performance of nanostructured bismuth antimony telluride bulk alloys. *Science* **320** pp. 634–638.
- PRIESTER, C. & LANNOO, M. 1995. Origin of self-assembled quantum dots in highly mismatched heteroepitaxy. *Phys. Rev. Lett.* **75** (1) pp. 93–96.
- QIN, Y., WANG, X. & WANG, Z.L. 2008. Microfibre–nanowire hybrid structure for energy scavenging. *Nature* **451** pp. 809–814.
- QU, L. & PENG, X. 2002. Control of photoluminescence properties of CdSe nanocrystals in growth. *J. Am. Chem. Soc.* **124** (9) pp. 2049–2055.
- RAAB, R.M. & STEPHANOPOULOS, G. 2004. Dynamics of gene silencing by RNA interference. *Biotechnol. Bioeng.* **88** (1) pp. 122–132.
- REISS, P. & PRON, A. 2002. Highly luminescent CdSe/ZnSe core/shell nanocrystals of low size

- dispersion. *Nano Lett.* **2** (7) pp. 781–784.
- ROGACH, A.L., KORNOWSKI, A., GAO, M., EYCHMÜLLER, A. & WELLER, H. 1999. Synthesis and characterization of a size series of extremely small thiol-stabilized CdSe nanocrystals. *J. Phys. Chem. B* **103** (16) pp. 3065–3069.
- ROSSETTI, R., ELLISON, J.L., GIBSON, J.M. & BRUS, L.E. 1984. Size effects in the excited electronic states of small colloidal CdS crystallites. *J. Chem. Phys* **80** (9) pp. 4464–4469.
- ROSSETTI, R., HULL, R., GIBSON, J.M., BRUS, L.E., ROSSETTI, R., HULL, R., GIBSON, J.M. & BRUS, L.E. 1985. Hybrid electronic properties between the molecular and solid state limits : Lead sulfide and silver halide crystallites. *J. Chem. Phys* **83** (3) pp. 1406–1410.
- SALAVATI-NIASARI, M., DAVAR, F. & LOGHMAN-ESTARKI, M.R. 2010. Controllable synthesis of thioglycolic acid capped ZnS(Pn)_{0.5} nanotubes via simple aqueous solution route at low temperatures and conversion to wurtzite ZnS nanorods via thermal decompose of precursor. *J. Alloys Compd.* **494** (1–2) pp. 199–204.
- SANTRA, S., WANG, K., TAPEC, R. & TAN, W. 2001. Development of novel dye-doped silica nanoparticles for biomarker application. *J. Biomed. Opt.* **6** (2) pp. 160–166.
- SANYAL, A., BALA, T., AHMED, S., SINGH, A., PITERINA, A. V, MCGLOUGHLIN, T.M., LAFFIR, R. & RYAN, K.M. 2009. Water dispersible semiconductor nanorod assemblies via a facile phase transfer and their application as fluorescent biomarkers. *J. Mater. Chem* **19** pp. 8974–8981.
- SAUNDERS, A.E., GHEZELBASH, A., SOOD, P. & KORGEL, B.A. 2008. Synthesis of high aspect ratio quantum-size CdS nanorods and their surface-dependent photoluminescence. *Langmuir.* **24** pp. 9043–9049.
- SCHÇNING, M.J. & KLOCK, P. 2007. About 20 years of silicon-based thin-film sensors with chalcogenide glass materials for heavy metal analysis : Technological aspects of fabrication and miniaturization. *Electroanalysis.* **19** pp. 2029–2038.
- SCHELLENBERGER, E.A., SOSNOVIK, D., WEISSLEDER, R. & JOSEPHSON, L. 2004. Magneto/Optical Annexin V, a Multimodal Protein. *Bioconjugate Chem* **15** pp. 1062–1067.
- SEGUINI, G., CASTRO, C., SCHAMM-CHARDON, S., BENASSAYAG, G., PELLEGRINO, P. & PEREGO, M. 2013. Scaling size of the interplay between quantum confinement and surface related effects in nanostructured silicon. *Appl. Phys. Lett.* **103** (2) pp. 023103-5.
- SELVAKANNAN, P.R., MANDAL, S., PHADTARE, S., GOLE, A., PASRICHA, R., ADYANTHAYA, S.D. & SASTRY, M. 2004. Water-dispersible tryptophan-protected gold nanoparticles prepared by the spontaneous reduction of aqueous chloraurate ions by the amino acid. *J. Colloid Interface Sci.* **269** (1) pp. 97–102.
- SHAFIZADE, R.B.R., IVANOVA, I.V.I. & KAZINETS, M.M.M. 1978. Electron diffraction study of phase transformations of the compound CuSe. *Thin Solid Films* **55** (2) pp. 211–220.

- SHENG, W., KIM, S., LEE, J., KIM, S., JENSEN, K. & BAWENDI, M.G. 2006. In-Situ encapsulation of quantum dots into polymer microspheres. *Langmuir*. **22** pp. 3782–3790.
- SHIH, I. 2001. The production of poly-(glutamic acid) microorganisms and its various applications. *Bioresour. Technol.* **79** pp. 207–225.
- SUN, X.W., HUANG, J.Z., WANG, J.X. & XU, Z. 2008. A ZnO nanorod inorganic/organic heterostructure light-emitting diode emitting at 342 nm 2008. *Nano Lett.* **8** (4) pp. 1219–1223.
- SUZUKI, A., TANAKA, T., MATSUNAMI, H. & IKEDA, M. 1977. Sic blue LED's by liquid-phase epitaxy. *IEEE Tran. Electr. Devices* **24** (958).
- TAKEMURA, Y., SUTO, H., HONDA, N., KAKUNO, K., SAITO, K., TAKEMURA, Y., SUTO, H., HONDA, N. & KAKUNO, K. 1997. Characterization of FeSe thin films prepared on GaAs substrate by selenization technique characterization of FeSe thin films prepared on GaAs substrate by selenization technique. *Am. Inst. Phys.* **81** (8) pp. 5177–5179.
- TALAPIN, D. V, ROGACH, A.L., KORNOWSKI, A., HAASE, M. & WELLER, H. 2001. Highly luminescent monodisperse CdSe and CdSe/ZnS nanocrystals synthesized in a hexadecylamine-trioctylphosphine oxide-trioctylphosphine mixture. *Nano Letters*. **1** (4) pp. 207–211.
- TANG, Z. 2002. Spontaneous organization of single CdTe nanoparticles into luminescent nanowires. *Science* **297** pp. 237–240.
- TAO, A.R., HABAS, S. & YANG, P. 2008. Reviews shape control of colloidal metal nanocrystals. *Nano-micro small*. **4** (3) pp. 310–325.
- THANIKAIKARASAN, S., MAHALINGAM, T., SUNDARAM, K., KATHALINGAM, A., DEAK, Y. & KIM, T. 2009. Growth and characterization of electrosynthesized iron selenide thin films. **83** (7) pp. 1066–1072.
- TIAN, X., WEN, J., WANG, S., HU, J., LI, J. & PENG, H. 2016. Starch-assisted synthesis and optical properties of ZnS nanoparticles. *Mater. Res. Bull.* **77** pp. 279–283.
- TOHGHA, U., DEOL, K.K., PORTER, A.G., BARTKO, S.G., CHOI, J.K., LEONARD, B.M., VARGA, K., KUBELKA, J., MULLER, G. & BALAZ, M. 2013. ligand induced circular dichroism and circularly polarized luminescence in CdSe quantum dots. *Acs. Nano* **7** (12) pp. 11094–11102.
- TRINDADE, T. & BRIEN, P.O. 1997. Synthesis of CdS and CdSe nanocrystallites using a novel single-molecule precursors approach. *Chem. Mater.* **9** (20) pp. 523–530.
- TRINDADE, T. & O' BRIEN, P. 1996. A single source approach to the synthesis of CdSe nanocrystallites. *J. Adv. Mater.* **8** (2) pp. 161–163.

- TRINDADE, T., PEDROSA DE JESUS, J. & O' BRIEN, P. 1994. preparation of zinc oxide and zinc sulfide powders by controlled precipitation from aqueous solution. *J. Mater. Chem* **4** (10) pp. 1611–1617.
- WANG, D., HE, J., ROSENZWEIG, N. & ROSENZWEIG, Z. 2004. Superparamagnetic Fe₂O₃ Beads-CdSe/ZnS quantum dots core-shell nanocomposite particles for cell separation. *Nano Lett.* **4** (3) pp. 409–413.
- WANG, Q., YE, F., LIU, P., MIN, X. & LI, X. 2011. Conjugation and fluorescence quenching between bovine serum albumin and L-cysteine capped CdSe/CdS quantum dots. *Protein Pept Lett* **18** (4) pp. 410–414.
- WANG, W., GENG, Y., YAN, P., LIU, F., XIE, Y. & QIAN, Y. 1999. Synthesis and characterization of MSe (M=Zn, Cd) nanorods by a new solvothermal method. *Inorg. Chem. Commun.* **2** (3) pp. 83–85.
- WENG, J. & REN, J. 2006. Luminescent quantum dots : A very attractive and promising tool in biomedicine. *Curr. Med. Chem.* **13** (8) pp. 897–909.
- WILLIAMS, J. V., ADAMS, C.N., KOTOV, N. A. & SAVAGE, P.E. 2007. Hydrothermal synthesis of CdSe nanoparticles. *Ind. Eng. Chem. Res.* **46** pp. 4358–4362.
- WON, B., PARK, I. & YI, G.C. 2004. Electroluminescence in n-ZnO nanorod arrays vertically grown on p-GaN. *Adv. Mater.* **16** (1) pp. 87–90.
- WU, X.J., ZHANG, Z.Z., ZHANG, J.Y., JU, Z.G., LI, B.H., LI, B.S., SHAN, C.X., ZHAO, D.X., YAO, B. & SHEN, D.Z. 2008. Growth of FeSe on general substrates by metal-organic chemical vapor deposition and the application in magnet tunnel junction devices. *Thin Solid Films* **516** pp. 6116–6119.
- WU, X.J., ZHANG, Z.Z., ZHANG, J.Y., JU, Z.G., SHEN, D.Z., LI, B.H., SHAN, C.X. & LU, Y.M. 2007. Structural and electrical characterizations of single tetragonal FeSe on Si substrate. *J. Colloid Interface Sci.* **300** pp. 483–485.
- WUISTER, S.F., DONEGA, C.D.M. & MEIJERINK, A. 2004. Luminescence temperature anti-quenching of water-soluble CdTe quantum dots: Role of the solvent. *J. Am. Chem. Soc.* **126** pp. 10397–10402.
- WUISTER, S.F., HOUSELT, A. VAN, DONEGA, C.D.M., VANMAEKELBERGH, D. & MEIJERINK, A. 2004. Temperature anti-quenching of the luminescence from capped CdSe quantum dots. *Angew. Chem. Int. Ed.* **43** pp. 3029–3033.
- WUISTER, S.F., SWART, I., DRIEL, F. VAN, HICKEY, S.G. & DONEGA, C.D.M. 2003. Highly luminescent water-soluble CdTe quantum dots. *Nano Lett.* **3** (4) pp. 503–507.
- WYTENBACH, T., WITT, M. & BOWERS, M.T. 2000. On the stability of amino acid zwitterions in the gas phase: The influence of derivatization, proton affinity, and alkali ion addition. *J. Am. Chem. Soc.* **122** pp. 3458–3464.

- XIE, Y., ZHENG, X., JIANG, X., LU, J. & ZHU, L. 2002. Sonochemical synthesis and mechanistic study of copper selenides Cu_{2-x}Se , CuSe , and Cu_3Se_2 . *Inorg. Chem.* **41** (2) pp. 387–392.
- XU, S., LAO, C., WEINTRAUB, B. & LIN, Z. 2008. Density-controlled growth of aligned ZnO nanowire arrays. *J. Mater. Res* **23** (8) pp. 2072–2077.
- XU, S., WANG, H., ZHU, J. & CHEN, H. 2002. Sonochemical synthesis of copper selenides nanocrystals with different phases. *J. Cryst. Growth* **234** pp. 263–266.
- YAN, D., ZHANG, L., QIN, M., BAI, L. & ZHAO, Y. 2014. Folic acid-conjugated silica-coated gold nanorods and quantum dots for dual-modality CT and fluorescence imaging and photothermal therapy. *J. Mater. Chem* **2** pp. 1945–1953.
- YANG, H., LUAN, W., WAN, Z., TU, S. & YUAN, W. 2009. Continuous synthesis of full-color emitting core/shell quantum dots via microreaction. *Cryst. Growth Des.* **9** (11) pp. 4807–4813.
- YIN, L., WANG, D., HUANG, J., CAO, L., OUYANG, H. & YONG, X. 2016. Morphology-controllable synthesis and enhanced photocatalytic activity of ZnS nanoparticles. *J. Alloys Compd.* **664** pp. 476–480.
- YU, S., ANTONIETTI, M., COLLFEN, H. & GIERSIG, M. 2002. Synthesis of very thin 1D and 2D CdWO_4 nanoparticles with improved fluorescence behavior by polymer-controlled crystallization. *Angew. Chem. Int. Ed.* **41** (13) pp. 2356–2360.
- ZHANG, A., MA, Q., WANG, Z., LU, M., YANG, P. & ZHOU, G. 2010. Controllable synthesis of copper selenide nanocrystals through a green paraffin-acetate method. *Mater. Chem. Phys.* **124** (2–3) pp. 916–921.
- ZHANG, B.P., YASUDA, T., SEGAWA, Y., YAGUCHI, H., ONABE, K., EDAMATSU, E. & ITOH, T. 1997. Naturally formed ZnCdSe quantum dots on ZnSe (110) surfaces. *Appl. Phys. Lett.* **70** (18) pp. 2413–2415.
- ZHANG, F., KONG, X., LI, Q., SUN, T., CHAI, C., SHEN, W., HONG, Z., HE, X., LI, W. & ZHANG, Y. 2016. Facile synthesis of CdTe @ GdS fluorescent-magnetic nanoparticles for tumor-targeted dual-modal imaging. *Talanta* **148** pp. 108–115.
- ZHANG, H., MA, X., JI, Y., XU, J. & YANG, D. 2003. Single crystalline CdS nanorods fabricated by a novel hydrothermal method. *Chem. Phys. Lett.* **377** (5–6) pp. 654–657.
- ZHANG, S., KOU, X., YANG, Z., SHI, Q., STUCKY, G.D., SUN, L., WANG, J. & YAN, C. 2007. Nanonecklaces assembled from gold rods, spheres, and bipyramids. *Chem. Commun.* (18) pp. 1816–1818.
- ZHONG, P., YU, Y., WU, J., LAI, Y., CHEN, B., LONG, Z. & LIANG, C. 2006. Preparation and application of functionalized nanoparticles of CdSe capped with 11-mercaptoundecanoic acid as a fluorescence probe. *Talanta* **70** (4) pp. 902–906.

- ZHONG, Z., QIAN, F., WANG, D. & LIEBER, C.M. 2003. Synthesis of p-type gallium nitride nanowires for electronic and photonic nanodevices. *Nano Lett.* **3** (2) pp. 343–346.
- ZHOU, H.L., CHUA, S.J., PAN, H., ZHU, Y.W., OSIPOWICZ, T., LIU, W. & ZANG, K.Y. 2007. morphology controllable ZnO growth on facet-controlled epitaxial lateral overgrown GaN/sapphire templates. *J. Phys. Chem.* **111** pp. 6405–6410.
- ZHU, J., PALCHIK, O., CHEN, S. & GEDANKEN, A. 2000. Microwave assisted preparation of CdSe, PbSe, and Cu_{2-x}Se nanoparticles. *J. Phys. Chem. B* **104** (31) pp. 7344–7347.
- ZHUANG, J., SHALLER, A.D., LYNCH, J., WU, H., CHEN, O., LI, A.D.Q. & CAO, Y.C. 2009. Cylindrical superparticles from semiconductor nanorods. *J. Am. Chem. Soc.* **131** (17) pp. 6084–6085.